BIOMECHANICAL MODELLING OF THE INTERPHALANGEAL JOINTS OF THE HUMAN HAND

A THESIS SUBMITTED TO
THE GRADUATE SCHOOL OF NATURAL AND APPLIED SCIENCES
OF
MIDDLE EAST TECHNICAL UNIVERSITY

BY

KORAY MELİH YATAĞAN

IN PARTIAL FULFILLMENT OF THE REQUIREMENTS
FOR
THE DEGREE OF MASTER OF SCIENCE
IN
MECHANICAL ENGINEERING

JULY 2021

Approval of the thesis:

BIOMECHANICAL MODELLING OF THE INTERPHALANGEAL JOINTS OF THE HUMAN HAND

submitted by **KORAY MELİH YATAĞAN** in partial fulfillment of the requirements for the degree of **Master of Science** i**n Mechanical Engineering, Middle East Technical University** by,

Prof. Dr. Halil Kalıpçılar
Dean, Graduate School of **Natural and Applied Sciences** _____

Prof. Dr. Sahir Arıkan
Head of the Department, **Mechanical Engineering** _____

Assoc. Prof. Dr. Ergin Tönük
Supervisor, **Mechanical Engineering, METU** _____

Prof. Dr. Gürsel Leblebicioğlu
Co-Supervisor, **Orthopaedics Dept., Hacettepe University** _____

Examining Committee Members:

Prof. Dr. Reşit Soylu
Mechanical Engineering, METU _____

Assoc. Prof. Dr. Ergin Tönük
Mechanical Engineering, METU _____

Assoc. Prof. Dr. M. Bülent Özer
Mechanical Engineering, METU _____

Prof. Dr. Halil İbrahim Açar
Anatomy Dept., Ankara Uni. _____

Prof. Dr. İlhami Kuru
Dept. Of Orthopedics and Traumatology, Başkent Uni. _____

Date: 15.07.2021

I hereby declare that all information in this document has been obtained and presented in accordance with academic rules and ethical conduct. I also declare that, as required by these rules and conduct, I have fully cited and referenced all material and results that are not original to this work.

Name Last name : K. Melih Yatağan

Signature :

ABSTRACT

BIOMECHANICAL MODELLING OF THE INTERPHALANGEAL JOINTS OF THE HUMAN HAND

Yatağan, Koray Melih
Master of Science, Mechanical Engineering
Supervisor : Assoc. Prof. Dr. Ergin Tönük
Co-Supervisor: Prof. Dr. Gürsel Leblebicioğlu

July 2021, 98 pages

In this study, the development process of a 3D unconstrained model of the interphalangeal (IP) joints is presented. The model agrees with the experimental studies. It can explain the change in the axes of the IP joints, the non-linear relationship between the tendon excursion and the flexion angle, the coordination between the IP joints and the tendon forces corresponding to the flexion angle. Furthermore, some controversial topics in the literature are investigated using the model, and four theses were developed.

Keywords: Biomechanics, Interphalangeal joints, Musculoskeletal model.

ÖZ

İNSAN ELİNİN INTERFALANGEAL EKLEMLERİNİN BİYOMEKANİK MODELLEMESİ

Yatağan, Koray Melih
Yüksek Lisans, Makina Mühendisliği
Tez Yöneticisi: Doç. Dr. Ergin Tönük
Ortak Tez Yöneticisi: Prof. Dr. Gürsel Leblebicioğlu

Temmuz 2021, 98 sayfa

Bu çalışmada, interfalangeal (IF) eklemlerinin kinematik sınırlamalar kullanılmadan 3B bir modeli oluşturuldu. Model literatürdeki deneysel veriler ile uyumluluk göstermekte olup, IF eklemlerinin dönme eksenlerindeki değişimi, tendon ekskürsiyonları ile fleksiyon açıları arsındaki doğrusal olmayan ilişkiyi, IF eklemlerinin koordine hareketlerini ve fleksiyon açısına karşılık gelen tendon kuvvetlerini açıklama kapasitesine sahiptir. Ayrıca bu model kullanılarak literatürdeki bazı tartışmalı konular incelenip, bu konular ile ilgili dört adet tez öne sürüldü.

Anahtar Kelimeler: Biyomekanik, İnterphalangeal eklemler, Muskuloskeletal model

To Ebru and Pampa

ACKNOWLEDGMENTS

First of all, I would like to thank my supervisor, Assoc. Prof. Dr. Ergin Tönük and my co-supervisor, Prof. Dr. Gürsel Leblebicioğlu. Without their guidance, I would easily get lost in the vast literature.

Many thanks to the Department of Anatomy in Ankara University, especially to Prof. Dr. İbrahim Tekdemir and Prof. Dr. Halil İbrahim Açar, for they allowed me to observe human anatomy closely.

Finally, I thank my family and mostly Ebru Bağlan and my little budgie friend Pampa for their love and support.

TABLE OF CONTENTS

LIST OF TABLES

TABLES

LIST OF FIGURES

FIGURES

LIST OF ABBREVIATIONS

ABBREVIATIONS

PP	Proximal phalanx
MP	Middle phalanx
DP	Distal phalanx
CMC	Carpometacarpal
MCP	Metacarpophalangeal
PIP	Proximal interphalangeal
DIP	Distal interphalangeal
PCL	Proper collateral ligament
ACL	Accessory collateral ligament
CR	Check rein
ORL	Oblique retinacular ligament
FDP	Flexor digitorum profundus
FDS	Flexor digitorum superficialis
EDC	Extensor digitorum communis
L1, L2, L3	Landsmeer's model I, II, III
AC	Ann and Chao's model
CP	Control point method
FHA	Finite helical axis
PCSA	Physiological cross-sectional area

CHAPTER 1

INTRODUCTION

The human hand is a very complex *mechanism*. It can perform both tasks requiring precision, such as writing or playing an instrument, and perform physically demanding tasks such as holding a hammer or lifting a weight. Considering it is almost impossible to work without our hands, the significance of understanding its biomechanics becomes apparent. In this study, a 3D model of the interphalangeal joints of the human finger is presented.

Experimental studies are crucial for they provide the most reliable results. However, it is not always possible or easy to perform experimentation. The number of specimens can be a limiting factor for the in vitro studies. For the in vivo studies, the risk of injuring the subject can be a limiting factor. In a mathematical model, one can perform many virtual experiments without worrying about wasting specimens or risking the patient's health. Another benefit is the ease of modifying anatomic structures. Parameters can be changed as desired, or some structures can be canceled to see their effects. Nonetheless, a mathematical model still needs to be validated experimentally. But it can help to reduce the number of experiments greatly.

The available finger models in the literature treat the interphalangeal joints as idealized hinge joints. These models can represent the joint's motion but cannot explain how that motion occurs. The questions such as "Which structures are responsible for a particular function?" or "How does the injury of a structure affect the finger's overall performance?" are left unanswered. The current study presents a 3D model that aims to answer those kinds of questions. The joints are modeled without using any idealized kinematic constraints. All six degrees of freedom of the bones are conserved and the motion is constrained by the ligaments.

In Chapter 2, background information is presented. Section 2.1 aims to familiarize the reader with the anatomy of the finger. In Section 2.2, the composition, structure, and mechanical properties of the ligaments and tendons are summarized. Lastly, in Section 2.3, the significant studies about the finger are presented.

Chapter 3 explains the modeling procedure. In Section 3.1, 3D geometry of the bones are presented. In Section 3.2, the modeling process of the proximal interphalangeal (PIP) joint is described. Since PIP and distal interphalangeal (DIP) joints are similar in structure, the modeling of the DIP joint is not presented in detail. In Sections 3.4 and 3.5, modeling of the oblique retinacular ligament (ORL) and the flexor digitorum profundus (FDP) is presented. Lastly, in Section 3.6, the material model used for the ligaments is explained, and also a new method for estimating the ligament parameters is proposed.

Chapter 4 presents the results of this study. In Sections 4.1-4.4, various experimental studies are virtually performed and compared to the literature. In Sections 4.5-4.8, controversial issues about finger anatomy are analyzed. As a result, four hypotheses are developed. Finally, in Chapter 5, the modeling procedure is summarized and the results are discussed.

CHAPTER 2

BACKGROUND

2.1 Anatomy of the Human Finger

The anatomy of the fingers from the index to the little finger is described in this part. The thumb has a different anatomy and is excluded. This part aims not to present the finger's complete anatomy but rather to familiarize the reader with the anatomical concepts. As a matter of fact, the details about the anatomy of the fingers have not been fully analyzed yet; there are still controversial issues that do not have a definite explanation. Those issues are not covered in this section, and detailed explanations are presented in the modeling section when necessary.

Anatomical structures are called proximal or distal according to their proximity to the heart. Structures close to the heart are defined as "proximal" and structures far from the heart are defined as "distal". In the coronal plane, structures close to the midline are called medial, and distant structures are called lateral. Structures located in front of the sagittal plane are called anterior, and structures located behind are called posterior. (Figure 2.1)

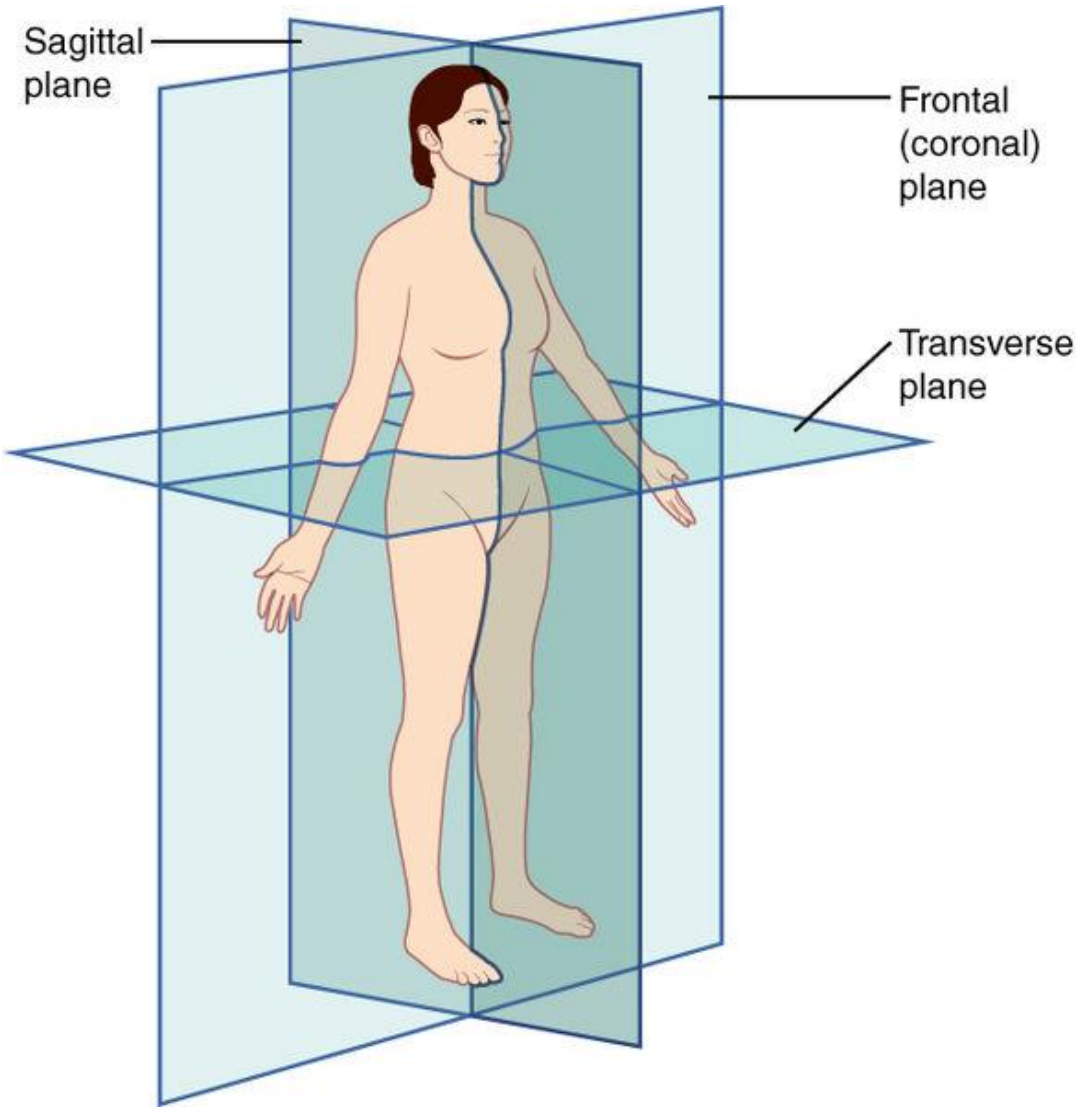

Figure 2.1. Body planes

The terms used in the clinical anatomy of the hand may show some differences. The palm faces anteriorly in the normal anatomical position. Structures in this direction are called “palmar” structures. The word palmar replaces the word volar. Since there is the radius bone on the lateral side of the hand and forearm, this lateral part is called the “radial” side. Since the ulna bone is located on the medial side of the hand and forearm, this part is called the “ulnar.” (Figure 2.2)

Bones are the essential stabilizing components of the body; they are the body's frame in mechanical terms. The bones of the finger are long bones. The "diaphysis" section

is the cortical bone-rich sections of the bones that carry mechanical loads. At the proximal and distal ends of the diaphysis, the segments that are specialized to form joints are called "metaphysis". In the literature, the proximal metaphysis is sometimes called "the base" and the distal metaphysis is called "the head". The most proximal bone of the finger is the metacarpal, and the other three are the proximal phalanx, the middle phalanx, and the distal phalanx. To differentiate between the bones of the different digits, each is assigned a number, the thumb being the first and the little finger being the fifth. The second metacarpal is the metacarpal of the index finger, for instance.

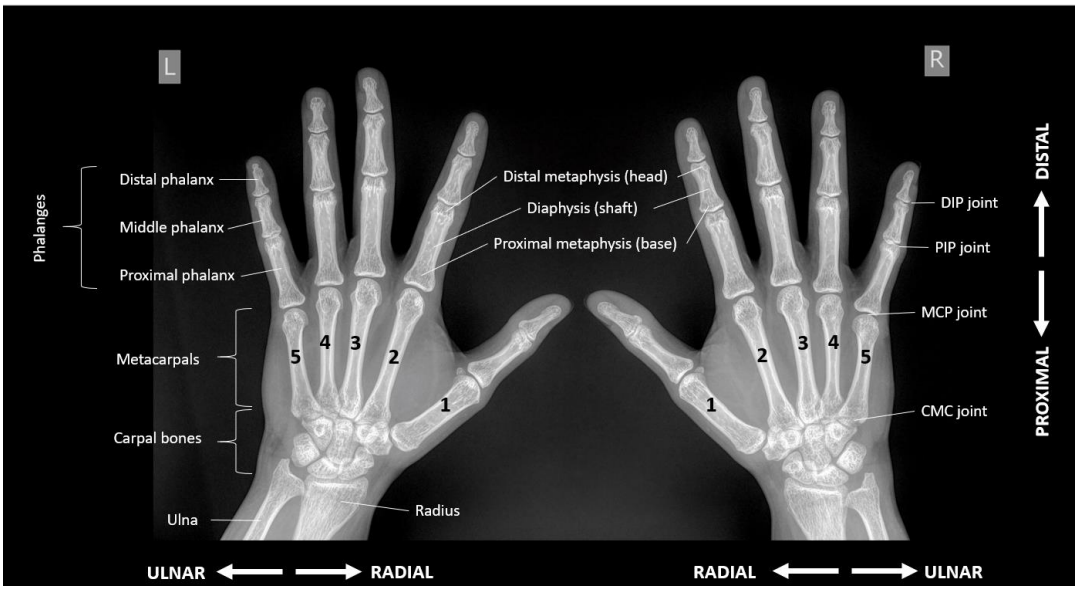

Figure 2.2. The bones and joints of the hand [1]

Two bones meet at the metaphyseal region to form a joint. These regions are covered with a very smooth surface called the articular cartilage. A joint is made into a compartment that is separated from the surrounding tissue by a structure called the "joint capsule". The "synovial" tissue in the joint capsule and various parts of the joint secrete joint fluid, both providing nourishment to the cartilage surface and reducing the frictional resistance between the joint surfaces. There are three different types of joints in the finger. These are the carpometacarpal (CMC) joint, metacarpophalangeal (MCP) joint, and interphalangeal (IP) joints (Figure 2.2).

CMC joint connects the metacarpals to the carpals (wrist bones) firmly. Each metacarpal is also connected to the adjacent metacarpals. Therefore, CMC joints do not allow much mobility. MCP joint connects the metacarpal bone to the proximal phalanx. It is capable of moving in flexion-extension and abduction-adduction [2]. CMC and MCP joints are not included in this study; therefore, they are not explained further.

IP joints connect the phalanges and are named as the proximal interphalangeal (PIP) joint and the distal interphalangeal (DIP) joint. Both of these joints are similar in structure. The PIP joint is formed by the proximal phalanx head and the base of the middle phalanx. It mainly moves in flexion-extension like a hinge. Rolling and gliding are also partially involved in this movement. The PIP joint's hinge-like motion is achieved partly by the articular surface geometry and partly by the ligaments surrounding the joint [3]–[5].

On both sides of the joint are the collateral ligaments. The essential function of the collateral ligament is to keep the joint in the normal anatomical position. The more dorsally located part is thicker and called the proper collateral ligament (PCL). The palmar portion is less pronounced and is called the accessory collateral ligament (ACL). It is thought to suspend the palmar plate.

Palmar to the joint is a thick ligamentous structure called the palmar plate (or volar plate). It prevents hyperextension of the joint. Distally it attaches to the middle phalanx metaphyseal region firmly; proximally attaches to the diaphysis of the proximal phalanx by two check-rein ligaments. The same structures are also present in the DIP joint.

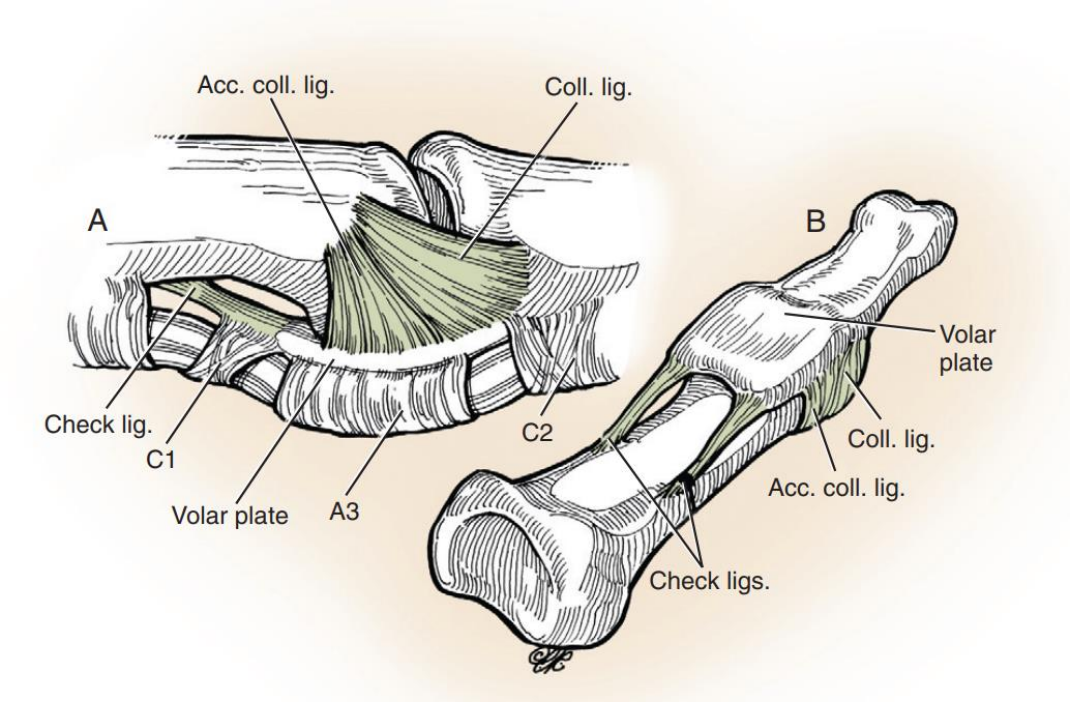

Figure 2.3. The PIP joint [6]

The PIP and the DIP joints are actuated by the flexor muscles, the flexor digitorum profundus (FDP), and the flexor digitorum superficialis (FDS). They are called extrinsic muscles since their muscle bellies are located outside of the hand. The muscle force is transferred to the joints by the tendons. FDP tendon attaches to the distal phalanx, thus flexes both the PIP and the DIP joints. FDS attaches to the base of the middle phalanx and flexes only the PIP joint. FDP is a larger, stronger muscle that provides the main flexion force, while FDS is a smaller muscle that acts as an active stabilizer of the joints. Flexor tendons pass through a number of special structures called flexor sheaths and pulleys. They guide the tendon and keep it close to the bone surface.

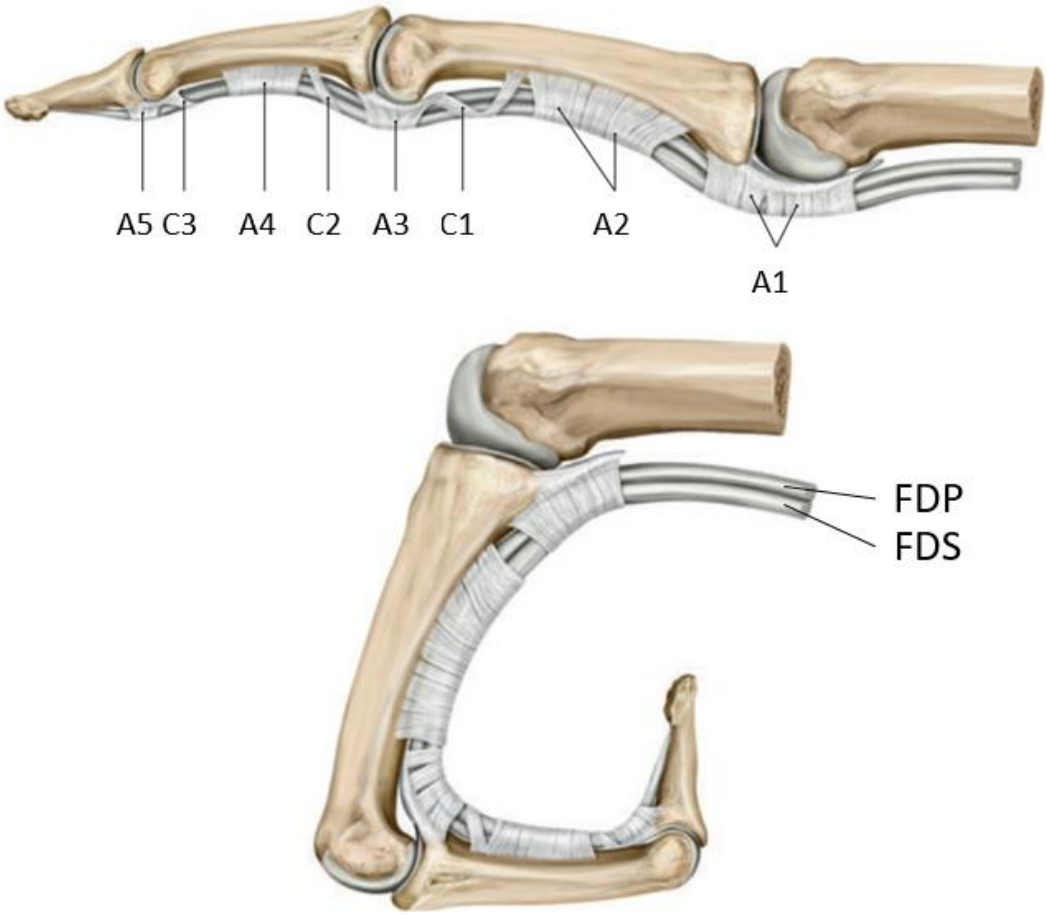

Figure 2.4. The flexor tendons and the pulleys of the finger [4]

The extension of the IP joints is achieved through the extensor mechanism. It is a complex web of tendinous bands covering most of the dorsal surface of the finger. Extrinsic long extensor muscles, the intrinsic lumbricals, and the interossei muscles have attachments to the extensor mechanism. The activation pattern of these muscles determines which part of it to be tensioned. The relation between the extensor mechanism and the different muscles acting on it is not straightforward. An investigation of this complicated relationship is out of the scope of this study. Only the parts of the extensor mechanism over the PIP and the DIP joints will be mentioned here.

Proximal to the PIP joint, the long extensor tendon diverges into two lateral slips and a central slip. Then, the central slip is joined by two slips coming from the interossei

and the lumbrical to form the medial band, which attaches to the base of the middle phalanx's dorsum. Lateral slips of the extensor tendon and the slips coming from the intrinsic muscles constitute the lateral band. The lateral bands then pass lateral to the PIP joint and unite distally to form the terminal tendon. The terminal tendon attaches to the base of the distal phalanx and extends the DIP joint. The triangular ligament and the transverse retinacular ligament provide stability to the lateral bands.

Another essential structure related to the PIP and DIP joints is the oblique retinacular ligament (ORL). The ORL originates from the proximal phalanx diaphysis, crosses the PIP joint obliquely, and attaches to the terminal tendon. Although not agreed generally, it is thought to have a role in the DIP and PIP joints' apparent coordinated motion [7].

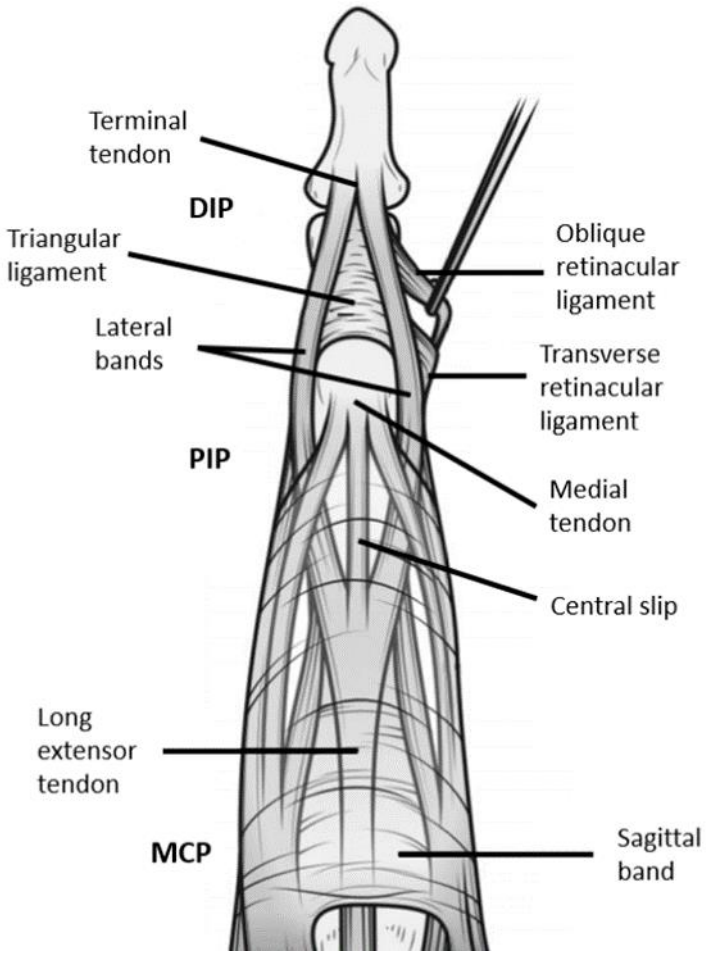

Figure 2.5. The extensor mechanism over the interphalangeal joints [8]

2.2 Composition, Structure and Mechanical Properties of Ligaments and Tendons

Tendons and ligaments are important components of the musculoskeletal system. An accurate mechanical model of the human finger requires an understanding of their functions, composition, structure and mechanical properties.

Tendons are mesenchymal tissues which internal fascicular arrangement is formed in parallel with mechanical forces. They are usually attached to a muscle at their proximal end and to a bone at their distal end. They transform the shortening in the muscles into movement and transmit it to the joints and bones. For example, the belly of the flexor digitorum profundus (FDP) muscle which flexes the fingers is located in the forearm. If it were to be attached directly to the finger joint, it would have to be located inside the hand thus its force capacity would be greatly reduced.

Ligaments are similar in structure to tendons but they connect bone to bone. They constraint motion and provide passive stability to joints. For instance, collateral ligaments found on both sides of the finger joints prevent sideways motion. Ligaments also coordinate motion between different joints. ORL (oblique retinacular ligament) connects proximal and distal interphalangeal joints (DIP and PIP) and it allows passive extension of DIP when PIP is flexed.

Ligaments and tendons have a specialized structure composed of different biological materials. One of these biological materials is the collagen which is the main structural material of the soft and hard tissues of the body. Fung states the importance of collagen in our body by comparing it to steel's importance in our civilization in his book *Mechanical Properties of Living Tissue* [9]. Different types of collagen are found all over the human body. These are named as type I, II, III, IV etc. 70-80 % dry weight of tendons and ligaments are composed of collagen type I and III [10]. Other types of collagens are also found in the muscle and bone junctions in trace amounts. Type I and III collagens are known as fiber forming collagens and they

provide high tensile strength of the tendons and ligaments. Fung reports the elastic modulus of a single collagen fiber around 1 GPa [9].

Elastin is another biomaterial which is found in ligaments in small amounts. It is responsible for the elasticity. Özkaya [11] states that elastin can deform linearly and reversibly up to 200% elongation with very low stiffness. It exhibits negligible hysteresis and strain rate dependence. Its elastic modulus is reported to be around 0.6 MPa [11].

Figure 2.6 shows the hierarchical structure of a collagenous tissue. Collagen molecules form into fibrils and fibrils organize into collagen fibers. Fibers are initially crimped and they show little resistance to strain until they are fully taut. Large groups of fibers are bundled together to form structures called fascicles. In tendons, fibers are strictly aligned parallel to loading direction. In ligaments, they are not completely parallel since ligaments sometimes need to carry lateral loads. Being a living tissue, ligaments and tendons also contain cells. But these cells do not affect the mechanical properties of the overall structure. Pridgen et al. [12] investigated the effects of de-cellularization of human FDP tendons on the elastic modulus and the ultimate stress. They did not find any statistically significant difference between the fresh specimens and the de-cellularized specimens.

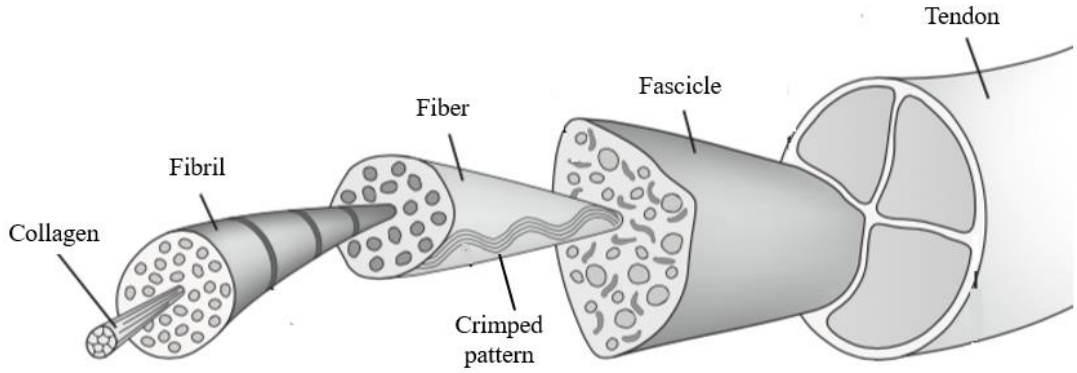

Figure 2.6. Hierarchical structure of tendons and ligaments [13]

Ligaments and tendons display non-linear viscoelastic behaviors. In this thesis, only the quasi-static behavior will be investigated. A typical stress-strain curve for a tendon or ligament is shown in Figure 2.7. Three distinct regions namely toe, linear and fracture regions can be identified. In the toe region, fibers are in crimped position and elongate with little resistance. As the strain increases, fibers become taut and the slope of the curve increases. In the linear region all fibers become taut and resist to strain linearly. In the fracture region some fibers start to rupture and eventually failure of the specimen occurs. Ligaments and tendons operate in the toe and linear regions in normal physiological range.

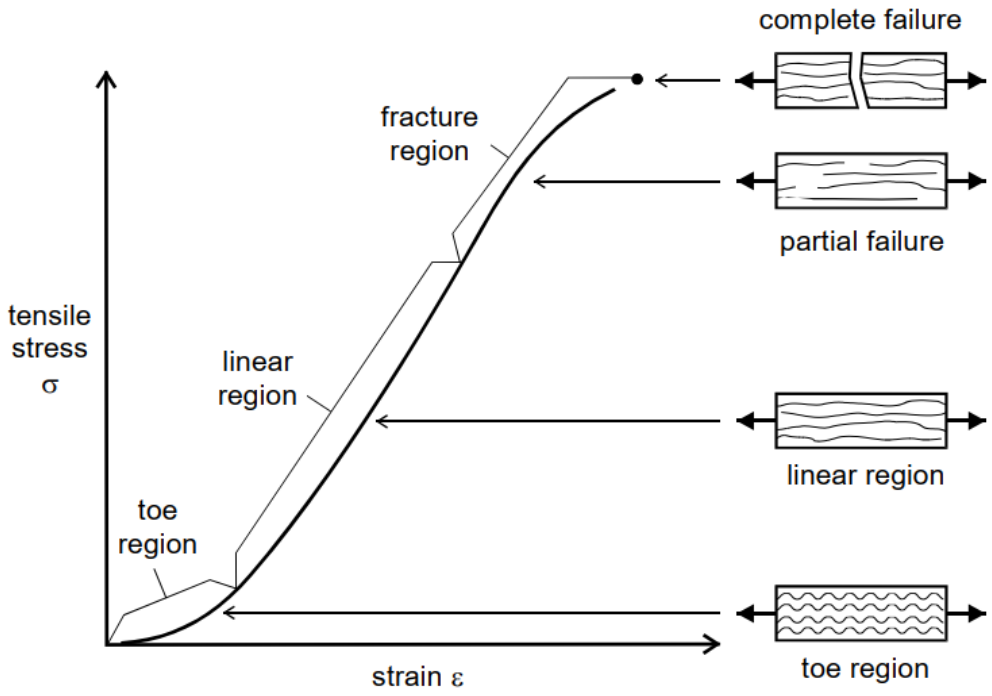

Figure 2.7. Typical stress-strain curve for ligaments and tendons [14]

Mechanical properties of ligaments and tendons vary depending on their composition and organization of their fibers. Up to date, many experiments are performed on tendons and ligaments to assess their mechanical properties. Various values for the elastic modulus of the linear region reported in the literature are presented in Table 2.1.

Table 2.1 Mechanical properties of tendons and ligaments reported in the literature

Ref	Tendon or ligament	Specifications	Tangent modulus (MPa)	Ultimate stress (MPa)	Ultimate strain (%)	Strain rate (%/s)
[15]	FDP	chicken	216 ± 8**	50±3.8**	x	0.05
[16]	UCL(thumb)	human	37.3 ± 5.1	11.4 ±1.2	x	0.88*
[17]	FDP	human	694±282	x	x	x
	FDS		800±238	x	x	x
	EDC		1230±641	x	x	x
[18]	DF	swine	1150±35**	95.1±5.2**	8.7±0.33**	0.333
	DE		647±107**	40.0±1.9**	9.0±0.41**	0.333
	MCL(knee)		10±3.3**	x	12±3	0.4
	MCL(knee)	mongrel dog	9.7±7.3**	x	14±1	0.4
[19]	FDP	chicken	324±17	x	x	<0.1
			427±10	x	x	0.6
			653±21	x	x	1.2
			837±11	x	x	5
[20]	ACL(knee)	human(old)	65.3 ±24	13.3±5	30±10.0	100
		human(young)	111±26	37.8±9.3	44.3±8.5	100
		rhesus monkeys	186±26	66.1±8.4	47±5.6	66
[21]	ACL(knee)	human(female)	99±50	22.58±8.92	27±8	100
		human(male)	128±35	26.35±10.08	30±6	100
		human(mixed)	113±45	24.36±9.38	28±7	100
[22]	MPFL(knee)	human	116±95	16±11	24.3±6.8	0.3
[23]	PT	human(young)	660±266	64.7±15	14±6	37*
		human(old)	504±222	53.6±10	15±5	37*
[24]	MCL(knee)	human	332.2±58.3	38.6±4.8	17.1 ±1.5	1
[25]	AT	human	816±218	71±17	7.5±1.1	1
			822±211	86±24	9.9±1.9	10

(Values are given as mean ± standard deviation. All the specimens in the papers are either freshly obtained or fresh frozen except [17] in which embalmed cadavers are used. "x": no data is provided. "*": Strain rate is not directly reported, it is obtained from elongation rate and the initial length. "**": Data is provided graphically, values are calculated from the given stress-strain plot. FDP: Flexor digitorum profundus. FDS: Flexor digitorum superficialis. UCL: Ulnar collateral ligament. DF: Digital flexor. DE: Digital extensor. MC: Medial collateral ligament. ACL: Anterior cruciate ligament. MPFL: Medial patella-femoral ligament. PT: Patellar tendon. AT: Achilles tendon)

Values presented in Table 2.1 show a large variability both in individual studies as a large standard deviation and among different types of tendons and ligaments studied. Mean elastic modulus values range between 9.7 MPa and 1.23 GPa, while ultimate

stress values range between 11.4 MPa and 95.1 MPa. Ultimate tensile strain also varies to a lesser extent (7.5% to 47%). Biological tissues in general are highly adaptable. Their properties change according to the function they need to accomplish. For instance, mean elastic modulus of the human Achilles tendon which needs to carry up to a few times of the body weight during walking and running is much greater (816 MPa) [25] compared to the ulnar collateral ligament (37.3 MPa) [16], which is a stabilizer of the thumb joint. Furthermore, ligaments seem to be less stiff compared to tendons in general. Properties also change with age and sex. Noyes and Grood [20] compared the mechanical properties of the anterior cruciate ligament (ACL) obtained from old and young adult humans. They found that mean values of elastic modulus and ultimate tensile stress are 1.7 and 2.8 times larger in the young group. Chandrashekar, Mansouri, Slauterbeck and Hashemi [21] investigated the effects of sex on the ACL and reported a 22.49% lower elastic modulus and 14.3% lower ultimate stress for the female group.

Apart from the intrinsic properties of the ligaments and tendons, some of the variability can be explained by the experimental procedure used during the material testing. Experimenting of the collagenous tissues is a challenging task and it is prone to error. Due to irregular geometry, cross sectional area of ligaments and tendons cannot be measured with high accuracy. In most of the papers it is measured with mechanical calipers by assuming its shape as rectangular or elliptical. The cross-sectional area also may change along the tested length. A few measurements are taken and averaged to find the cross-sectional area. Another problem is the measurement of strain. Slippage of the specimens is very common and it results in higher strain measurements than the actual values. Special viscoelastic features such as preconditioning and strain rate effects also cause some variability. If a specimen is loaded and unloaded cyclically at a constant strain rate between a lower and upper limit and left to rest and then tested again, it will be found that the stress strain curve is shifted to right. This behavior is called preconditioning. If the upper and lower limits are changed, the specimen needs to be preconditioned again. Some papers overlook this behavior, which can explain some variability. It is reported in the

literature that as the strain rate increases, the tangent modulus of the linear portion increases. Ng, Chou, Lim and Chong [15] investigated 75 chicken FDP tendons to assess the effect of strain rate on mechanical properties. They found significant change in the elastic modulus of the linear region and ultimate stress values but no statistically significant change in the toe region. Wu [19] also conducted experiments on chicken FDP tendons at different strain rates. He reported no strain rate dependence below 0.001/s and a significant increase in the elastic modulus between 0.003/s and 0.1/s (e.g. 427±10 MPa for 0.006/s and 837±11 MPa for 0.05/s).

In conclusion, ligaments and tendons are very specialized complex collagenous structures with nonlinear viscoelastic behavior. Their properties vary depending on their function and adapt to the loading patterns during the lifetime. Significant variations related to age and sex are also observed. Furthermore, the material testing is difficult and error-prone. Careful control of the strain rate is essential for usable results. In the literature, large variations in mechanical properties are found between the different ligaments and tendons and also within the same type of ligament or tendon for the sample set.

2.3 Current State of the Literature on the Human Finger

Most of the work in the literature models the finger as a chain of rigid bodies connected to each other by kinematic constraints. DIP and PIP joints are modeled as hinge joints that work in flexion-extension only and MCP joints are modeled as universal joints with two degrees of freedom in flexion-extension and abduction-adduction. Elastic and viscous resistance of the ligaments and joint capsule are neglected. Muscles are modeled as either constant forces or using Hill's three element muscle model. For the modeling of tendon excursions, four models namely Landsmeer's models 1, 2, 3 [26] and An and Chao's [27] model (commonly referred as control point or sliding point models) become prominent. These models will be referred as L1, L2, L3 and AC here. They describe the tendon excursions over joints

with different geometrical approaches. Landsmeer's models are planar and AC model is applicable to both planar and 3D cases.

In L1 [26] model, it is assumed that the tendon wraps around a constant radius pulley which has a center coinciding with the joint (Figure 2.8). The excursion is formulated as:

$$exc = R * \theta \qquad \text{(Equation 1)}$$

where R is the radius of the pulley and approximated by the average radius of the metaphysis of the phalanx that is proximal to the joint.

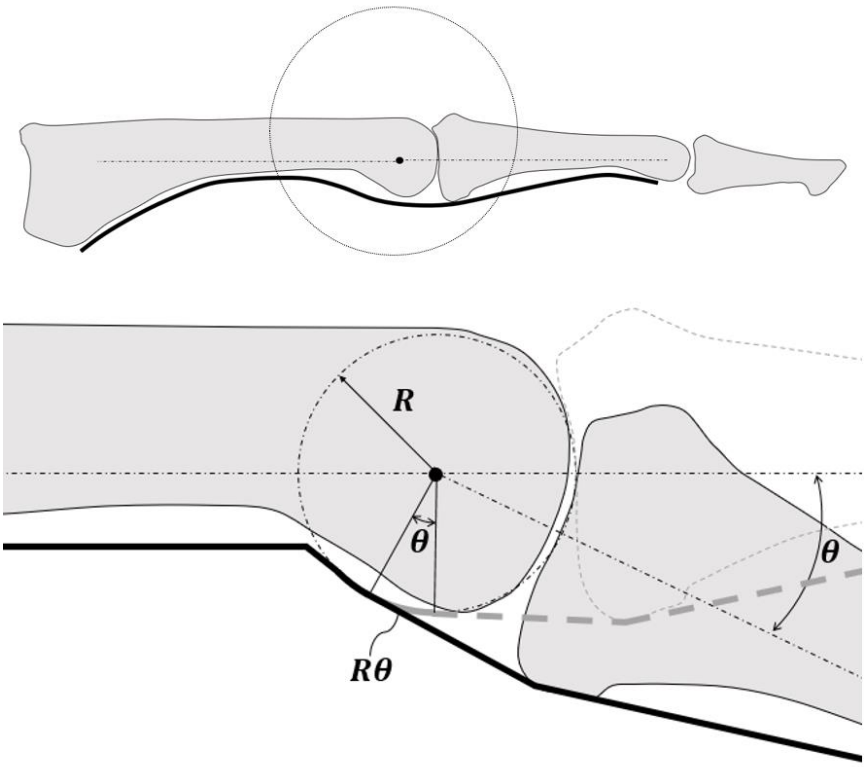

Figure 2.8. Landsmeer's Model I [26]

In L2 [26] model, a link with length R which is free to rotate around the joint center is used to constraint the tendon when passing through the joint. Proximal and distal segments of the tendon are parallel to the long axis of the corresponding phalanges and they meet at the end point of the link. For satisfying the static equilibrium, the

link bisects the angle created between the long axis of the phalanges (Figure 2.9). The excursion over the tendon is calculated by considering the change of the tendon length over the joint with respect to the full extension.

$$exc = 2R * \sin(\theta/2) \quad \text{(Equation 2)}$$

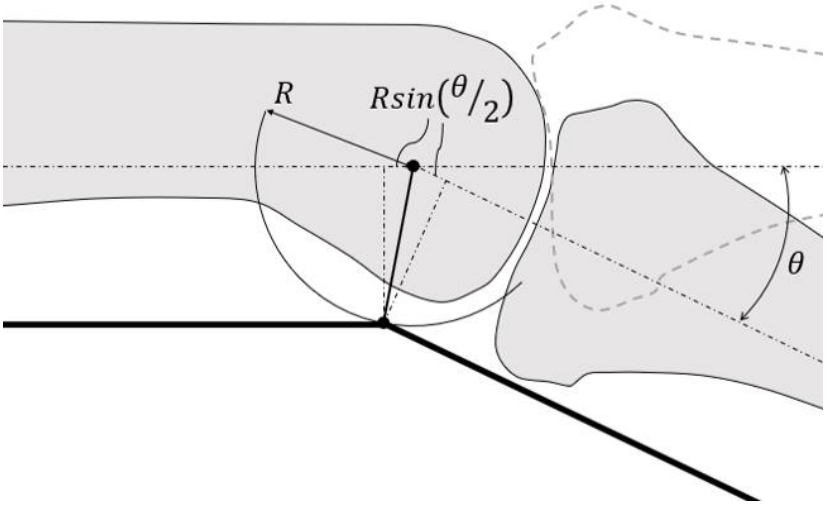

Figure 2.9. Landsmeer's Model II [26]

L3 [26] model also assumes that the tendon passes over a circular arc similar to L1 model but with changing radius and center. Center is determined as the intersection of the two lines which are located at a distance of y to the joint center and perpendicular to the respective phalanx long axis. Furthermore, the linear segments of the tendon are parallel to the phalanx long axes at a distance d and tangent to the circular arc. (Figure 2.10). Initial tendon length over the joint is $2y$. The excursion is calculated by taking the difference between the tendon length at an angle θ and the initial length.

$$exc = \theta d + y\left[2 - \frac{\theta}{\tan(\theta/2)}\right] \quad \text{(Equation 3)}$$

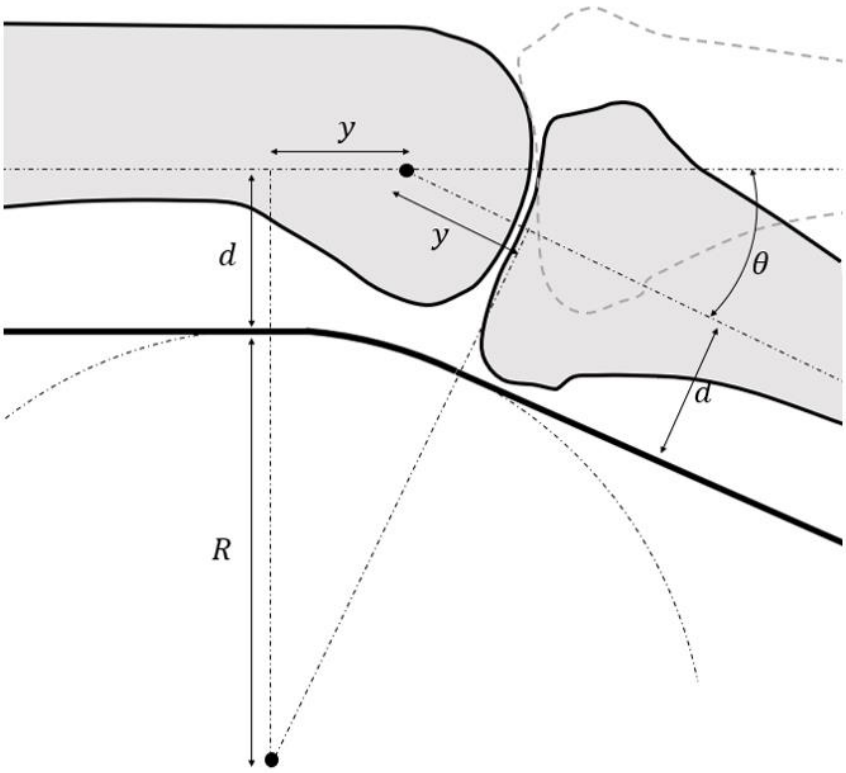

Figure 2.10. Landsmeer's Model III [26]

AC [27] model has a more straightforward approach. Tendon over the joint is represented by a line segment between two control points (commonly referred as slide points or control points) P1 and P2 (Figure 2.11) attached to both phalanges. After necessary coordinate transformations, the distance between the points is calculated. The change in length with respect to the fully extended position yields the excursion.

$$exc = |\overline{P_1P_2}|_\theta - |\overline{P_1P_2}|_{\theta=0} \qquad \text{(Equation 4)}$$

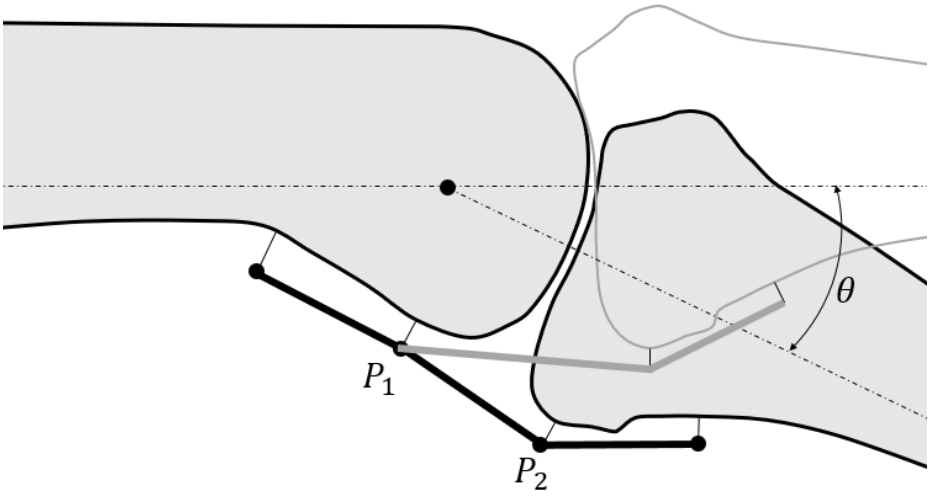

Figure 2.11. An and Chao's Model [27]

Armstrong [28] conducted experiments on several cadaver hands to compare Landsmeer's models. FDP and FDS tendons were displaced in 2 mm increments and the resulting joint angles were observed. The data were fit to equations given by L1, L2 and L3 models (equations 1-3) with least square errors. y parameter of L3 model is found to be less than zero for most cases, therefore L3 model is rejected as a usable model. Upon comparison of the residual errors of L1 and L2 models, it is concluded that L1 represents the data better although both fit reasonably well. An empirical model relating the tendon excursions to joint angles obtained by curve fitting all 976 observations from different cadavers and fingers is provided.

$$\begin{aligned} Tendon\ displacement\ (mm) \\ &= 0.1034X_5 + 0.004211X_4X_5 - 0.0162X_3X_5 \\ &- 0.03043X_1X_5 - 0.06818X_2X_5 \\ &+ 0.03679X_1X_3X_5 \end{aligned} \qquad \text{(Equation 5)}$$

Equation 5 yields the tendon excursions of FDP and FDS for corresponding displacements of DIP, PIP or MCP joints only. The definitions of the parameters X_1 to X_5 are as follows:

$X_1 = 1$ for PIP and 0 for other joints

$X_2 = 1$ for DIP and 0 for other joints

$X_3 = 1$ for FDP and 0 for FDS

X_4 =joint thickness in mm

X_5 =joint angle in degrees measured from fully flexed position

Kociolek and Keir [29] compared AC and L1 on an Opensim (an open source biomechanics software) model. They tuned the wrapping radius of L1 model and the control points of AC model to minimize the difference between Armstrong's empirical model mentioned above (Equation 5). L1 model fitted slightly better compared to AC model. However, this does not mean L1 performs better in general since tuning AC model is a manual task where one changes the control points by hand. From the results of this paper, it can be said that they both describe the tendon excursions equally well.

Buchner, Hines and Hemami [30] constructed a model to study the interphalangeal joint coordination. They modeled DIP, PIP and MCP as hinge joints and included FDP, FDS, EDC, interossei and lumbrical muscles. They modeled the extensor mechanism with middle band, lateral bands and the terminal tendon. EDC tendon passes over MCP joint and divides into the middle band and the lateral bands proximal to the PIP joint. Middle band inserts to the base of the middle phalanx and the lateral bands proceed and merge to form the terminal tendon proximal to the DIP joint. Terminal tendon passes over the DIP joint and inserts to the base of the distal phalanx. They used L1 model and a modified version of L3 model proposed by Fischer [31] to model the tendon excursions (Equation 6)

$$exc = (R + R'\theta)\theta \qquad \text{(Equation 6)}$$

Assuming that there is no slackness on the terminal tendon, the lateral bands and the middle band, they equated the combined excursions of the terminal tendon and the lateral bands to the excursion of the middle band. This resulted in a quadratic relationship between the joint angles of DIP and PIP as follows:

$$\theta_{DIP} = \beta\theta_{PIP}^2 \qquad \text{(Equation 7)}$$

Resulting equilibrium equations of this system was found to be statically indeterminate. This is a common problem in most biomechanical models since number of muscles acting on a joint are more than the joint degrees of freedom. To solve this problem, they introduced a performance index J, which is the sum of the normalized muscle forces obtained by dividing each muscle force to its physiological cross-sectional area (PCSA). By minimizing J, the tendon forces corresponding to a given set of joint angles are calculated.

A dynamic model to calculate the tendon forces for a given motion trajectory was also introduced. In the dynamic model, tendon forces at each time step are calculated by the static optimization model mentioned above and corrected with a feedback loop to minimize the error between the instantaneous joint angles and the desired trajectory.

Yokogawa et. al. [32] utilized the model of Buchner et. al. [30] and they introduced the concept of force manipulability. It is defined as the set of possible fingertip forces for a given set of joint angles. Muscle forces are limited by their maximum stress and their PCSA obtained from the literature.

Yamaguchi et.al. [33] extends the work of Yokogawa et. al. [32]. They state that calculating the maximum fingertip forces at positions close to the joint limits results in unrealistically high tendon forces and propose a model based on the finger soft tissue deformation. Two forces are defined as F_{muscle} and $F_{deformation}$ to be calculated at any given position and a desired fingertip force direction. Then the smallest of these two forces is taken as the maximum available fingertip force. F_{muscle} is the maximum fingertip force calculated from static equilibrium equations with optimization methods. $F_{deformation}$ is calculated considering the maximum fingertip soft tissue deformation. Maximum fingertip deformation in the direction of the desired force is searched by changing θ to $\theta + \Delta\theta$ within joint limits. They performed experiments on subjects to measure the force corresponding to fingertip deformation. An exponential curve is fitted to this data and used to calculate $F_{deformation}$. With this approach, if the given positions are close to the joint limits,

smaller forces are calculated from the deformation approach compared to the unrealistically high fingertip forces calculated in previous studies.

Wu et. al. [34] used inverse dynamics to study the muscle forces during finger tapping using a commercial software package AnyBody (a multibody dynamics software). They obtained the time histories of typical impact forces at the fingertip and the corresponding joint angles from a previous study [35]. The model is driven with these data and the required joint torques are calculated. With the calculated joint torques, they determined the muscle forces by minimizing the sum of the normalized muscle forces. Normalization is achieved by dividing each muscle to its maximum isometric force value.

Image processing is commonly used to measure the kinematics of the hand. One such example is provided by Vignais and Marin [36] where they attached reflective markers to the fingers and the forearm of the subject and recorded the motion during cylinder grasping with a motion capture system. Their approach is similar to Wu et. al [34] except they model the whole hand instead of a single finger.

The compliant effects of ligaments are rarely introduced in the literature. Sancho-Bru et. al. [37] modeled the collateral ligaments of the MCP joint in their dynamic finger model created to assess the muscle forces during fast free movements. They modeled both ulnar and radial collateral ligaments as line segments between two attachment points. A quadratic formula (Equation 8) is employed to relate the deformation to force. K, x and x_0 are the stiffness coefficient, length and initial length respectively.

$$F_{lig} = K(x - x_0)^2 \qquad \text{(Equation 8)}$$

Other aspects of their model are similar to previously mentioned papers. They used inverse dynamics and optimization techniques to calculate the forces with and without the ligaments. They observed much lower forces and significant changes in muscle activation patterns between the two cases.

An experimental investigation of the 3D motion of PIP joint is published by Hess et. al. [38]. In the experiment they fixed the proximal phalanx and pulled both FDP and FDS with the same force until PIP joint is fully flexed. They attached markers to both proximal and middle phalanx to capture both displacement and orientation changes. Bone geometry is obtained by computed tomography (CT) scanning of the specimen. Through FHA (finite helical axis) analysis, they estimated the instantaneous rotation axis at each step. They found out that the axis of rotation varied up to 10.5°. Most of the change occurred between 0-50° and then the rotation axis was stationary until full flexion (Figure 2.12). Translation along the FHA was smaller than 0.31 mm between 1° steps. A fixed coordinate system which would minimize the translational and the rotational changes during motion is determined through optimization. Center of this coordinate system is found to be in the center of the articular curvature in the lateral view. However, it was on the ulnar side in the anterior-posterior view. They observed -1.5 to 1.5 degrees abduction-adduction and -1.1 to 2.2 degrees rotation with respect to the fixed coordinate system throughout the motion.

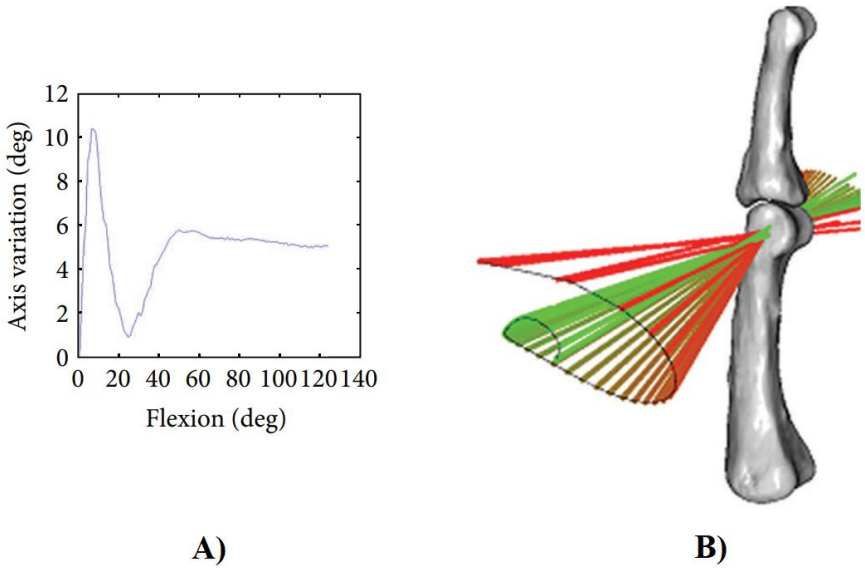

Figure 2.12. A) Variation of the instantaneous rotation axes with respect to the initial axis. B) PIP joint rotation axis trajectory from neutral (red) to full flexion (green) [38]

Another outcome of this study was the investigation of the joint gap. The smallest distance between each point on the articular surface of the proximal phalanx to the middle phalanx is calculated for all steps and presented as a color map. (Figure 2.13). Contact is distributed to a wide region initially and shifts to the dorsal-radial side as flexion angle increases.

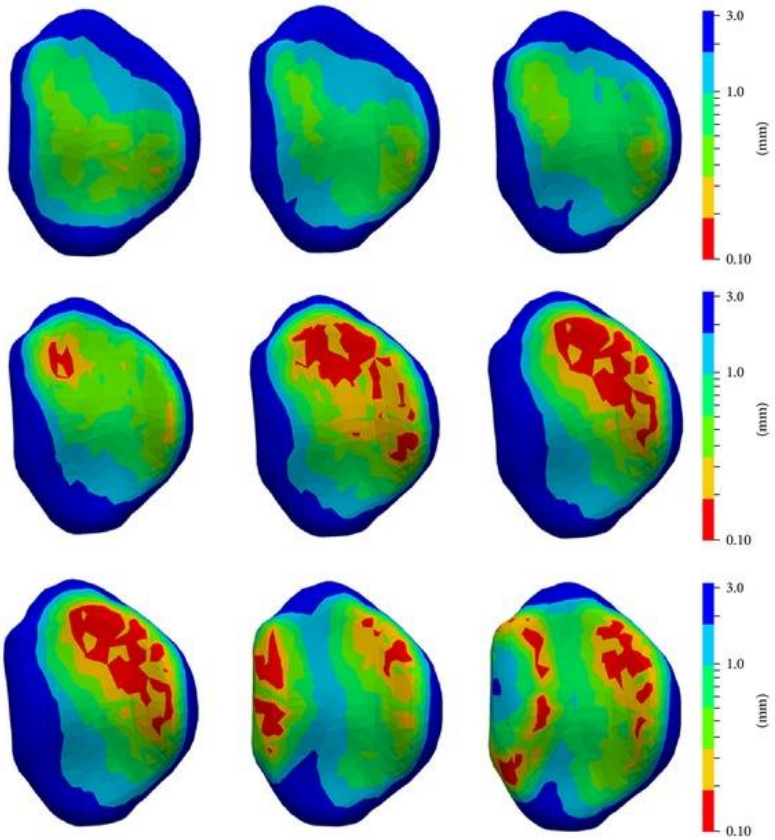

Figure 2.13. Change in joint gap of PIP joint during flexion shown with 15^{o} steps. (First image corresponds to the fully extended position and the last one corresponds to fully flexed position.) [38]

All the musculoskeletal models reviewed here approach to the finger as a chain of rigid bodies connected by kinematic constraints. Resulting static or dynamic equations are indeterminate due to muscle redundancy. This problem is solved with optimization methods by trying to guess the objective function of the neuromuscular control system. These models are sufficiently complex for studying the kinematics

of the finger and the neuromuscular control action, yet insufficient for studying the injury mechanics. In reality, the characteristic degrees of freedom of the joints are dictated by the surrounding connective tissue and the articular surface geometry. Injury of one of these structures may lead to loss of normal function of the finger. Thus, it is necessary to model their contribution to sustain the normal anatomical motion for an understanding of the injury mechanics.

CHAPTER 3

METHODOLOGY

3.1 Modelling the Bones

Proximal, middle, and distal phalanges are included in the finger model. They are modeled as rigid bodies. A 3D laser scan of the left hand's third digit is used for the geometry. The files are obtained from an open source website [39].

Geometries are anatomically checked; all the anatomical features are visible. Images of the geometries are presented in Figures 3.1, 3.2 and 3.3. There are some important anatomical landmarks on the metaphysis regions of the phalanges. These landmarks are shown for the proximal phalanx head and the middle phalanx base. Although less pronounced, the same landmarks are also observed on the middle phalanx head and the distal phalanx base.

The head of the proximal phalanx consists of two condyles separated by an inter-condylar concavity (Figure 3.1). In the dorsal view, the misalignment of the condyles can be observed. This misalignment is not found in the middle phalanx head. On the lateral sides of the condyles, a shallow concave area is present [5], which is commonly believed to be the origin of the collateral ligaments.

The middle phalanx base has two ellipsoid-shaped concavities that correspond to the proximal phalanx's condyles (Figure 3.2). The median ridge bifurcates these concavities and forms into the palmar lip and the dorsal tubercle palmarly and dorsally. The dorsal tubercle slopes towards the lateral tubercles. Just palmar to the lateral tubercles, there are smaller tubercles on each latero-palmar side.

Ash and Unsworth [40] studied 83 PIP joints to design a surface replacement prosthesis. They reported various dimensions of the proximal and middle phalanges.

The same dimensions are also measured for the geometries used (Figures 3.1 and 3.2). They are within the reported range.

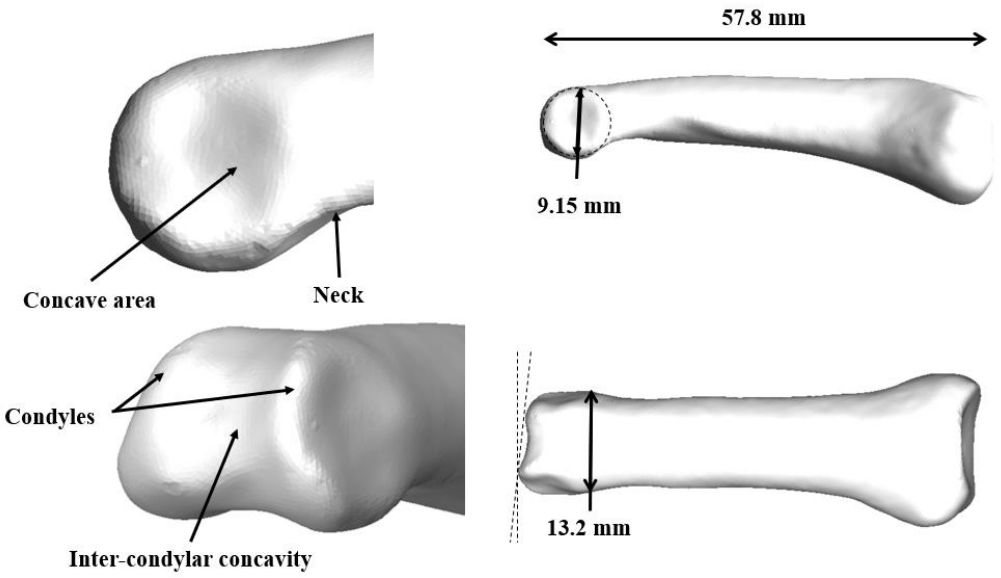

Figure 3.1. Geometry and anatomical landmarks of the proximal phalanx

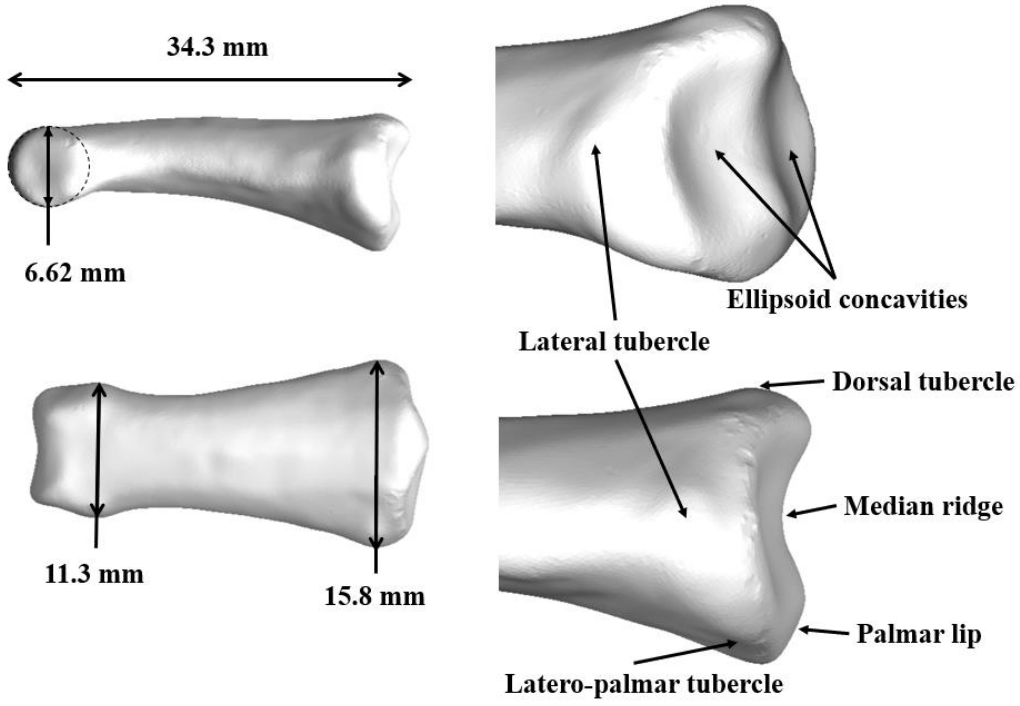

Figure 3.2. Geometry and anatomical landmarks of the middle phalanx

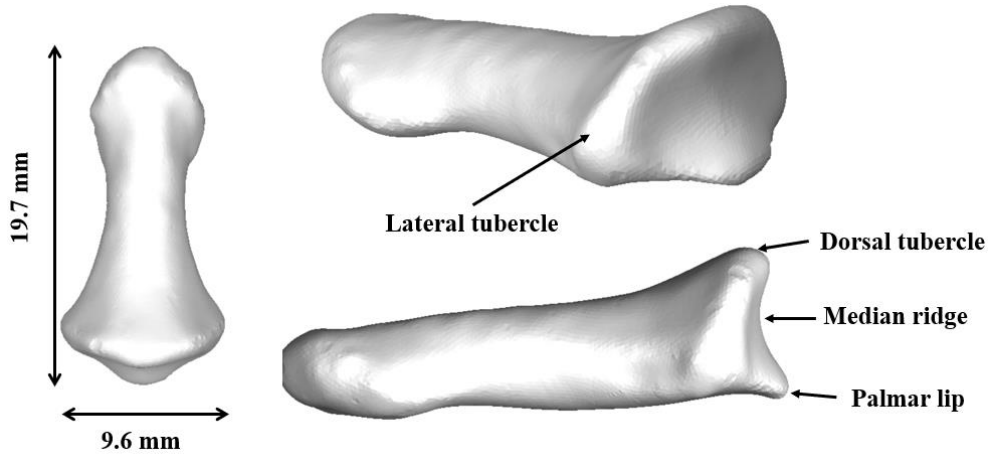

Figure 3.3. Geometry and anatomical landmarks of the distal phalanx

3.2 Modelling the PIP Joint

3.2.1 Modelling the Articulation

The articulation of the phalanges on each other is modeled using the rigid 3D contact in MSC ADAMS (a commercial multibody dynamics software), which is essentially a nonlinear spring. Figure 3.4 presents a summary of its algorithm.

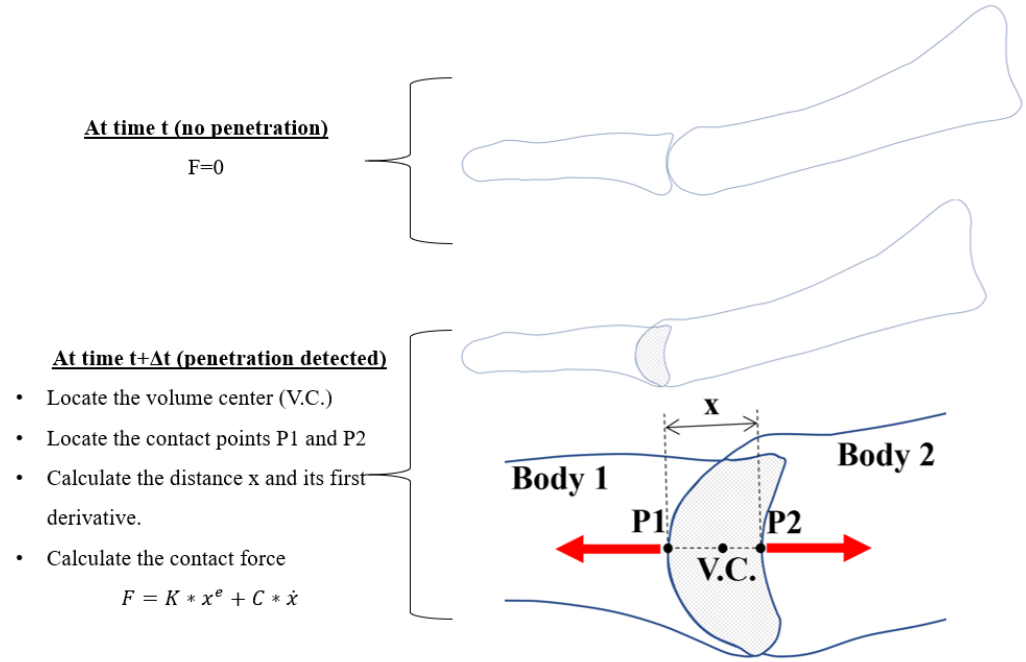

Figure 3.4. Algorithm of the rigid body contact method in MSC ADAMS

The contact force is defined between two geometries. In every time step, ADAMS calculates the penetrating volume (gray region in Figure 3.4) and determines the geometric center (V.C. in Figure 3.4) if it detects any penetration between the bodies.

The closest points on the surface to the volume center (P1 and P2 in Figure 3.4) are identified for each body. The contact force act on body 1 at P1 and body 2 at P2 along the line connecting these points. The magnitude of the force is calculated as:

$$F = K * x^e + C * \dot{x} \qquad \text{(Equation 9)}$$

In equation 9, K is the stiffness coefficient, x is the distance between P1 and P2, e is the force exponent, and C is the damping coefficient. Contact force behaves as a softening spring for e<1, as a linear spring for e=1, and as a stiffening spring for e>1. The parameters K, e, and C are taken as 1000 N/mm, 1, and 1 N.s/mm, respectively.

In reality, articular cartilage shows nonlinear, viscoelastic, and anisotropic behavior. It releases synovial fluid in response to pressure to decrease friction. Although articulation is very complicated, the rigid body contact method is sufficient for this study. The dynamics of the contact is not a concern since it is aimed to model the

quasi-static behavior. Furthermore, the deformations at the cartilage are negligibly small compared to the rigid body displacements. It does not matter if the deformation is calculated accurately provided that it is very small. An accurate determination of the parameters K, e, and C are also not crucial for the same reasons. Choosing a too high value for K resulted in high-frequency oscillations, which forced the ADAMS solver to take smaller time steps. That increased the run time and caused noise in the results. K is chosen by trial and error to keep contact deformation below 0.1 mm without compromising the run times. C value is chosen to damp out oscillations.

3.2.2 Modelling the PCL

To the best knowledge of the author, there is not a single definitive anatomical description of the collateral ligaments (PCL) in the literature. While some investigators define it as a thin oblique band, others as a broad structure parallel to the middle phalanx at all angles. Three different descriptions by Kuczynski [5], Bowers [41] , and Allison [42] are prominent in the literature.

Kuczynski [5] defines a concave area on the lateral surface of the proximal phalanx located eccentrically to the joint center. The proper collateral ligament originates from the concave area. Insertion is at the lower part of the lateral tubercles found at the base of the middle phalanx. Some of the fibers pass on to the small tubercles found on both sides of the middle phalanx's palmar surface and merge with the palmar plate's insertion. He depicts the proper collateral ligament as an insubstantial structure compared to the accessory collateral ligaments (ACL).

Bowers [41] also locates the origin of the proper collateral ligament at the concavity of the proximal phalanx. The distal attachment is broader than Kuczynski's description and takes the lower third of the lateral tubercle. He also observes the merging of the collateral ligament and palmar plate insertions. At the palmar side of the lateral tubercles, the fibers of the collateral ligament and the palmar plate merge. He names this region as “*the critical corner*”.

Allison [42] describes a much broader PCL. It is parallel to the middle phalanx's long axis on the dorsal aspect and becomes more oblique on the palmar part. The origin is crescent-shaped and extends dorsally and proximally to the concave area. The attachment covers most of the middle phalanx's lateral surface, not just the lower third of the lateral tubercle. He observed no merging of the fibers at the critical corner, although he acknowledged that they are very close and reported a bare area devoid of fibers. Figure 3.5 shows PCL as described by Kuczynski, Bowers, and Allison's papers.

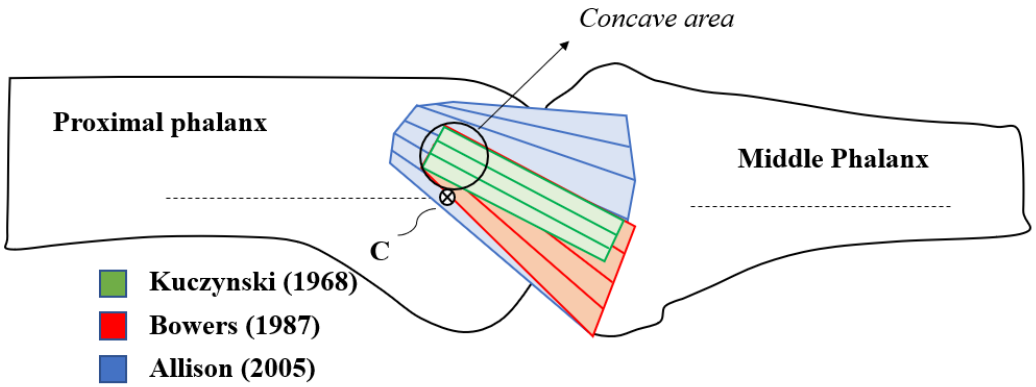

Figure 3.5. Different descriptions of the PCL

The PCL is an essential stabilizer of the PIP joint. An accurate model of it requires an accurate description. A simple 2D geometrical model of the PIP joint is used to evaluate the PCL's different descriptions in terms of stability and select one of them as the basis for modeling (Figure 3.6). The middle phalanx is connected to the proximal phalanx with a hinge joint. Its center "C" is coincident with the condyle's center of curvature. A hypothetical collateral ligament fiber, which has an origin at O and insertion at "I" is considered.

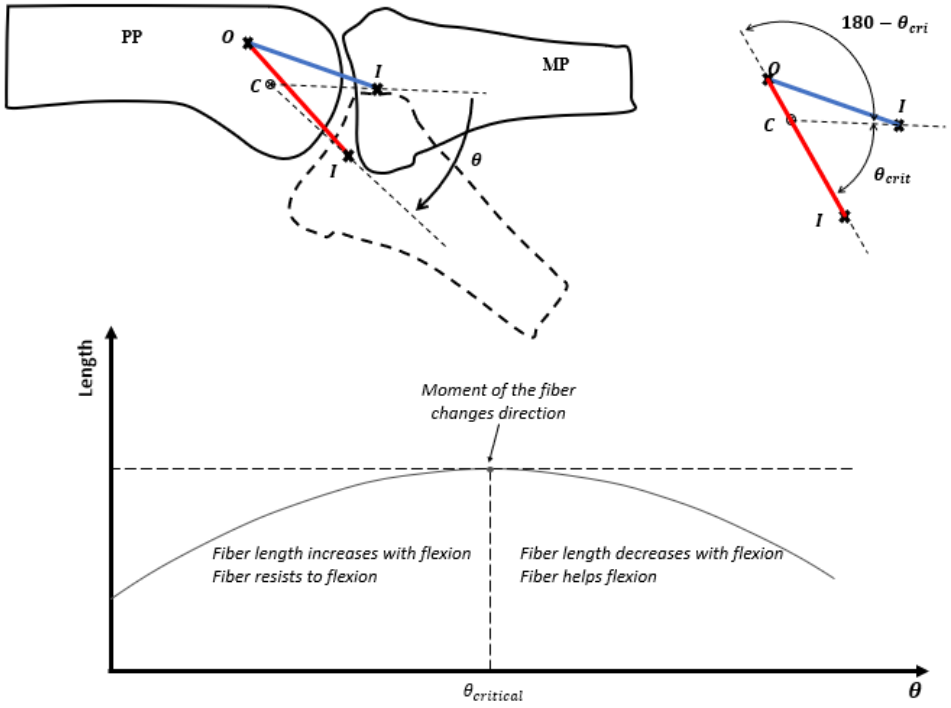

Figure 3.6. 2D graphical model of the PIP joint

Now let us investigate the length change of the fiber with the flexion angle (θ). As θ increases, the point "I" will move with the middle phalanx while origin "O" is stationary. The fiber will elongate with flexion until the critical angle, (θ_{crit}), is reached. It is defined as the angle at which the "OI" line coincides with the joint center, "C". The fiber will reach its maximum length at this angle, and the tensile force in the fiber will start to decrease beyond this angle. A more important consequence is that the moment created by the tensile forces change direction at this angle. While the fiber resists flexion before the critical angle, it will help flexion beyond the critical angle, thus contributing to instability. Based on this simple model, the critical angle is calculated geometrically as the supplementary angle of the angle $\widehat{OCI}$.

$$\theta_{crit} = 180 - \widehat{OCI} \qquad \text{(Equation 10)}$$

More dorsally located fibers will have a higher critical angle. There are no significant passive structures dorsal to the collateral ligament. Suppose the flexion angle reaches beyond the critical angle of the most dorsal fiber of the PCL. In that case, it will not be possible for the joint to return to its resting position without the help of the extensor tendon or an external force. In other words, the joint will be locked in flexion beyond the critical angle. Since such behavior is not observed in the normal physiological function of the PIP joint, it can be concluded that the critical angle must be very close to the endpoint of the joint's range of motion if not out of the range.

This model can be used to compare the three descriptions. According to the sketch given in Figure 3.5, Kuczynski's and Bower's models have a critical angle at about 80 degrees, and Allison's model has a critical angle at about 120 degrees. For sure, these estimates are quite rough; however, it is evident that the collateral ligaments will continue to resist flexion for a larger portion of the joint's range of motion in Allison's description. For this reason, the PCL model presented in this study is based on his studies. PCL is divided into three segments, namely dorsal, central, and palmar (Figure 3.7). Every segment is modeled as a force between 2 points as non-linear spring elements. Strain versus stress data is provided to MSC ADAMS as a table of values and stress is converted to force. Section 3.6 explains the material model and the choice of the required parameters in detail. A small amount of damping is also added to every segment for a smoother simulation.

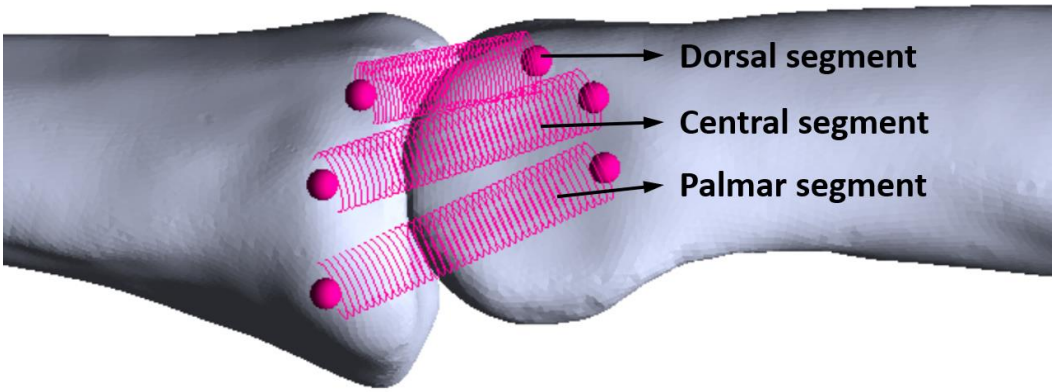

Figure 3.7. PCL segments

3.2.3 Modeling the Palmar Plate

The palmar plate consists of a distal fibrous part and a proximal membranous part. Distally it attaches to the bone firmly only at the lateral sides. The central portion attaches loosely by blending into the periosteum [43]–[46]. Bowers et al. [44] report that the central attachment takes about 80% of the total attachment surface. The palmar plate becomes thinner in the distal attachment region; therefore, it can easily bend like a hinge joint with the PIP joint flexion. Proximally the soft membranous palmar plate attaches to the diaphysis of the proximal phalanx via check rein ligaments (CR). The check reins blend into the periosteum just inside of the proximal margin of the A2 pulley [44], [46].

It is thought that the function of the palmar plate is to resist hyperextension of the PIP joint; however, it also provides a gliding surface for the flexor tendons. Saito and Suzuki [47] investigated the palmar plate's motion during flexion using ultrasonography. As the flexion angle reaches 30 degrees, the flexor tendons tighten and push against the A3 pulley, which causes the palmar plate to elevate. This elevation is not observed in pathological cases and is believed to be crucial for smooth operation.

If only the extension resisting function of the palmar plate were to be modeled, a nonlinear spring connecting the proximal phalanx to the middle phalanx would suffice. The relation between the flexor tendon excursion and the flexion angle is dependent on the elevation of the palmar plate. Therefore, in this study, the palmar plate's distal fibrous part is modeled as a rigid plate. Rigid body assumption is plausible since the palmar plate is made of fibrocartilage and quite thick. The deformation of the palmar plate is negligible compared to the surrounding ligaments and the rigid body displacements. Figure 3.8 shows the geometric modeling of the palmar plate. Its dimensions are based on the anatomical descriptions and the experimental measurements given by Kömürcü et al. [48] and Schreiber et al. [49].

The distal attachment is modeled with a revolute joint that connects the palmar plate to the middle phalanx. Its axis of rotation coincides with the lateral axis. Rigid contact is defined between the palmar plate and the proximal phalanx to prevent penetration. Proximal attachment is through the check rein ligaments, which are modeled as nonlinear springs (Figure 3.8). The material model and the related parameters are explained in Section 3.6.

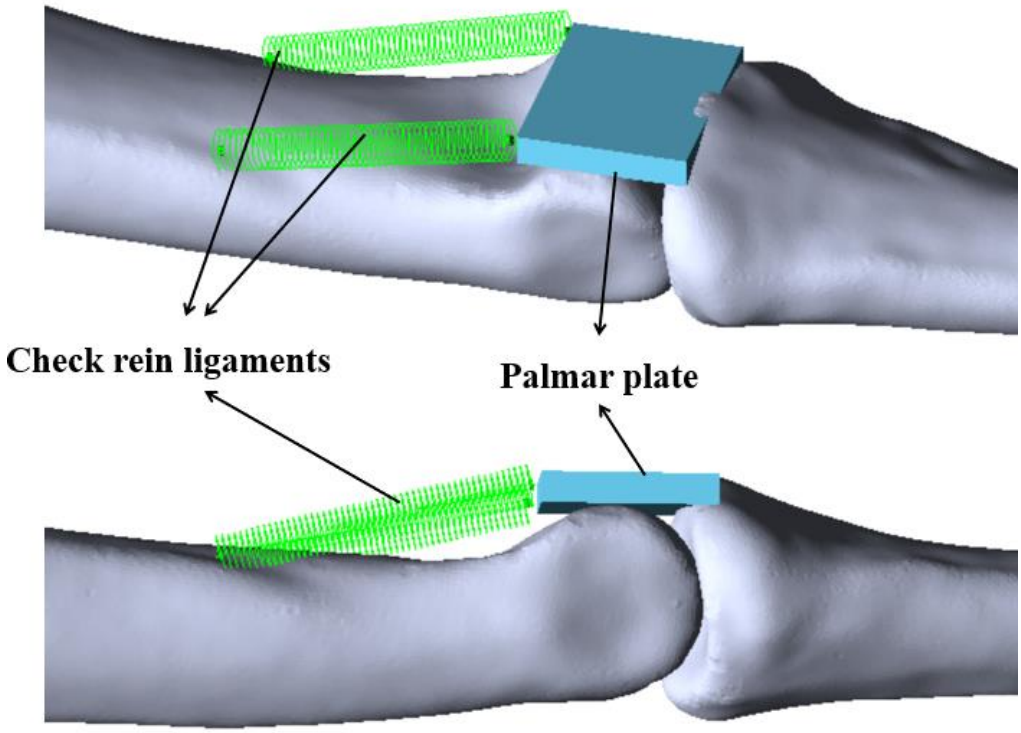

Figure 3.8. Palmar plate model

3.2.4 Modelling the ACL

The anatomy of the ACL is controversial in the literature. It is not easy to distinguish it from the PCL. Generally, it is believed to be a suspender of the palmar plate and a lateral stabilizer of the PIP joint to a lesser extent. It originates from the PCL's palmar side and inserts to the palmar lateral tubercles of the proximal phalanx and dorsolateral margin of the palmar plate. Its orientation changes from dorsal-palmar

to oblique [41], [42], [44]–[46], [50]. Recent studies show it as an insubstantial, thin structure compared to PCL [42].

In this study, ACL is represented with two segments, a dorsal segment, and a palmar segment, respectively (Figure 3.9). Both originate palmar to the PCL's origin. The dorsal segment inserts to the palmar lateral tubercle of the middle phalanx, and the palmar segment inserts to the midline of the palmar plates lateral margin. They are modeled with nonlinear springs. After a few trial analyses, it is seen that resulting elongations of the palmar segment were very large, more than 100% to which no ligament reported in the literature reaches. Therefore, this type of modeling is abandoned for the palmar segment. However, its function of suspending the palmar plate still needed to be modeled, since otherwise, the palmar plate oscillated wildly and this significantly increased the simulation time. A small constant force of 0.1 N is applied normal to the palmar plate to press it against the proximal phalanx, as shown in Figure 3.9. Effect of this force is insignificant to cause noticeable changes in the force requirements and reaction forces, yet enough to prevent the palmar plate moving freely.

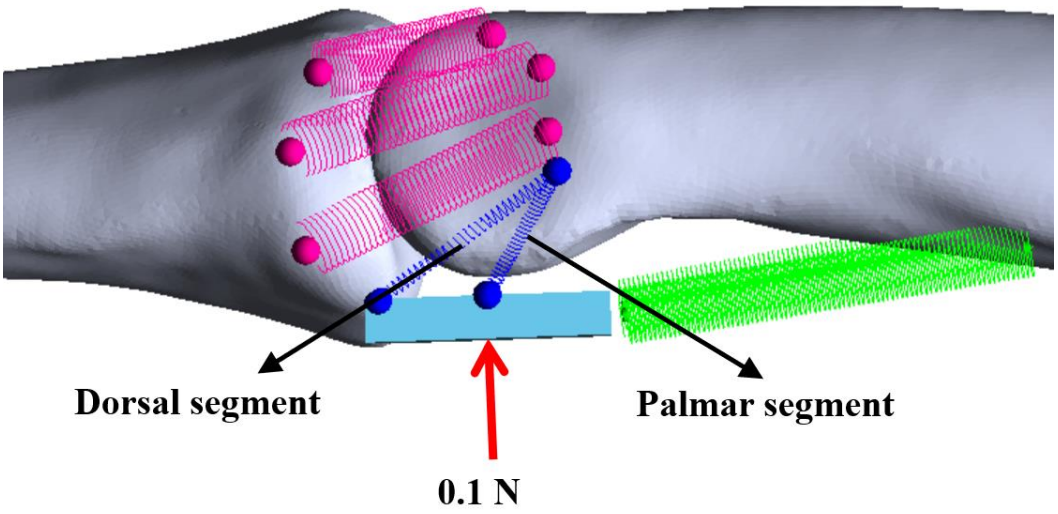

Figure 3.9. ACL model

3.3 Modelling the DIP Joint

The distal interphalangeal (DIP) joint is modeled the same as the PIP joint (Figure 3.10). The choice of parameters for the ligament segments are explained in Section 3.6.

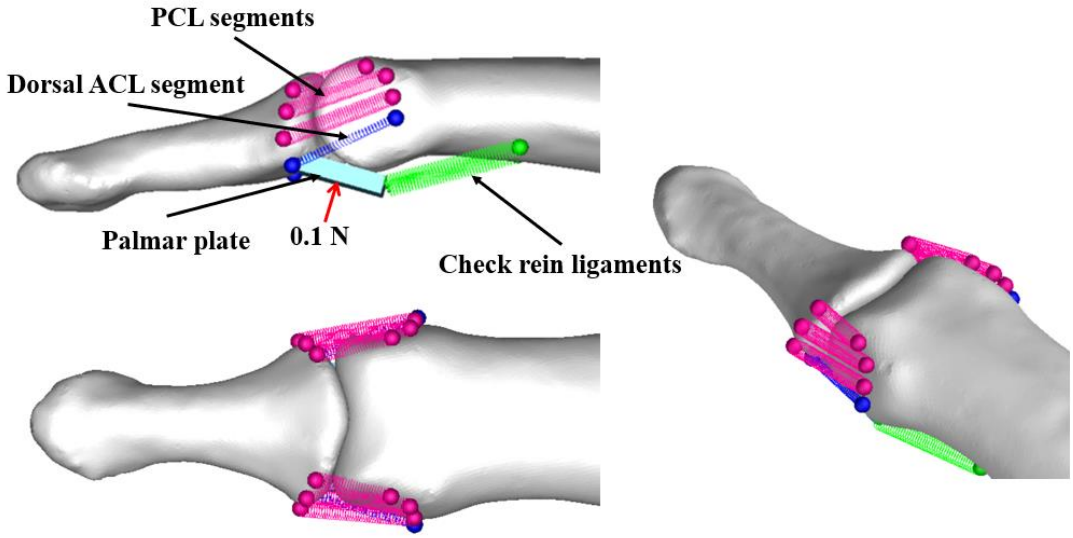

Figure 3.10. DIP joint model

3.4 Modelling the Oblique Retinacular Ligament

Landsmeer, in 1949 [51], first coined the term oblique retinacular ligament (ORL) in his work "the anatomy of the dorsal aponeurosis of the human finger and its functional significance", which he believes coordinates the interdependent motion of the interphalangeal joints. The ORL originates from the proximal phalanx at the level of the A2 pulley, passes obliquely palmar to the PIP joint, and inserts to the most lateral sides of the terminal tendon (Figure 3.11). Length of the ORL decreases with PIP joint flexion and increases with extension. Conversely, elongate and shorten with DIP joint flexion and extension, respectively.

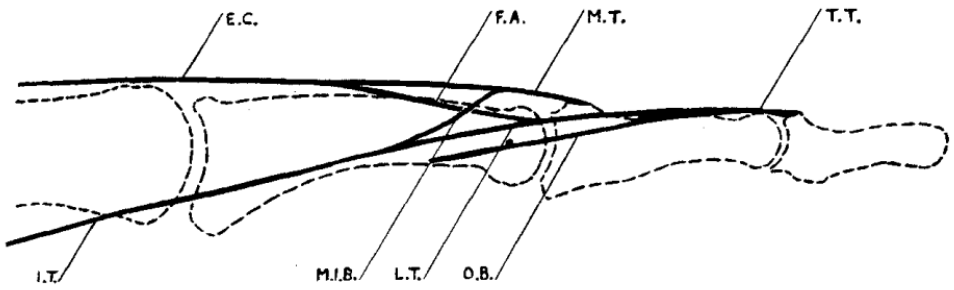

Figure 3.11. Landsmeer's ORL definition [51]
(O.B. is short for oblique band which is another name given to the ORL by Landsmeer. T.T. is terminal tendon, L.T. is lateral tendon)

According to Landsmeer, as the DIP flexes, the ORL tightens and transfers some of the flexion force to the PIP joint. Passive or voluntary flexion of the DIP joint will result in the PIP joint flexion. However, a passive or an active flexion of the PIP joint by the flexor digitorum superficialis does not necessarily mean flexion of the DIP joint.

Another conclusion is made regarding the active extension of the PIP joint, followed by an obligatory extension of the DIP joint. Contrary to the common misconception, Landsmeer never wrote that this depends solely on the ORL tightening. The active full extension of the PIP joint is only possible by tightening the central tendon of the extensor communis muscle, which is difficult without tensioning the lateral tendons, thus extending the DIP joint. The PIP joint extension will result in the tightening of the ORL and further help with the DIP joint extension. A passive extension of the DIP joint does not necessarily mean the extension of the PIP joint.

Since Landsmeer's first paper in 1949 [51], a controversy regarding the anatomy and function of the ORL ligament continues up today. Different papers with contradictory results are published, and a complete picture is yet to be found. Haines [52], in 1952, independently recognized the same structure. He attributed the same function to it, which is apparent from the name "link ligament" he gives. He reported that when the PIP is held in extension, the DIP joint did not extend more than 45

degrees in most subjects and up to 60 degrees in some. Stack [53] also reported that the ORL tightened at approximately 45 degrees when the PIP joint is fully extended.

Harris and Rutledge [54] worked on a fresh finger and stated that ORL is a tiny structure " if it is to be found at all". When the PIP joint is held in full extension, the ligament did not tighten until 70 degrees of DIP flexion and did not tighten when the PIP joint flexed more than 30 degrees. They observed no marked change in interphalangeal coordination upon incision of the ORL. They concluded that the ORL is not involved in the interphalangeal joint coordination and helps centralize the lateral tendons over the middle phalanx.

Shrewsbury and Johnson [55] dissected fourteen preserved and two fresh hands. They could identify a complete form of the ORL in 40-50% of the specimens, except in the ring finger's ulnar side with a frequency of 90%. They reported that the ORL tightened in the first half of the DIP flexion range independent of the PIP joint angle. They agreed with Harris and Rutledge [54] on its function.

El-Gammal et al. [56] studied the ORL in twenty fresh frozen index finger specimens for developing a mathematical model. They found the ORL in 95% and 90% of the specimens on the radial and ulnar sides, respectively. The ORL tightened when the DIP joint flexed more than 60 degrees. They refuted the ORL's coordination function and proposed that the ORL acted as a lateral stabilizer of the PIP joint during hook grip.

Some of the important studies about the ongoing controversy are mentioned above. Most of these studies do not have well-controlled and well-defined experimental procedures, at least as they are presented. Instead of statistically evaluated, quantitative results, approximate anecdotal evidence are given. Ueaba et al. [57], in 2011, filled this gap in the literature. They tested 40 fresh frozen fingers on a custom-designed jig. All the extrinsic and intrinsic muscles are sectioned, and only the extensor digitorum communis is loaded with 200 g (about 2 N). DIP joint flexed through an eye screw inserted to the palmar surface of the DP, and the force is measured with a force transducer. For each measurement, the DIP joint is cycled

through 0-45 degrees 18 times to allow the joint to precondition, and the last six measurements are taken. The maximum force required to flex the DIP joint, for different combinations of MCP (0, 45, 90) and PIP (0, 30, 60, 90) joints with both ORL and the central slip intact, only the ORL incised, both the central slip and the ORL incised are collected. They reported that the MCP joint has no statistically significant effect on DIP flexion. The ORL contributed 25% to the flexion force when the PIP is at 0 degrees, 31% at 30 degrees, 18% at 60 degrees, and 3% at 90 degrees. The incision of the central slip did not affect the results significantly except for 90 degrees PIP flexion.

To the author's knowledge, there is no mathematical model of the ORL. Including this structure may provide additional insight to the ongoing controversy. Apart from that, the addition of the ORL to the finger model was a necessity. The behavior of the interphalangeal joints was unacceptably abnormal before the inclusion of the ORL. Upon the excursion of the FDP, DIP joint fully flexed much before the PIP joint flexed even a few degrees. To limit the DIP joint's excessive flexion, the best candidate in the literature was the ORL structure.

The ORL is modeled with 1D nonlinear force elements in the manner the other ligamentous structures are modeled. The ORL's path on the ulnar side of the finger is represented with spheres in Figure 3.12. Sphere 1 is on the distal phalanx, 10 is on the proximal phalanx, and the others are fixed on the middle phalanx. Any palmar or dorsal shift of the ORL is neglected. The force definition is made between the points 2-3 and 9-10. The ORL length is calculated as the total distance between the spheres, and the magnitude of the force is calculated as a nonlinear function of this length. Details are explained in Section 3.6.

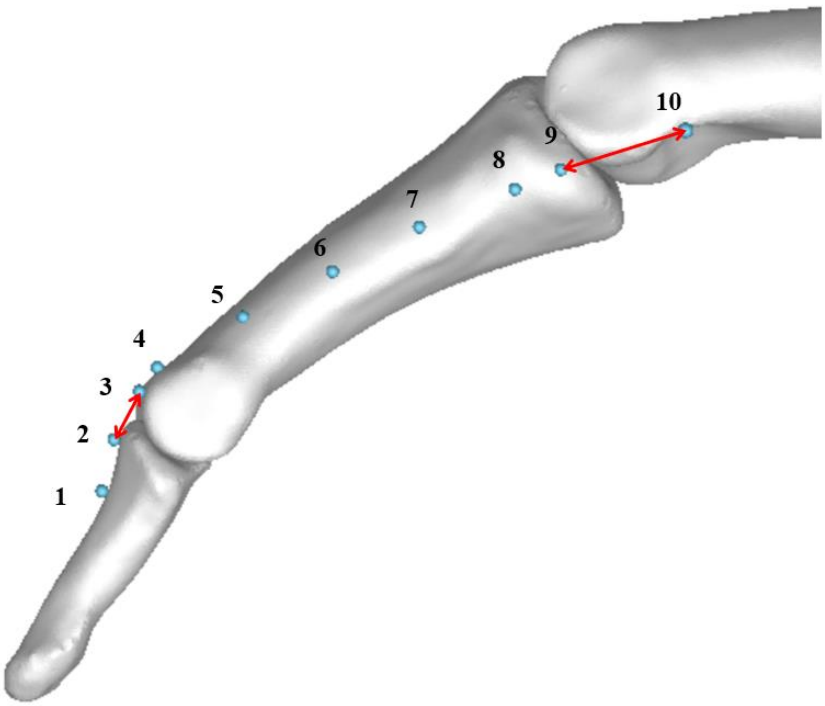

Figure 3.12. ORL model

3.5 Modelling the FDP Tendon and Annular Pulleys

The control point (CP) method mentioned in Section 2.3 is used for the modeling of the FDP tendon. The control points are placed to best represent the anatomical position of the FDP. They are presented in Figure 3.13, along with the flexor sheaths (or pulleys). The flexor sheaths are just for visual purposes and do not affect the behavior of the model. CP 1 is on the distal phalanx, CP 2 and 3 are on the A5 pulley which is fixed to the palmar plate. CP 4 to 7 represent the path of the FDP on the middle phalanx and through the A4 pulley. CP 8 and 9 are on the A3 pulley, which is fixed to the PIP palmar plate. CP 10 is on the proximal phalanx. Finally, CP 11 is on a separate body named "profundus". This body can slide with respect to the proximal phalanx in the direction shown. Tendon is assumed to be composed of line segments connecting the control points. The translational motion of the profundus body corresponds to the excursion of the FDP.

1D forces are defined between points 1-2, 3-4, 7-8, 9-10, and 10-11 to represent the tendon forces acting on the bodies. $l_{1-2}, l_{2-3}, \dots l_{10-11}$ corresponds to the distances between the control points. l_{1-2} and l_{3-4} will change with DIP flexion, l_{7-8} and l_{9-10} will change with PIP flexion and l_{10-11} will change with the excursion. l_{prof} is the summation of these distances and represents the length of the tendon. The elastic tendon force is a function of the change of Δl_{prof} . See Section 3.6 for the parameters of the tendon force formulation.

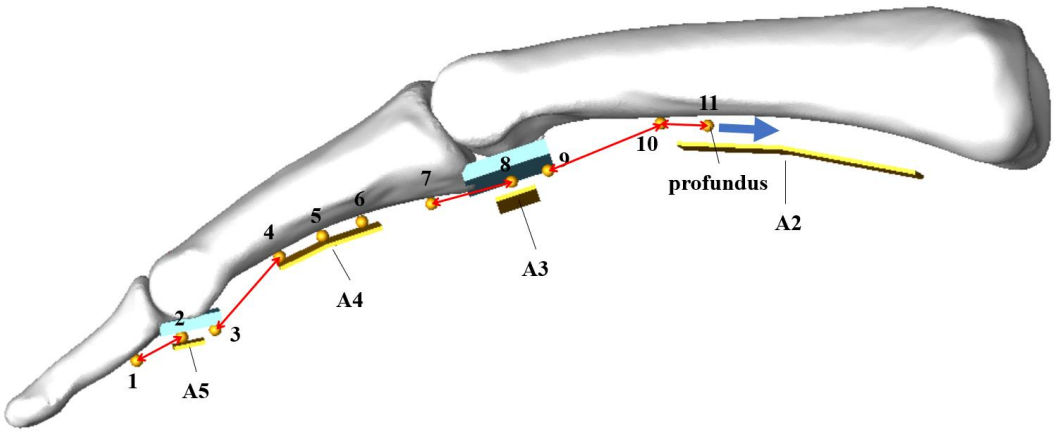

Figure 3.13. FDP tendon model

3.6 Material Models of the Ligaments

Ligaments and tendons are usually modeled as linear springs in the musculoskeletal models found in the literature. This approach is plausible for tendons since they are less extensible compared to ligaments. They transfer the force or the displacement inputs coming from the muscles to the joint. Little deformation that might occur along their length is negligible compared to the joint's displacements. In fact, it is entirely plausible to model them as inextensible cables. However, for the ligaments, a linear elastic model would vastly overestimate the tension. Figure 3.14 shows the elastic behavior of a hypothetical ligament, which reaches its final tangent modulus value of 100 MPa at 10% strain. It is modeled both nonlinearly and linearly with the

same tangent modulus. At 5 % strain, the linear model estimates the stress 5.7 times and 10% strain 2.1 times larger than the nonlinear model.

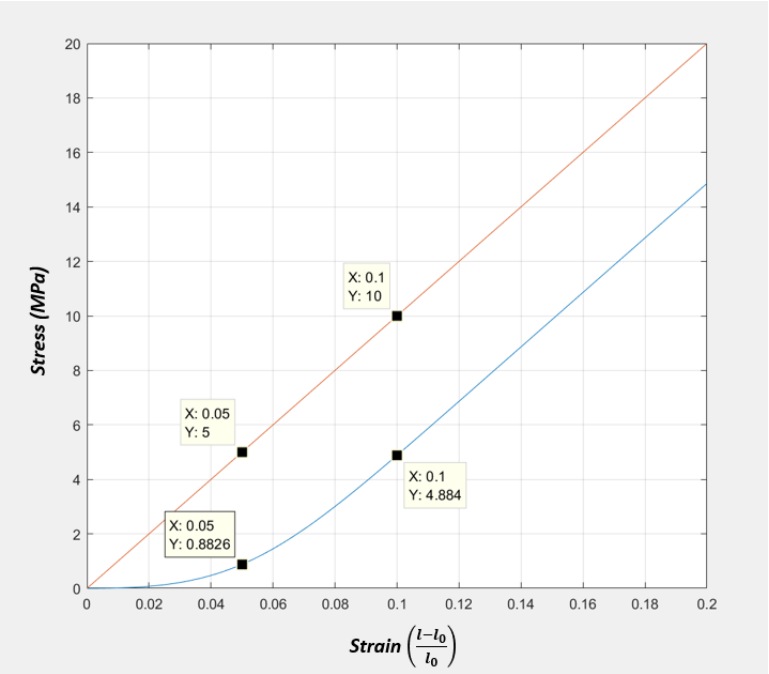

Figure 3.14. Nonlinear modelling vs linear modelling

Ligaments need to be less stiff at some part of the joint's range of motion to allow smooth operation and be stiff at other parts to restrain excessive motion. Assigning them a single stiffness value would either make the joint too stiff or unstable. Therefore, in this study a nonlinear elastic model is used. A method for the estimation of the material parameters is also proposed.

3.6.1 Decraemer et al.'s Model

A ligament bundle consists of many fibers that have different initial lengths. Under light microscopy, these length differences are observed as differences in crimp frequency. The ligament's tangent modulus increases as more and more fibers are recruited and eventually reach a stable value when all the fibers become taut. Decraemer, Maes and Vanhuyse [58] proposed a structural model that takes this

"*gradual fiber recruitment*" into account. This material model is adopted in this study because its parameters have direct physical interpretation (Figure 3.15).

The original model is modified. The derivation of the stress-strain relationship is slightly different from the original study. Furthermore, although the number of parameters remained the same, they are chosen such that they have different physical meanings.

It is considered that the ligament has a large number of fibers with different initial lengths, l_i. l_i is normally distributed around a mean length μ with a standard deviation σ (Figure 3.15). l_0 is the total ligament's free length. All fibers have the same cross-sectional area and are perfectly linear with the same elastic modulus. When the ligament extends up to a length l, fibers with $l > l_i$ will be stretched. The number of those fibers is directly proportional to the tangent modulus of the total ligament, which can be expressed as follows:

$$E \propto \int_{l_0}^{l} p(l)\, dl \qquad \text{(Equation 11)}$$

In equation 11, $p(l)$ is the normal distribution function. At this point it will be more convenient to change the variable from length, l to strain, $\varepsilon = {(l - l_0)}/{l_0}$. After expanding the normal distribution function, the tangent modulus E is written as follows:

$$E(\varepsilon) = E_\infty K \int_0^{\varepsilon} \frac{1}{\sigma\sqrt{2\pi}} e^{-\frac{1}{2}\left(\frac{\varepsilon-\mu}{\sigma}\right)^2} d\varepsilon \qquad \text{(Equation 12)}$$

Here E_∞ is the tangent modulus at infinity, and K is a constant such that the tangent modulus approaches to E_∞ when $\varepsilon \to \infty$. Then K is calculated as follows:

$$K = \frac{1}{\int_0^{\infty} \frac{1}{\sigma\sqrt{2\pi}} e^{-\frac{1}{2}\left(\frac{\varepsilon-\mu}{\sigma}\right)^2} d\varepsilon} \qquad \text{(Equation 13)}$$

To reduce the number of parameters, a new parameter linearity strain, ε^* (Figure 3.12) is defined and it is assumed that it has the following relation with the standard deviation, σ and the mean value, μ:

$$\varepsilon^* = 4\sigma, \varepsilon^* = 2\mu \qquad \text{(Equation 14)}$$

According to this assumption, when $\varepsilon = \varepsilon^*$ elastic modulus reaches 97.6% of its final value. Putting together equations 12, 13 and 14 together $E(\varepsilon)$ can be expressed as:

$$E(\varepsilon) = E_{\infty} \times \frac{\int_0^{\varepsilon} e^{-2\left(\frac{2\varepsilon-\varepsilon^*}{\varepsilon^*}\right)^2} d\varepsilon}{\int_0^{\infty} e^{-2\left(\frac{2\varepsilon-\varepsilon^*}{\varepsilon^*}\right)^2} d\varepsilon} \qquad \text{(Equation 15)}$$

E is by definition first derivative of the stress, $\sigma(\varepsilon)$ with respect to strain.

$$\sigma(\varepsilon) = \int_0^{\varepsilon} E(\varepsilon) d\varepsilon \,, \sigma = 0 \; when \; \varepsilon = 0 \qquad \text{(Equation 16)}$$

Equations 15 and 16 yields the stress strain behavior with 2 parameters, tangent modulus in the linear region E_{∞} and the linearity strain ε^*. Both have direct physical meaning and can quickly be identified from a given stress-strain curve. Figure 3.15 presents an example.

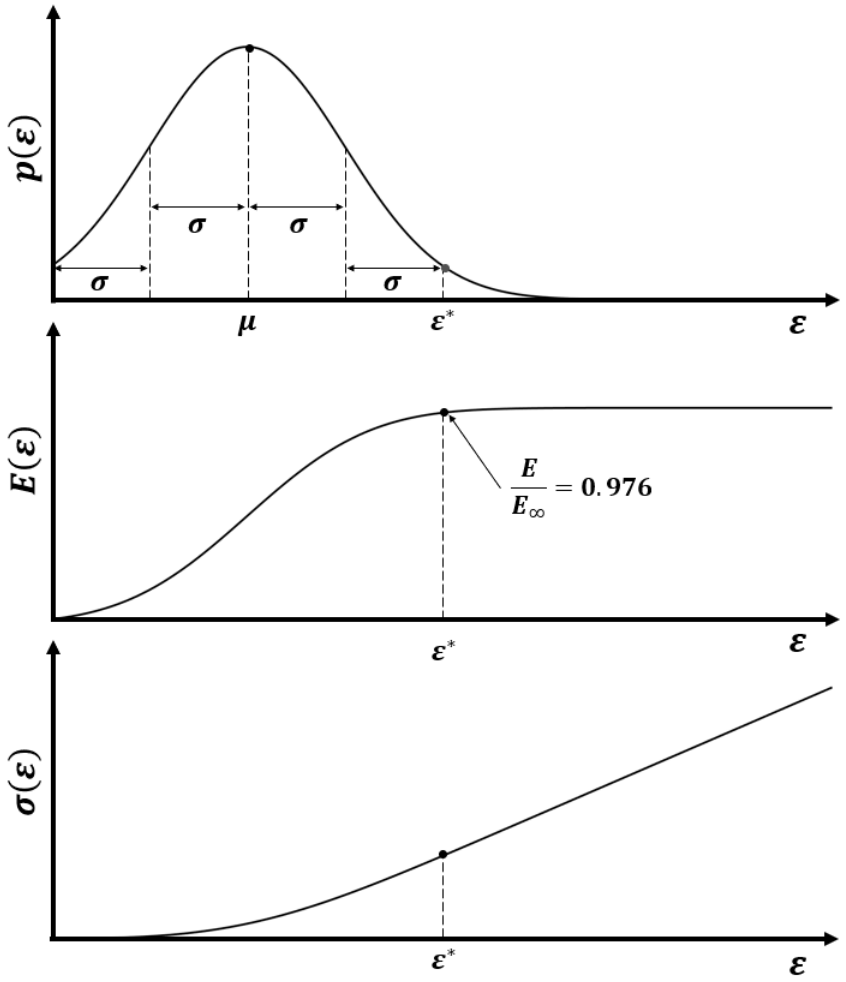

Figure 3.15. Modified version of Decraemer et al.'s 1D model

Equations 15 and 16 cannot be solved analytically; since they include the error function. Instead, they must be tabulated for a suitable range of ε, and since the integrals of Equations 15 and 16 contain ε^* values, these tables must be separately generated for every ligament segment. Then during the numerical analysis, the stress on a ligament can be determined from the tables. Constructing a different table for every ligament segment is quite cumbersome. A further change of variable from ε to $t = {\varepsilon}/{\varepsilon^*}$ can reduce the number of required tables to one. Then the stress (σ) becomes:

$$\sigma[t(\varepsilon)] = E_\infty \varepsilon^* \frac{1}{\int_0^\infty e^{-2(2t-1)^2} dt} \int_0^t \left[\int_0^t e^{-2(2t-1)^2} dt \right] dt \qquad \text{(Equation 17)}$$

$$\sigma[t(\varepsilon)] = E_\infty \varepsilon^* \bar{\sigma}(t) \qquad \text{(Equation 18)}$$

In equation 18, $\bar{\sigma}(t)$ is tabulated for the range 0-2, which covers the range from 0 strain to double the amount of the linearity strain. Although each ligament will have a different t value, their relation to $\bar{\sigma}(t)$ will be the same. For modeling different ligaments, it is enough to change E_∞ and ε^* values using a single table.

The stress expression given in Equation 18 must be must be multiplied with width, w_i and thickness, t_i of each ligament to obtain the force. Then the force in ith ligament becomes:

$$F_i \left[\mathrm{t_i} = {}^{\varepsilon_\mathrm{i}}/_{\varepsilon_\mathrm{i}^*} \right] = E_{\infty,i} \cdot w_i \cdot t_i \cdot \varepsilon_\mathrm{i}^* \cdot \bar{\sigma} \qquad \text{(Equation 19)}$$

3.6.2 Determination of the parameters for the ligaments

ε^* and E_∞ values will vary depending on many factors. They will be different for every ligament, every individual, and even be different for a single individual at different times. Linearity limit ε^* can be thought of as a switch that determines when the ligament will be active or not. The ligament will respond weakly to displacement inputs for strains far lower than this value, while at strains close to this value, it will respond strongly. E_∞ value will determine the strength of the response. In other words, the shape of any curve related to the joint's kinematics will largely depend on the ε^* and the E_∞ value will act as a scaling factor.

Another critical parameter is the load free length (l_0) of the ligament. It is especially hard to determine since the slopes are too small at the beginning of the toe region, and it is hard to identify the zero-stress state. It is a challenging task to determine these parameters. No emphasis is given on the determination of them throughout the

literature. Usually, values obtained from other experimental studies are used. It is often impossible to find the parameters for the studied ligament, and the data for other ligaments are utilized, causing erroneous results since ligaments are highly specialized tissues. For instance, ε^* is at about 13% strain and 45% strain for the UCL (ulnar collateral ligament) of the thumb's MCP joint [16] and ligamentum flavum of the vertebral joint [59], respectively. If the parameters for the ligamentum flavum were used for a model of the MCP joint, the thumb would be unstable. Conversely, if the vertebral joint were modeled using the UCL data, it would behave much stiffer compared to the actual behavior. Clearly, ligaments adapt to the displacement and stability requirements of their joints.

Ligaments also change their properties in response to immobilization and exercise [60]–[65]. Noyes et al. [60] investigated the effects of immobilization and exercise on rhesus monkeys' anterior cruciate ligaments. After 8 weeks of immobilization, they observed 39% decrease in maximum load to failure and 32% decrease in energy absorbed. Strains at linearity (same as ε^*) were 33.00 ± 9.86 % and 39.24 ± 8.52% for the immobilized and control groups respectively. Another group is first immobilized and later reconditioned by allowing normal activity to see the effect of exercise. Strain at linearity did not return to normal levels but got closer to the control group (36.21 ± 9.91%). They also observed a decrease in stiffness in the immobilized group, the reconditioning group had slightly lower stiffness compared to the control. There is a positive or negative change in the ligament's properties depending on the strains they are exposed to. Consequently, there must be a point where the adaptation speed is zero which is commonly called "the mechanostat theory". Some amount of strain is needed to be maintained for the anabolic and catabolic activities to balance.

When no force is exerted on the PIP joint, it has a resting position at about 30 degrees [66]. If the ligaments' adaptation continued significantly at this angle, it would not be possible to have a stable resting position since the ligaments' force equilibrium would change constantly. So, it is thought that the mechanostat strain of the PIP joint ligaments should be close to the strains at the resting angle. Wren et al. [67] proposed

an adaptation model for ligaments and tendons that tries to maintain strain levels between 1.5 and 3% and they used these limits unchangingly for any ligament or tendon believing that this interval corresponds to physiological strain values. Here it is assumed that the mechanostat strain should be in proportion to the maximum strain capacity of a ligament and it is taken as one-fourth of the linearity limit, ε^*. Also, the mechanostat strain should be close to the strains at the resting position of the joint, ε_{rest} (Equation 20).

Finally, it is known that the ligaments operate in mostly toe region and at the beginning of the linear region. If the strain increases more, the ligament will rupture. Therefore, the maximum strain induced on a specific ligament belonging to a certain joint should not be exceeding the linearity limit ε^* too much. It is assumed that the maximum strain of a ligament is $5\varepsilon^*/4$.

Two assumptions made above about ε^* can be summarized as:

$$\varepsilon_{rest} = \frac{l_{rest} - l_0}{l_0} = \frac{\varepsilon^*}{4} \qquad \text{(Equation 20)}$$

$$\varepsilon_{max} = \frac{l_{max} - l_0}{l_0} = \frac{5\varepsilon^*}{4} \qquad \text{(Equation 21)}$$

Then it is possible to estimate $\varepsilon^*$and l_0 for every ligament of the PIP joint provided that the length at resting, l_{rest} and maximum length, l_{max} are given:

$$\varepsilon^* = \frac{4(l_{max} - l_{rest})}{5l_{rest} - l_{max}} \qquad \text{(Equation 22)}$$

$From\ equations\ (3) and\ (4) \rightarrow$

$$l_0 = \frac{4l_{rest}}{\varepsilon^* + 4} \qquad \text{(Equation 23)}$$

Equations 22 and 23 provide a systematic method for approximating ε^* and l_0 given that the rest length and the maximum length of the ligament are known. An iterative process can refine these approximations (See Figure 3.16). The proposed approximation method is not validated by any experimental results. However, it ensures that the ligaments operate in the toe region and a small portion of the linear region during normal anatomical motion.

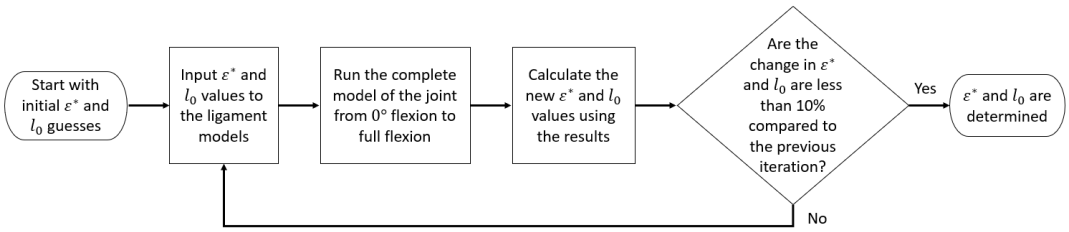

Figure 3.16. Approximation of ε^* and l_0

E_∞ is reported varyingly starting from a few MPa to 1 GPa (See Table 2.1). No paper that is directly reporting the collateral ligament tangent modulus is found in the literature. In one study, thumb MCP joint UCL is reported as 33 MPa [16]. Since it is similar to the PIP joint, it can at least be said that the order of magnitude should be the same. Endress et al. [68] studied the PIP joint collateral ligaments to be used as an allograft for scapholunate ligament reconstruction, however they did not directly report the tangent modulus values. They reported the width of the collateral ligaments as 6.8 ± 2.9 mm, thickness as 3.1 ± 0.4 mm and free length as 15.8 ± 2.5 mm. Instead of tangent modulus, stiffness (defined as the slope in the linear region in the study) is provided as 44 ± 9 N/mm. Using the stiffness value and the geometric properties, tangent modulus is estimated as 33 ± 6.8 MPa. This value is used for all the ligament segments in this study except for the ORL.

For the PIP joint PCL segments, the thickness is taken as the value reported in Endress et al.'s study (3.1 ± 0.4mm). The same value is used in the DIP joint PCL segments by scaling according to the condyle radius. Width is a geometric parameter

and readily available in the model. ACL thickness is estimated as one-fourth of the PCL thickness, by observing the histological sections provided in Allison's study [42]. For the CR (check rein) segments, width is taken as 10% of the palmar plate width [44], and the thickness is taken as the palmar plate's lateral thickness reported in Kömürcü et al.'s study [48]. Since the parameters E_{∞}, w_i and $\mathrm{t_i}$ cannot be known with certainty, it is not very meaningful to keep them as separate variables. They are lumped into a single parameter K_i.

$$F_i = K_i \cdot \varepsilon_i^* \cdot \bar{\sigma} \; where \; K_i = E_{\infty,i} \cdot w_i \cdot \mathrm{t_i} \qquad \text{(Equation 24)}$$

Equation 22 yields the force of each ligament as a function of its strain. K_i, ε_i^* and l_0 are the required parameters. ε^* and l_0 are calculated iteratively by Equations 19 and 20 starting with linear springs. K_i and ε_i^* values used in this study are tabulated in Table 3.1.

Table 3.1 Ligament parameters

Ligament segment		K_i (N)	ε_i^* (%)
PIP joint	**PCL-dorsal-ulnar**	306	36.0
	PCL-central-ulnar	300	4.84
	PCL-palmar-ulnar	294	3.22
	PCL- dorsal-radial	290	31.0
	PCL-central-radial	281	3.24
	PCL-palmar-radial	271	3.72
	ACL-dorsal-ulnar	89	16.5
	ACL-dorsal-radial	92	10.2
	CR-ulnar	73	37.4
	CR-radial	73	25.9
DIP joint	**PCL-dorsal-ulnar**	117	27.1
	PCL-central-ulnar	114	1.96
	PCL-palmar-ulnar	102	2.06
	PCL- dorsal-radial	114	23.5
	PCL-central-radial	111	1.45
	PCL-palmar-radial	102	2.52
	ACL-dorsal-ulnar	25	7.42
	ACL-dorsal-radial	27	6.73
	CR-ulnar	40	15.6
	CR-radial	40	11.5
ORL ulnar		1500	7.26
ORL radial		1500	5.78
FDP		5000	1

CHAPTER 4

RESULTS AND VALIDATION

4.1 Finite Helical Axis Analysis

Hess and colleagues' experimental study [38] was mentioned in Section 2.3. They investigated the change of the finite helical axis (FHA) of a PIP joint during flexion. While performing the FHA analysis, they used increments of 1-degree of flexion. They observed that the axis of rotation changed up to 10.5 degrees and drew a spiral shape.

A similar investigation of the PIP joint is also carried out in this study. In ADAMS, it is possible to obtain the orientation of a coordinate system relative to another coordinate system in the form of Euler parameters. They are defined by an axis of rotation ($\vec{n}$) and a rotation angle φ:

$$E_0 = \cos\left(\frac{\varphi}{2}\right) \quad \text{(Equation 25)}$$

$$E_1 = n_x \sin\left(\frac{\varphi}{2}\right) \quad \text{(Equation 26)}$$

$$E_2 = n_y \sin\left(\frac{\varphi}{2}\right) \quad \text{(Equation 27)}$$

$$E_3 = n_z \sin\left(\frac{\varphi}{2}\right) \quad \text{(Equation 28)}$$

A coordinate system on MP is arbitrarily chosen. For determining the helical axis at the angle (θ_i), Euler parameters of this coordinate system should be obtained relative to the same coordinate system at the angle (θ_{i-1}). The angle difference between the frames is chosen as 1-degree. It is not possible to directly enter a reference coordinate system at a previous time frame in MSC ADAMS. Therefore, a secondary model consisting of only two bodies which are named MP_1 and MP_2 is created. An analysis is performed on the primary model simulating the movement from the fully

extended position to full flexion. The kinematic data to drive the MP is obtained and used as an input to MP_1 body in the secondary model. The same data is used as an input to MP_2 with a delay of 1-degree. Euler parameters are measured between MP-1 and MP_2, and the direction vector ($\vec{n}$) of the helical axis is obtained. Finally, the position vector of the helical axis that is perpendicular to it is calculated using the coordinates of an arbitrary point on the MP_1, as explained in Appendix 1.

The variation of the helical axis is measured as the angle it made with the initial axis. Although the results have many oscillations, it can still be observed that the axis variation reaches its peak during early flexion, similar to Hess et al.'s study. (See Figure 4.1). The maximum angle change is more than twice the value reported by Hess et al. One possible explanation for this may be the choice of 0-degree flexion which is usually designated as the angle that the phalanges are parallel to each other visually. It is quite possible that the 0-degree angle will be designated by a few degrees difference by different investigators. Since at the beginning of the flexion, the axis angle change is very steep, this difference in 0-degree flexion may affect the results.

The oscillations in the results are due to the weakness of the model to lateral angulations. Since the wrapping behavior of the ligaments is not included in the current model, small lateral angulations are not eliminated effectively. This oscillatory lateral motion reflects as an axis change in the FHA analysis. To be able to see the general trend without the oscillations, polynomials are fit to the input data, and the analysis is remade. All the polynomial fits have an R^2 value of more than 0.99999. In figure 4.1.C, the results of the smoothed analysis are presented.

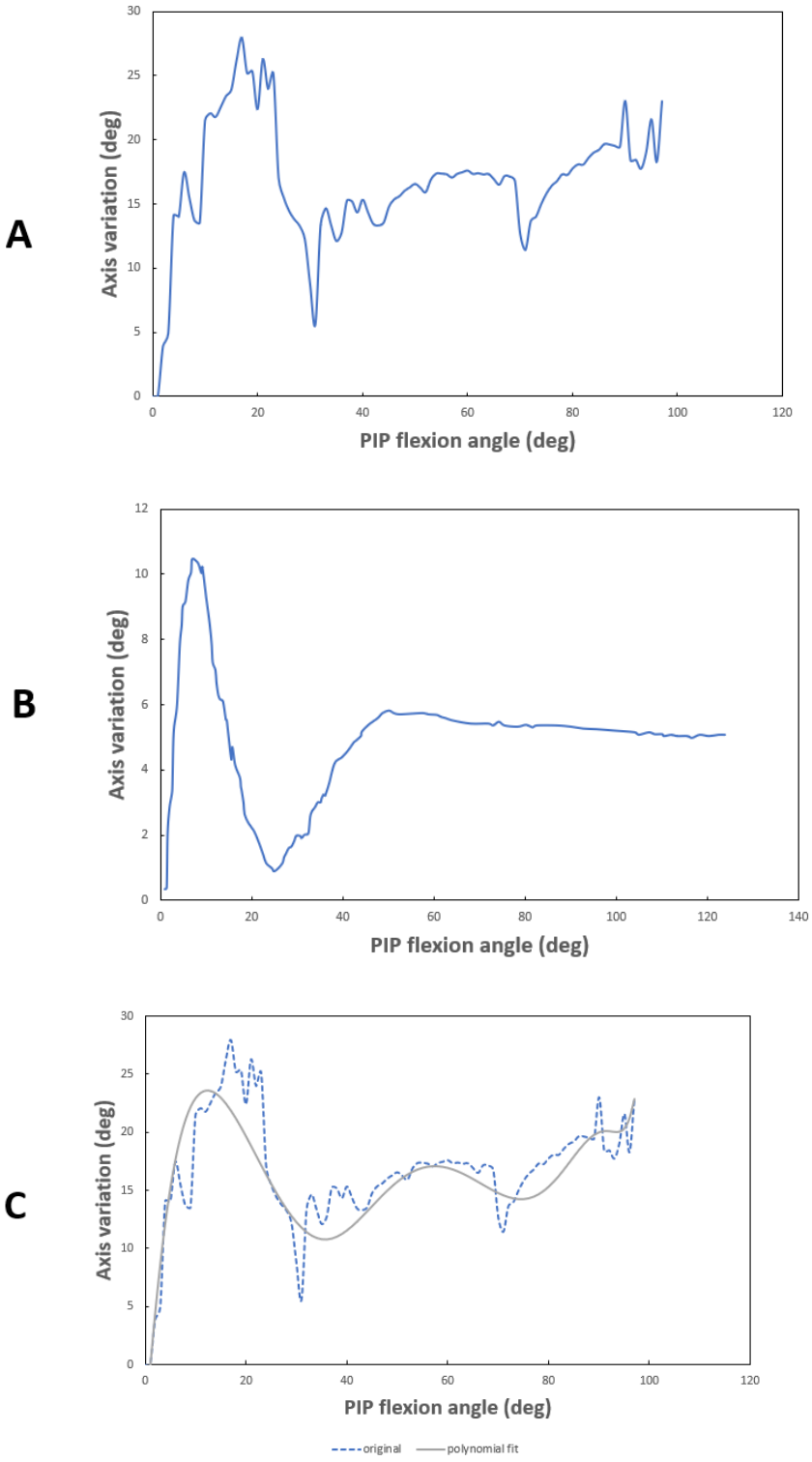

Figure 4.1. Angle between the helical axis at an angle with the initial axis

A) Current model B) Hess et al.'s study C) Original results and the smoothed results

In Figure 4.2 the change of the helical axis is presented visually. Its trajectory has a spiral shape except for the end of the flexion, similar to what Hess et al. observed. The axes pass through roughly from the center of curvature of the condyle.

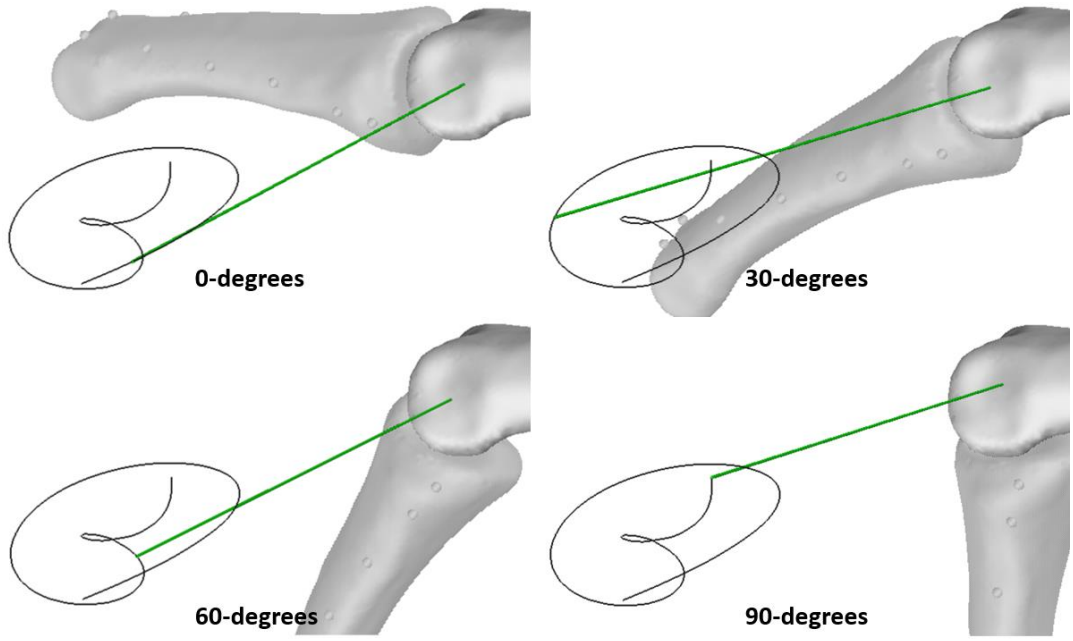

Figure 4.2. Position and trajectory of the helical axis

4.2 Excursion-Flexion relation

The amount of excursion over a joint is important for assessing the normal function of the finger. The muscle moment arms are also dependent on the relation between the excursion and flexion angle. Therefore, many investigators focused on this subject.

Here the results of the different investigators will be compared with the current model to assess its plausibility. The excursion angle relation is reported in various forms such as mm/10 degrees, mm/100 degrees, or as the moment arm, mm/radians. All the reported data are converted into the moment arm form, mm/rad, to avoid confusion.

Armstrong and Chaffin [28] created a regression model for the excursion of the joints, as previously mentioned (Section 2.3, Equation 5). They also constructed a regression model for the joint moment arms as a function of the joint thickness. This regression model is used with the PIP joint thickness (15.8 mm) and the DIP joint thickness (11.3 mm) of the current model. (Table 4.2)

Franko et. al [69] reported that the relation between the excursion and angle started as a nonlinear curve and became linear at the end of the flexion. They fitted third and first-order polynomials to the excursion data and calculated the instantaneous moment arms. Third-order fits showed an increasing trend with the flexion angle. The moment arms obtained from the linear fits are presented in Table 4.2. Ann et al. [70] and Horibe et al. [71] also reported moment arm values in their studies (Table 4.2).

In the current model, the finger is flexed from the extended position to full flexion by pulling the FDP tendon. The excursions over the IP joints are plotted against the flexion angle in Figure 4.3. Third and second-order polynomials and a linear equation are fitted to this data (Table 4.1) to calculate the instantaneous moment arm.

$$M = \frac{d(exc)}{d(angle)} \qquad \text{(Equation 29)}$$

In Figure 4.4, moment arms obtained by different fits are plotted for both PIP and DIP joints.

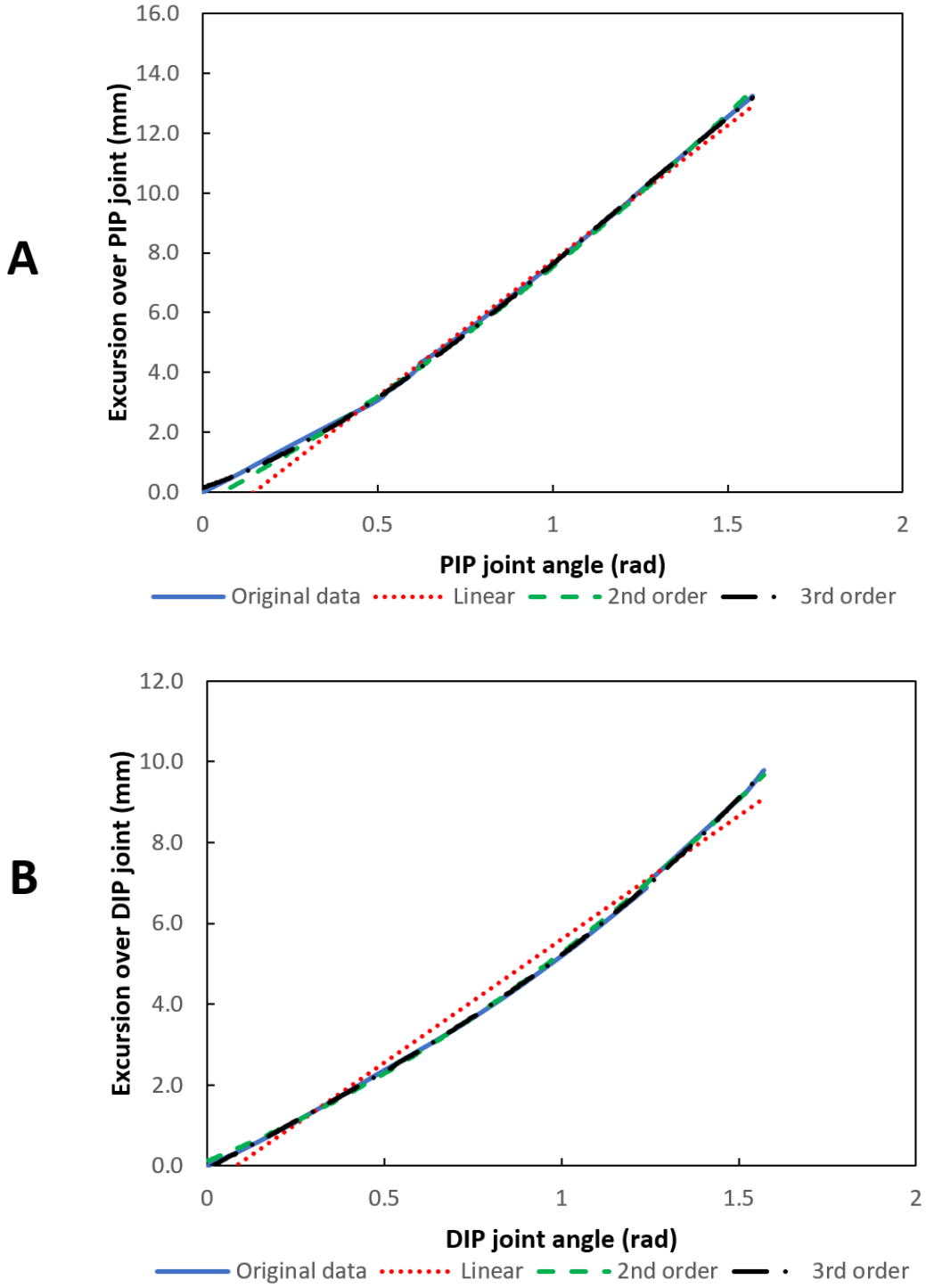

Figure 4.3. Excursion versus angle

A) FDP excursion over the PIP joint vs PIP joint angle B) FDP excursion over the DIP joint vs DIP joint angle

Table 4.1 Coefficients of the polynomial fits to the excursion data.

	3rd order fit	**2nd order fit**	**Linear fit**
PIP	$-1.40x^3 + 5.02x^2 + 3.84x + 0.156$ $R^2 = 0.9997$	$1.57x^2 + 6.30x - 0.346$ $R^2 = 0.9990$	$9.06x - 1.33$ $R^2 = 0.9955$
DIP	$0.705x^3 - 0.110x^2 + 4.70x - 0.0735$ $R^2 = 0.9999$	$1.63x^2 + 3.52x - 0.120$ $R^2 = 0.9997$	$6.10x - 0.498$ $R^2 = 0.9921$

x is the angle of the corresponding joint in radians. R^2 is the coefficient of determination.

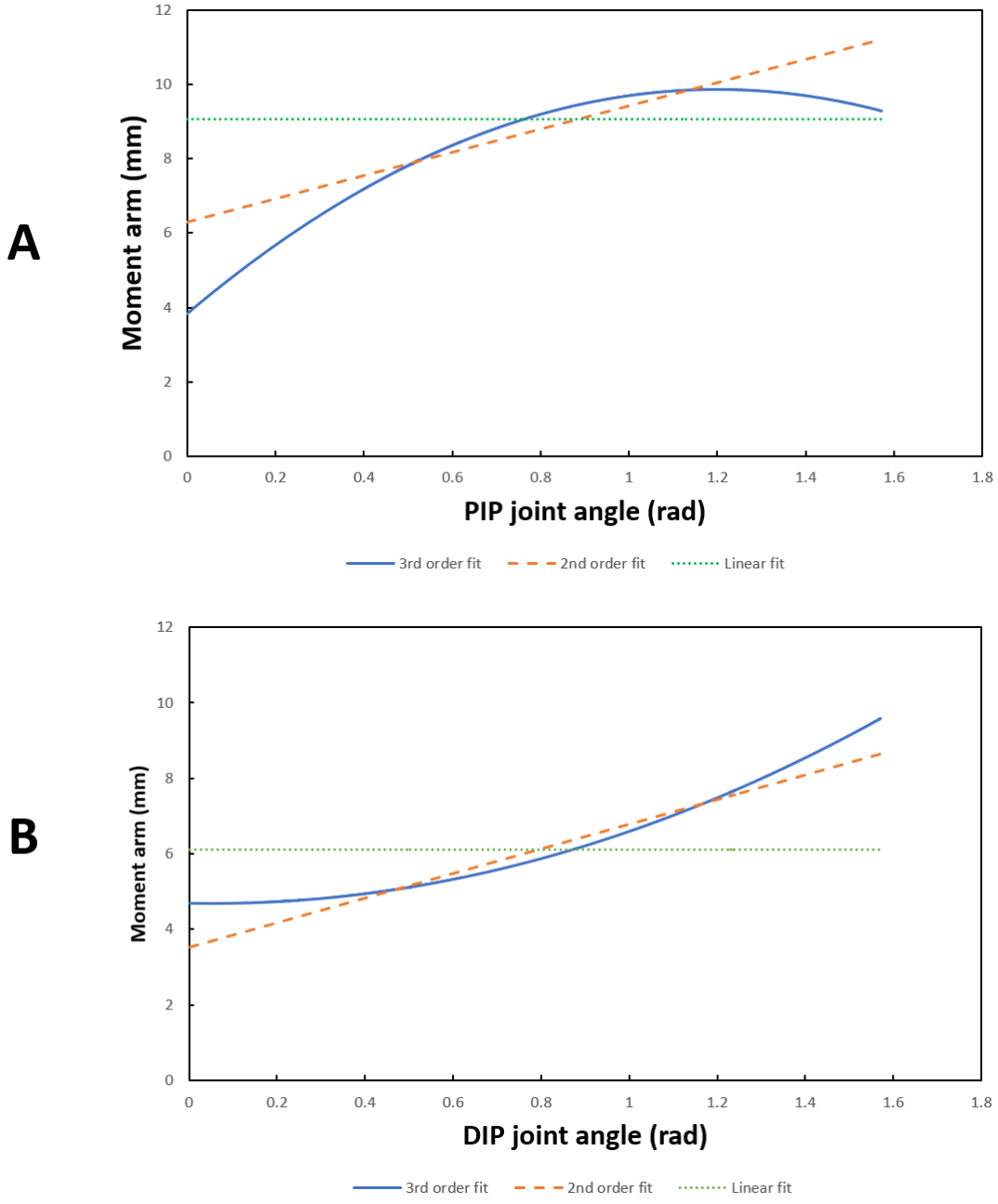

Figure 4.4. Moment arms obtained from the polynomial fits.

A) PIP joint moment arm versus PIP joint angle B) DIP joint moment arm versus DIP joint angle

A comparison of the moment arms obtained from the different studies with the current study is given in Table 4.2. The flexion range that the measurements are

taken is different for each study. Therefore, a linear fit of the excursion data is repeated for each study's range for a better comparison. The difference between the reported values are not greater than the variability in the literature, therefore it can be concluded that the current models' results are acceptable.

Table 4.2 Comparison with the moment arms reported in the literature

Author	**PIP**	**Angle range**	**Current study**	**DIP**	**Angle range**	**Current study**
Armstrong and Chaffin	9.075*	0-90**	9.06	3.93	0-90	6.10
An et al.	7.9±1.1	0-90	9.06	4.1±1.4	0-50	5.08
Horibe et al.	9.17±0.57	0-50	7.68	5.73±0.57	0-22	4.70
Franko et al.	11.81±0.93	2.8-63	8.50	7.77±0.62	3.4-36	5.01

*the value is calculated from the regression equation given in the study. **The range is not specified, it is obtained visually from the plots provided in the study

4.3 PIP-DIP Coordination

The experimental studies indicate that the interphalangeal joints of the finger move in a coordinated manner. In this part of this study, the relation between the PIP and DIP joints is obtained and compared with the data found in the literature.

Darling et al. [72] investigated the coupled motion of the interphalangeal joints at various speeds and reported that the relationship does not depend on the speed or direction of the movement. They stated that the relationship is roughly linear. Interestingly, in some individuals, the PIP joint moved without DIP joint motion in the early flexion.

Hahn et al. [73] also observed a linear relationship except s-shaped at the beginning and the end of the flexion range. The slopes of the linear fits varied much among the different individuals. The reported slopes for the left hand are between 1.17-0.55.

In a recent study, Zwieten et al. [74] fitted S-curves to the experimental data obtained from a normal and pathological finger. They calculated the slope as a function of the PIP angle and argued that the change of the slope might be significant in differentiating the healthy and pathological cases.

The current model is simulated from the extended position to full flexion by an excursion through the FDP. The relation between the PIP and DIP is plotted in Figure 4.5. The shape of the curve resembles an S-curve. DIP moves relatively less compared to the PIP at the beginning and the end of the range. A linear equation is fitted to the data ($R^2 = 0.978$) to compare with the slopes given in Hahn et al.'s study [73]. The slope is obtained as 1.20, which is slightly out of the range given by Hahn et al.

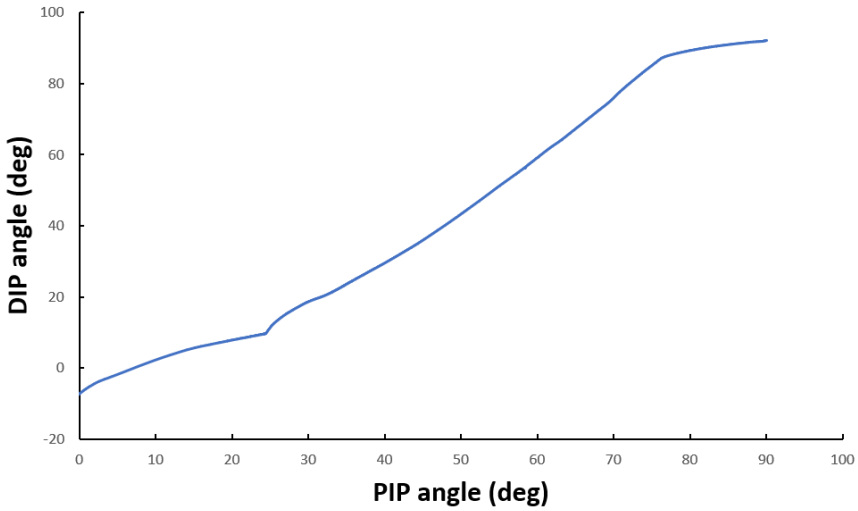

Figure 4.5. DIP angle versus PIP angle

An S curve is also fitted to the data with a coefficient of determination of $R^2 = 0.997$. The change of the slope is obtained as the derivative $d\theta_{DIP}/d\theta_{PIP}$. (Figure 4.6) The slope reached up to a value of 1.81 and peaked at around 55-degree similar to Zwieten et al.'s study.

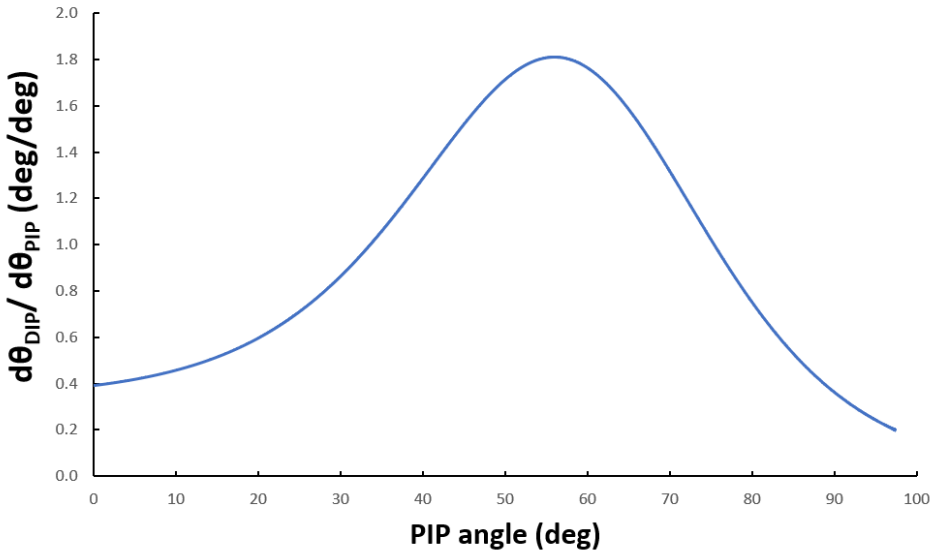

Figure 4.6. The slope of the fitted S curve to the DIP-PIP angle data

4.4 Tendon Force – Angle Relation

Most of the finger models in the literature use hinge joints to model the IP joints. (Section 2.3) The elastic forces due to the surrounding ligaments are neglected. Tendons pull the joints without any resistance, and a tendon force can be calculated only when an external force acts on the finger. However, this does not reflect reality. Tendons need to be loaded up to 10 N to flex the finger fully [75].

Experimental studies about the angle change of the free finger for a force acting on the tendons are limited. Horibe et al.'s [71] study about the tendon excursion was mentioned in the previous section. They loaded the FDP tendon with a 2 N force while all the joints are free to rotate. They also loaded the tendon when only a single joint was free to rotate and the other joints are at approximately 90 degrees. Their results for the both cases are reported in Table 4.3

Nimbarte et al. [75] loaded the FDP tendon with 10% of its maximum force capacity which they reported as 13.2 N. The resulting flexion angles are reported in Table 4.3. They also obtained the relationship between the angle corresponding to the FDP force and found out it was nonlinear. Initially for a small range of force the angle of

both PIP and DIP joints increased rapidly. Then the curve started flatten as the tendon force increased.

In the current study, the finger model is pulled from the FDP tendon with a displacement input until the finger is fully flexed and the resulting force is obtained. In Figure 4.7.A the force required to keep the finger at an angle is plotted against the PIP and DIP angles. The force reached a local peak at mid-flexion with a value of 11.0 N and reached its global maximum in full flexion. The same data is used to plot the angle change for a given tendon force in Figure 4.7.B. The angle increases linearly with the FDP force that is different than Nimbarte et al.'s study [75]. However, close to the maximum flexion, the angle rises rapidly in a small range of force and flattens out, similar to Nimbarte et al.'s study.

To be able to compare with Horibe et al.'s study, [71] a second analysis is performed. PIP joint is held fixed at 90-degrees, and a force of 2 N is applied on the FDP tendon. The analysis is repeated with DIP fixed at 90 degrees and PIP free to rotate. All the numerical results are presented in Table 4.3. The results are similar except for the DIP joint angle at 13.2 N FDP force.

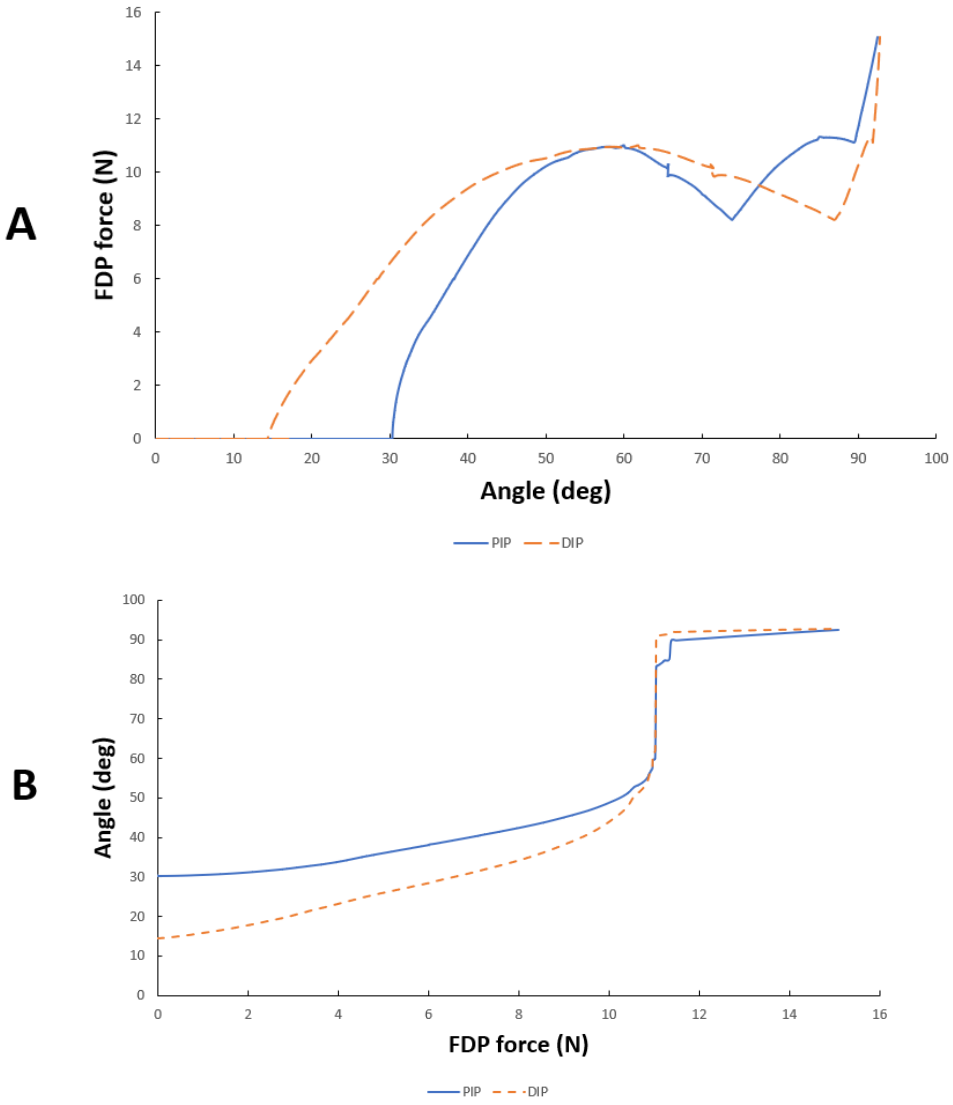

Figure 4.7. A) FDP force versus joint angles B) Joint angles vs FDP force

Table 4.3 Comparison of the angle changes to a corresponding FDP force.

Study	Force	PIP angle	Current study	DIP angle	Current study
Horibe et al. 1*	2 N	32.3±7.2	31.2	15±4.7	17.7
Horibe et al. 2**	2 N	50.2±10.1	73.0	21.8±2.1	28.7
Nimbarte et al	13.2 N	91.5±17	91.2	46.6±17.8	92.42

*All joints of the finger are free to rotate. **The joints other than the measured one is kept at a 90-degrees flexion.

4.5 A Suggestion About the Function of the PCL

In Section 3.2.2, three different definitions of the PCL were compared with each other using a 2D model with a stationary center of rotation. Allison's definition of the PCL was adopted since it was found to be more advantageous mechanically. The moment created by the PCL fibers may change direction depending on their initial position and orientation. The flexion angle at which this change occurred is defined as the critical angle, θ_{crit}. Here this idea is tested on the 3D model.

The most dorsal segment of the PCL, as defined in Section 3.2.2, is canceled for the PIP joint. The distal phalanx is fixed to the middle phalanx to observe only the PIP joint. A force of 2.5 N is applied to the FDP tendon starting from the equilibrium angle (37 degrees for the current simulation). After the PIP joint is fully flexed, the tendon force is set to zero. The change of the tendon force and the PIP angle is presented in Figure 4.8.

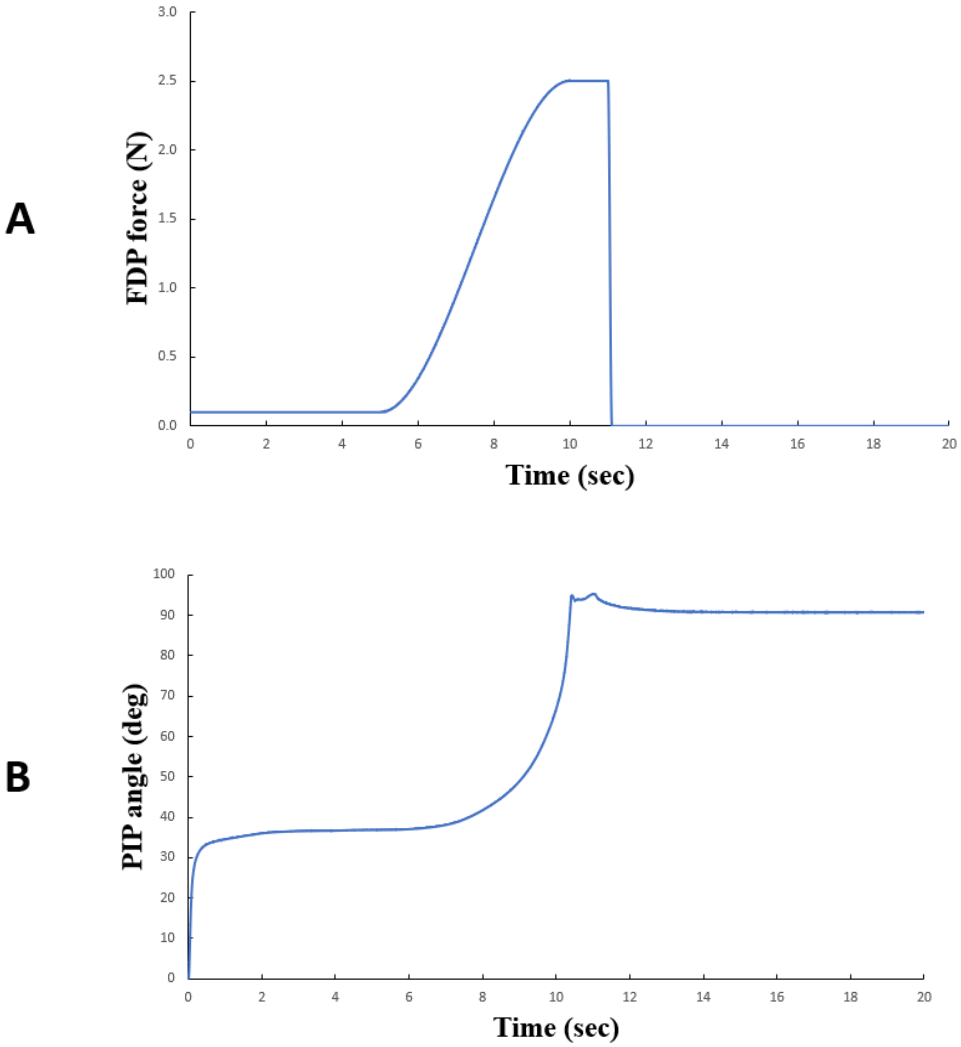

Figure 4.8. A) FDP force versus time B)PIP angle versus time

After removing the tendon force, the PIP joint angle remained constant at an angle about 90 degrees instead of getting back to the initial equilibrium position. This behavior is expected, as explained in Section 3.2.2. Without the most dorsal segment, there is no structure to extend the joint. In Figure 4.9 the images of the joint for 40, 50, 60, 70, 80 and 90 degrees of flexion for the ulnar side is presented. Initially, the central segment is above the joint center, and it resists the flexion movement. However, as the flexion proceeds, at some angle, its line of action goes beyond the center of rotation. This angle was defined as the critical angle in Section 3.2.2.

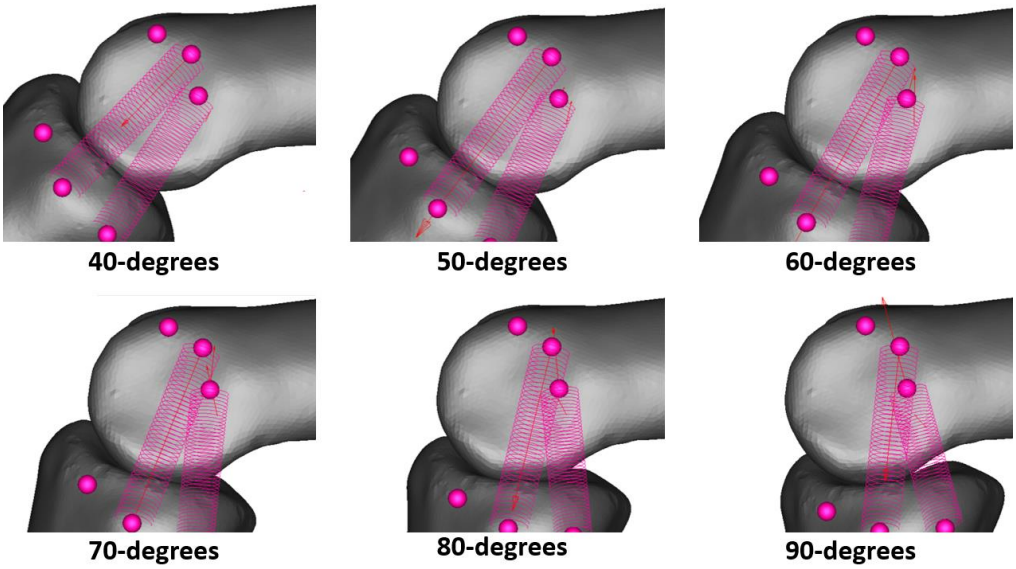

Figure 4.9. Position and orientation of the PCL segments during flexion

The critical angle is also the angle at which the increasing trend in length changes to a decreasing trend. In Figure 4.10, the lengths of the ulnar and radial central segments are plotted. The turning points correspond to 60 degrees for the ulnar side and 75 degrees for the radial side. The critical angle of the whole joint should be somewhere between these two values.

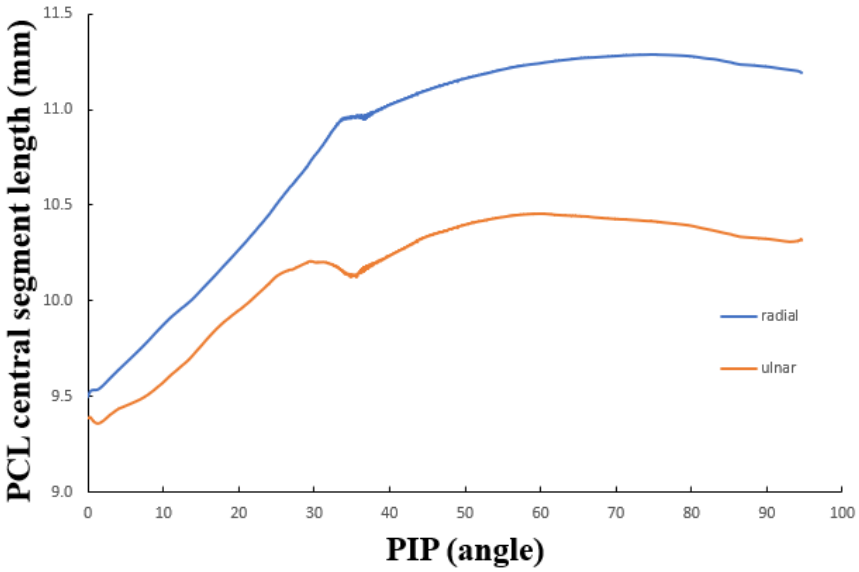

Figure 4.10. PCL central segment length change versus PIP angle

A slightly different analysis is performed to determine the critical angle better. This time instead of force input, a displacement input is applied to the profundus tendon. The force requirement is plotted against the PIP angle in Figure 4.11. The force value reached a value around 2.5 N at 47 degrees. At about 73 degrees, the tendon force required to flex the joint decreased below 0.1 N. This can be thought of as the critical angle of the whole joint. In other words, if the joint is further flexed, it will not come back to its initial equilibrium position without the application of an extension force and it will be locked in flexion.

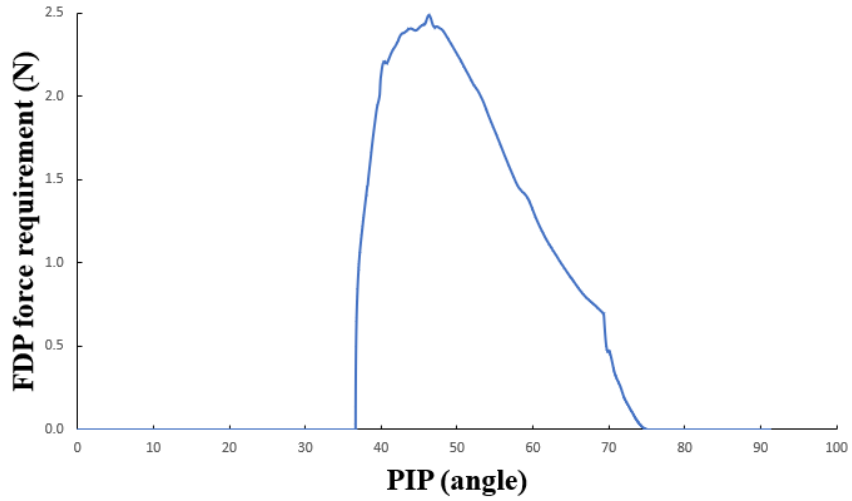

Figure 4.11. FDP tendon force requirement to hold the PIP at an angle

In reality, this locking behavior may not be observed since the tension on the structures dorsal to the PCL can still extend the joint. However, it can still cause a disturbed flexion since the force requirement of the tendon would decrease suddenly. It is believed that experimental studies are required to clarify this subject further.

4.6 The Significance of ORL

In this part, the significance of ORL is investigated. Its stiffness (K) is changed from 0 to 0.25, 0.5, 1, 2, and 4 times its original value (K_0), and a flexion simulation from the extended position to full flexion is performed. DIP-PIP angle data is plotted in

Figure 4.12. When K/K_0 is zero, the DIP flexes without hardly any flexion in the PIP joint. When the DIP reaches full flexion, the PIP joint is only at 35 degrees. This behavior contradicts the experimental results mentioned in Section 4.3. Figure 4.13 presents images from the simulations with and without ORL. Clearly, such angulation of the DIP joint is not possible in the healthy finger.

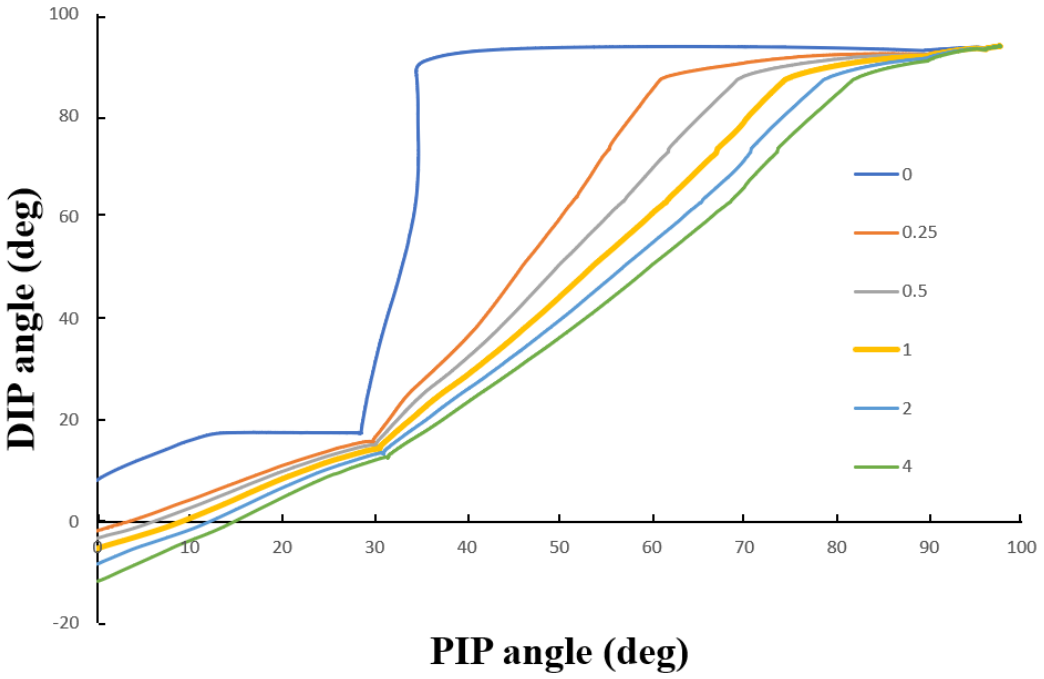

Figure 4.12. DIP-PIP angle plots for different ORL stiffness ratios (K/K_0)

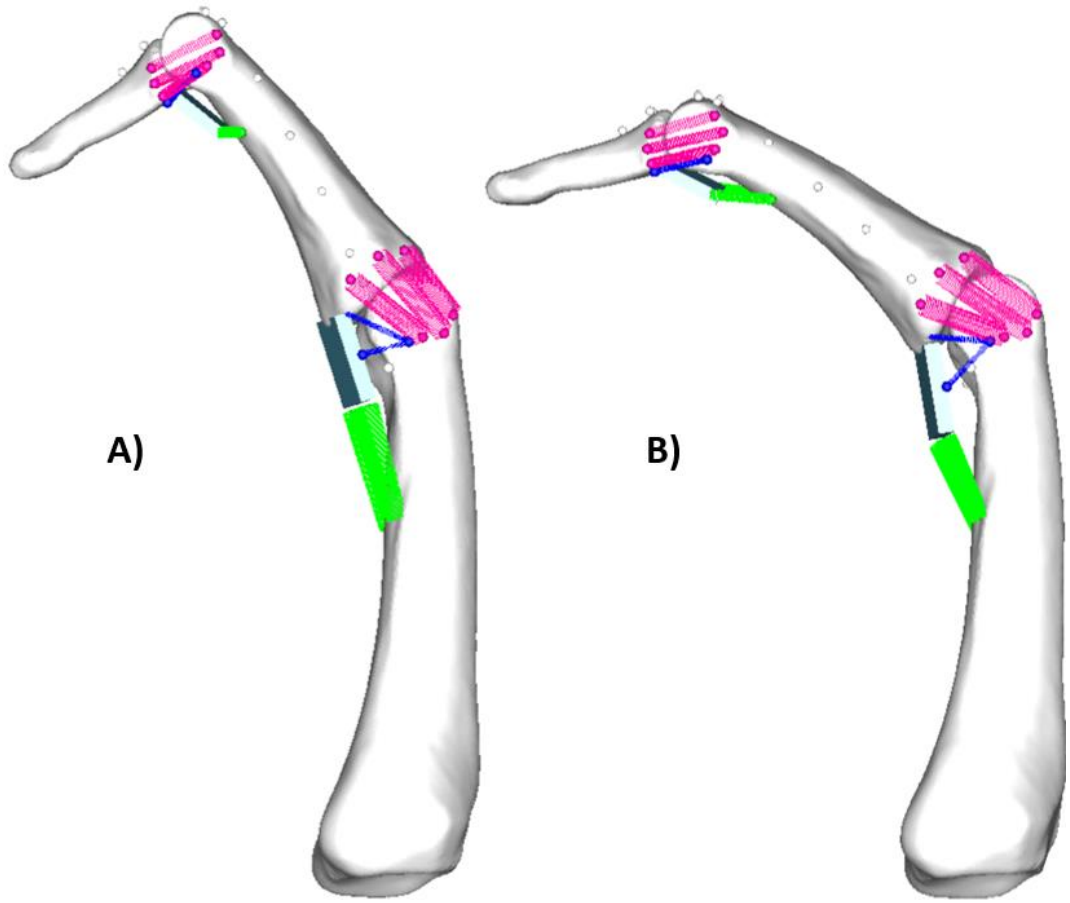

Figure 4.13. Images from the simulations without (A) and with (B) ORL

As the stiffness increased to 0.25 and 0.5 times of its original value, some coordination is introduced. Further raising the stiffness by two times and four times results in a minor change in the curve. The slopes of the curves in the linear regions are calculated by linear fits and plotted against K/K_0 (Figure 4.14). It can be seen that the slopes converge to a value of about 1.4 as the stiffness is increased. This indicates that at high stiffness, the DIP-PIP relationship is a kinematical relationship.

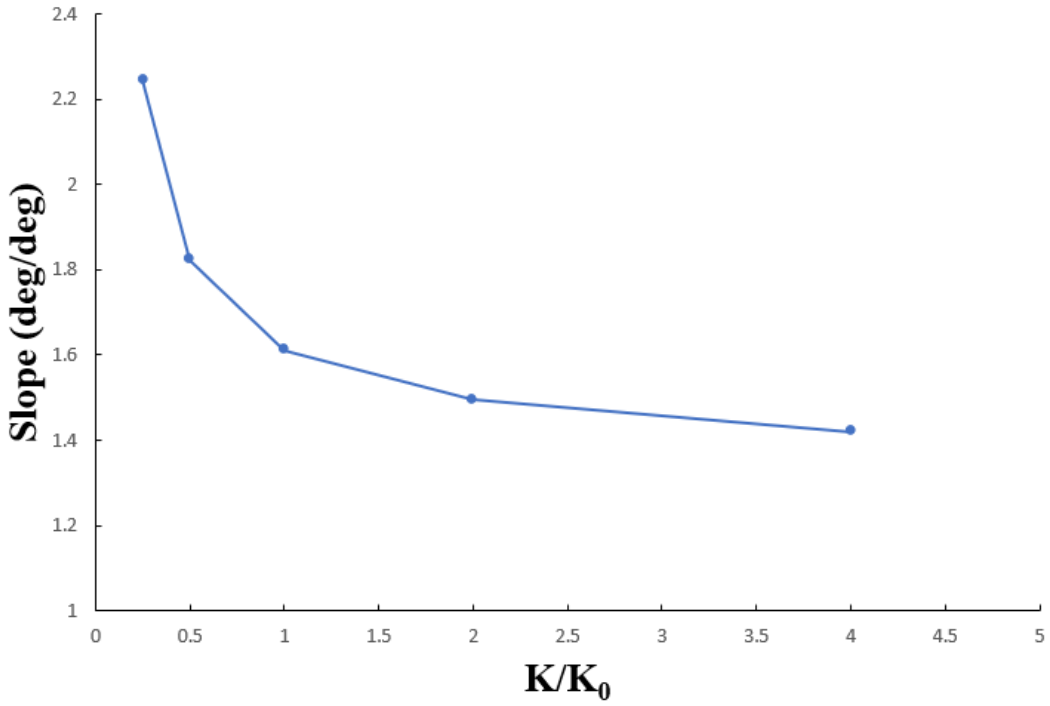

Figure 4.14. The slope in the linear region versus ORL stiffness ratio

Another significant consequence of the ORL is observed when the FDP tendon force requirements to flex the PIP joint are examined. The FDP tendon force is plotted against the PIP angle for the simulation with and without ORL in Figure 4.15. The peak forces in the mid-flexion range almost double for the no ORL case. The force values converge in the late flexion; this is to be expected since the ORL loosens with the PIP joint flexion.

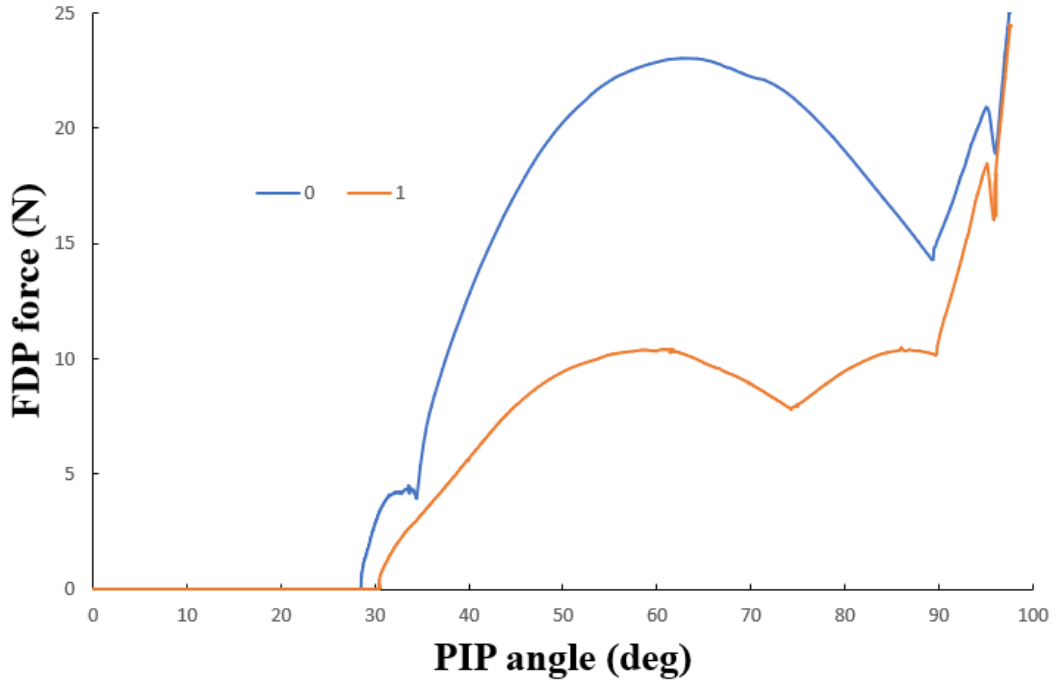

Figure 4.15. The FDP force requirement to flex the PIP joint with and without ORL

In conclusion, the current model point outs that the ORL or an equivalent structure with the same function is required for the coordinated motion of the interphalangeal joints. Furthermore, without the ORL, the necessary force for the PIP joint to flex increases significantly. Experimental studies are required to clarify this subject. Such an experimental procedure is suggested as follows: The MCP joint should be disarticulated to eliminate any coupling that can exist between the MCP joint and the PIP joint. The extensor tendons should be free of tension to prevent any effect. Then the FDP force-angle relationship for the PIP joint should be obtained when the DIP joint is fixed at different angles, when the DIP joint is free to move, and finally when the DIP joint is disarticulated. If ORL or a similar structure with the same function exists, the obtained force-angle data should drastically differ.

4.7 Elevation of the Palmar Plate and A3 Pulleys Role

Saito et al. [47] studied the motion of the PIP joint palmar plate using ultrasonography. At the beginning of the flexion, the palmar plate slid proximally while in contact with the condyles of the proximal phalanx. At about 30-degrees, the palmar plate elevated from the surface of the condyles. The same motion was not observed in the pathological fingers with no A3 pulley. They argued that the A3 pulley might be an elevator of the palmar plate.

The elevation of the palmar plate is also observed in this study. The position of the palmar plate at different angles is presented in Figure 4.16. Unlike Saito et al.'s observations, the contact between the condyles and the palmar plate is lost much earlier (around 5-degrees). The gap progressively increases with flexion.

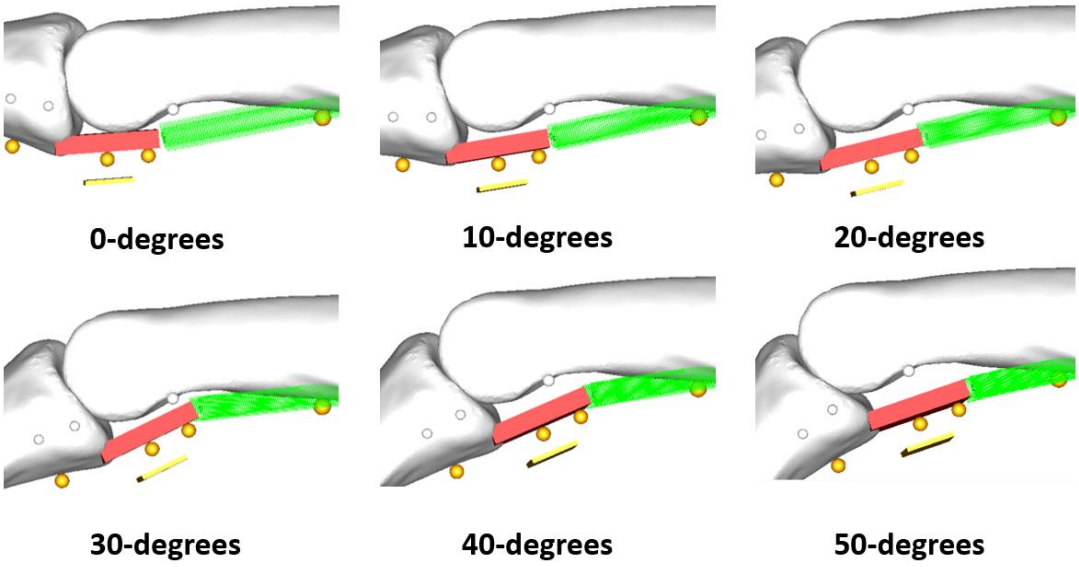

Figure 4.16. Position of the palmar plate (shown in red) during flexion

The reason for the elevation is the tendon forces acting on the VP through the A3 pulley. In Figure 4.17, forces acting on the palmar plate are marked for 0 degrees and 30 degrees. The palmar plate can rotate around its attachment to the middle phalanx. $F_{CR}, F_T, F_{T,net}$ and F_{ACL} are the forces of the check rein ligaments, tendon

forces acting through the A3 pulley, net forces of the tendons, and the forces of the ACL, respectively.

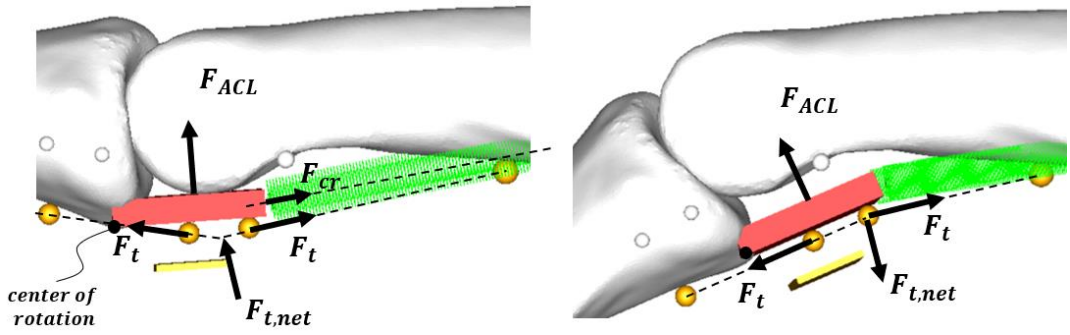

Figure 4.17. Forces acting on the palmar plate (left at 0 degrees, right at 30 degrees)

Considering the moment around the center, F_{CR} can be neglected because its magnitude diminishes with flexion, and almost no force is left on it at around 30 degrees. Also, its line of action is quite close to the center of rotation. F_{ACL}'s moment about the center of rotation pushes the palmar plate against the condyles at all angles. $F_{T,net}$ is the sum of the tendon forces F_T acting indirectly on the palmar plate through the A3 pulley. The direction of its moment changes with flexion. At 0 degrees, it acts together with the F_{ACL} to press the palmar plate onto the condyles, while at 30 degrees, it acts against the palmar plate and causes it to elevate. Both the magnitude and the direction of the net tendon force determine the position of the palmar plate. When the direction of the net tendon force is suitable as in at 30 degrees, tendon forces still should be large enough to balance the ACL force and elevate the palmar plate. In the current study, the ACL force was too weak (Section 3.2.4), and it started to elevate much earlier than Saito et al. reported. [47]

The analysis here shows that the main elevator of the VP is the A3 pulley, since FDP forces can only be transferred to the palmar plate via the A3 pulley. Without the A3

pulley, the ACL forces would be left unbalanced, and the palmar plate would firmly be pressed onto the proximal phalanx surface. This could possibly cause an impingement of the palmar plate, as suggested by the deformed shape of the palmar plates observed in Saito et al.'s studies on pathological fingers. The elevation of the palmar plate may also be associated with the change of the moment arms during flexion since the distance between the tendon and the joint increases. Saito et al.'s findings and the current study indicate that the A3 may be a significant structure for the normal anatomical function of the palmar plate contrary to the current view in the literature.

4.8 Elongation of the ACL

While modeling the ACL's palmar segment which attaches to the palmar plate, it was mentioned that the elongations were more than 100%. Therefore, modeling it as an elastic element was abandoned, and a constant normal force was applied on the palmar plate to represent its effect. In this section, the elongation of the ACL is investigated in detail, and a modified definition of the ACL is suggested.

In Figure 4.18, the length of the ACL's palmar segment is plotted against the PIP joint angle for both sides. If the free length is taken as the length at 30 degree flexion, which is roughly the resting position of the PIP joint [66], the elongations reach up to 56% for the radial side and 130% for the ulnar side. To the author's knowledge, no ligament reported in the literature reaches this high level of elongation. The maximum value found in the literature is for the ligamentum flavum [59], which elongated up to around 40-50%.

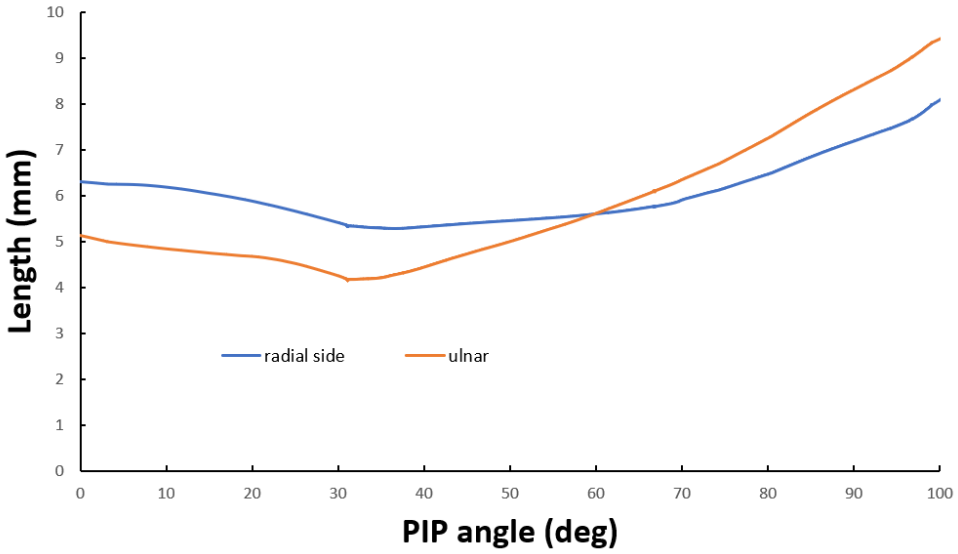

Figure 4.18. Length change of the ACL's palmar segment

One might argue that this excessive elongation is the result of the palmar plate elevation mentioned in the previous section. However, the maximum elongations occur at angles which the palmar plate is not elevated (Figure 4.19).

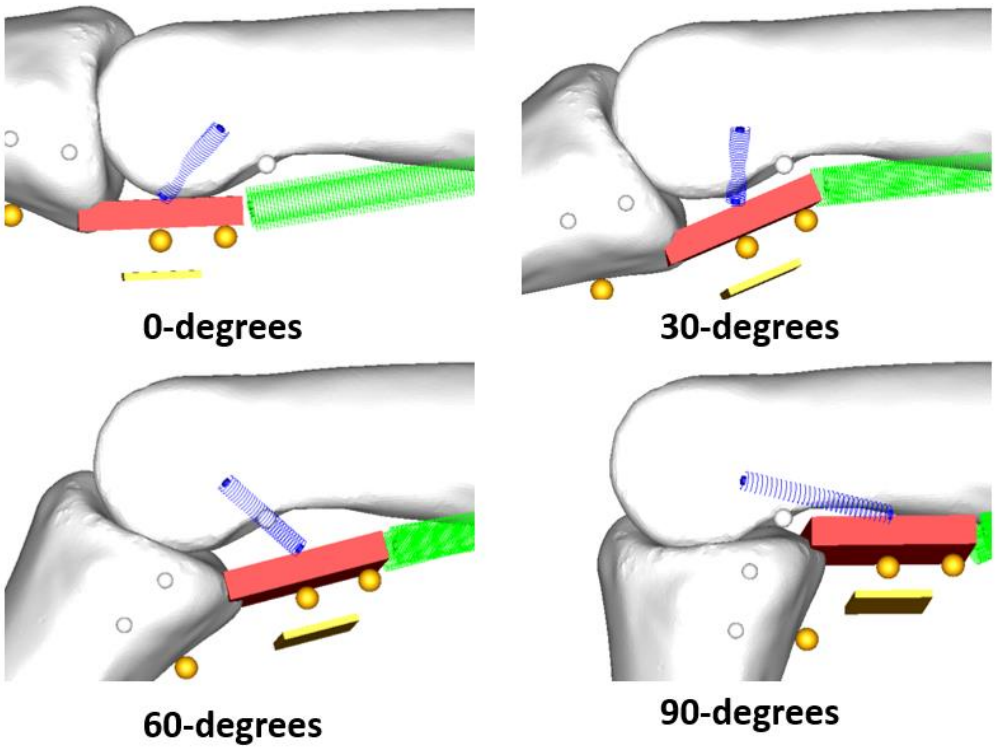

Figure 4.19. Position and orientation of the ACL during flexion

ACL is a tiny structure hard to isolate from other structures. The information about it in the literature is very scarce. The abnormal elongations encountered here might be due to an incomplete definition of it. In the current model, a slight modification in the ACL's definition resolves the problem. If ACL is defined as a single continuous structure originating from one side of the proximal phalanx, traveling under the palmar plate, and inserting on the other side, the elongations reduce to acceptable levels. The lengths at both sides and the length over the palmar plate (13 mm) are added together and plotted against the PIP angle in Figure 4.20. Again, taking the length at 30 degrees as the free length, the maximum elongation reduces to 36%.

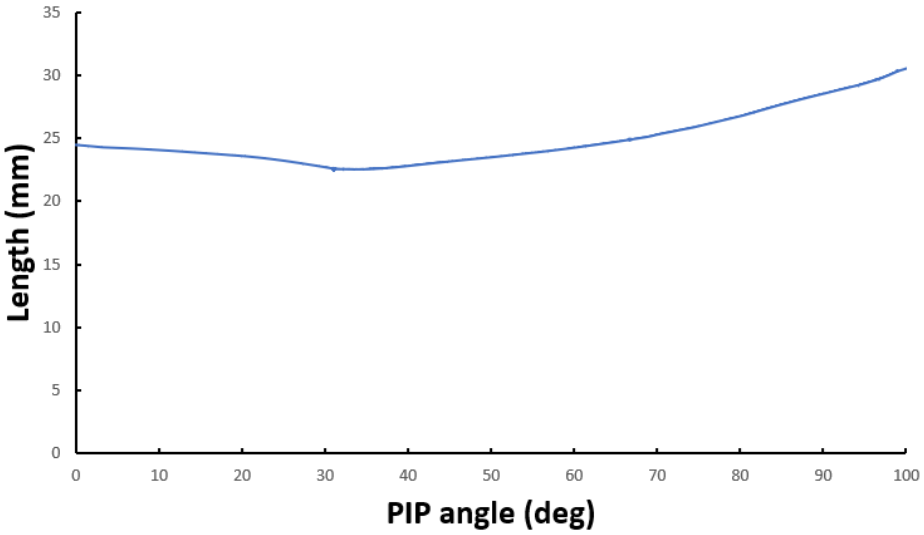

Figure 4.20. Length change of the ACL defined as a single continuous structure.

Two different studies done by William et al. [45] and Watanabe et al. [76] supports this definition of a single continuous ACL. They both investigated fiber layers of the palmar plate and reported a transverse layer at the most palmar surface. The fibers of this layer were reported to be continuous with the ACL's fibers. If the continuous ACL hypothesis presented here is correct, any disruption of its continuity may result in a stiffer ACL by creating two different ACL ligaments. This in turn might restrict palmar plate motion and possibly cause a stiffness in flexion of the joint.

CHAPTER 5

DISCUSSION AND CONCLUSION

The aim of this study was to explain the development process of a 3D model of the interphalangeal joints. The model's plausibility is assessed by comparing it with the results found in the literature. Furthermore, four controversial issues are analyzed using the model, and four hypotheses are developed.

Both the PIP and the DIP joints are modeled without using any idealized kinematic constraints. Anatomically correct 3D geometries are used for the bones. The articulation is modeled using the contact model in MSC ADAMS. The motion of the joint is constrained by the surrounding ligamentous structures. The proper and accessory collateral ligaments, the palmar plate, and the check rein ligaments are included in the model. In order to model the coupling between the two interphalangeal joints, the oblique retinacular ligament is also added to the model. Finally, the flexor digitorum profundus is modeled to be able to actuate the finger.

The modeling of the bones and the contact between them was straightforward. The study mainly focused on the modeling of the ligamentous structures. One of the difficulties encountered during modeling was the lack of precise definitions of the ligaments. Three different definitions of PCL are prominent in the literature. Although the differences between them may seem small, they affect the biomechanics of the joint significantly. A simple 2D model is utilized to compare them, and Allison's [42] definition is found to be the most advantageous mechanically. Another problem was encountered in the modeling of ACL. When it is modeled as described in the literature, it elongated more than twice its initial length. Because of these challenges, the modeling was a highly iterative process, unlike the manner, it is explained here. For this reason, simulation durations were a constant concern during modeling. Simulation parameters, contact stiffness values,

and damping values are carefully tuned to give satisfactory results without increasing the solution time too much. Typical simulation durations were around 10 minutes, although it occasionally reached up to 1 hour on a typical laptop computer.

The ligaments are modeled as 1D non-linear force elements. A modified version of Decraemer et al.'s [58] model is utilized. The derivation of the formulation is slightly changed, and the parameters are chosen differently such that they have a different physical meaning. The used parameters were the tangential modulus and the linearity strain.

Another problem with ligament modeling was the determination of the parameters. There is not much data about the ligaments of the finger. It is not surprising since they are tiny and hard to work with. Ligaments are highly adaptive structures, and their properties may vary a lot; therefore, it is not meaningful to use values reported for different ligaments. For this reason, a method to estimate ligaments' free length and the linearity strain is proposed. This method relied on two main assumptions. First, the ligaments have a mechanostat point where there is no adaptation, which corresponds to the joint's neutral position. Second, the ligaments operate in the toe region and the initial portion of the linear region in joints ROM. Although there is no experimental basis for the proposed method, it ensured that the ligaments operated in the toe region.

In order to assess the model's plausibility, the results are compared with the literature. First, the 3D kinematics of the PIP joint is investigated using finite helical axis analysis. Hess and colleagues [38] showed that the axis of the joint changed during flexion. The angular variation of the axis reached its peak in early flexion and remained stationary after 50 degrees. Although the max values differed, a similar trend is observed in the current study. The trajectory of the helical axis followed a spiral shape similar to Hess et al.'s study.

Secondly, the relation between the FDP tendon excursion and the flexion angles is investigated. This relationship is usually expressed as a constant moment arm (mm/rad) for a specified angle range. Here the moment arms are calculated for the

same flexion range by fitting linear equations to the excursion-angle data. The values were in good agreement with the literature. Also, the instantaneous moment arms are calculated from third-order and second-order fits of the excursion data. The moment arms of both joints significantly increased with the flexion angle.

Thirdly, the relationship between the interphalangeal joints is investigated. The DIP-PIP angle curve resembled an S curve. The slope of the curve obtained by a linear fit conformed with the values reported in the literature. A sigmoid function is also fitted to the data, and the instantaneous change of the slope is calculated. According to this fit, the slope reached a maximum at about 55 degrees and decreased as the flexion increased.

Finally, the relationship between the FDP tendon forces and the joint angles is investigated. The force requirements to hold the joint at an angle had a local maximum at around 60 degrees. Close to the full flexion, the force values increased rapidly and reached the maximum value. The reverse relation, which is the angle corresponding to a given force, is also obtained. The angle increased steadily with the force until about 60 degrees. It then rose rapidly and flattened near the full flexion. Nimbarte et al. [75] also obtained the same relation for both DIP and PIP joints. The results were similar for the PIP joint. Horibe et al. [71] loaded the FDP both when all joints are free and when only one joint is free to rotate. Their reports for PIP and DIP angles for the two cases were very close to the values found in this study.

A good model should be able to explain the experimental findings but should also be able to make some predictions. For this reason, the less known areas of the finger are analyzed using the model. The first one is about the function of the PCL. It is known as the lateral stabilizer of the joint. Based on the results here, it is believed that it also helps stabilization in the flexion movement. When the most dorsal segment of it was canceled, the joint locked in flexion even after the flexion force was removed. The central segment of the PCL moves below the axis of rotation after a certain angle

which causes their moments to change direction and help flexion instead of resisting it.

A second prediction was made about the significance of the ORL. When ORL is omitted in the model, the DIP joint flexed unrealistically without hardly any PIP joint motion. Increasing the ORL stiffness resulted in a higher slope of the DIP-PIP angle curve. The slopes converged to a value of about 1.4 in the mid-flexion region as the stiffness is further increased, suggesting a kinematic relationship between the DIP and PIP joints. It is concluded that the ORL or a similar structure with the same function is necessary for interphalangeal coordination. Furthermore, when the ORL is not present, the forces required to flex the PIP joint was almost doubled. It is suggested that experimental studies should focus on ORL's effects on the force-angle relationships of the interphalangeal joints instead of trying to visually identify its existence since some other structure might be responsible for the observed coordinated motion.

The third analysis was about the palmar plate elevation mentioned in Saito et al.'s study. They did not observe the same motion in the fingers with no A3 pulley and argued that A3 might be responsible for the elevation. The same elevation is also present in the current study. An analysis of the forces acting on the palmar plate revealed that the balance of the tendon forces acting through the A3 pulley and the ACL forces determines the palmar plate's position. The elevation also depends on the angular position of the joint since the net tendon forces do not act against the ACL at all angles.

Lastly, an anomaly encountered while modeling the ACL is investigated. When the ACL is modeled as described in the literature, the resulting elongations were unreasonably high. However, a slight modification of its definition resolved the problem. It is assumed that the ACL is a single continuous ligament originating from one side of the proximal phalanx, traveling under the palmar plate and attaching to the other side. The observed continuity of the palmar plate and the ACL fibers

support this hypothesis [45], [76]. If this hypothesis is to be true, a disturbance of the continuity might result in the stiffening of the ACL by creating two separate ACL's.

The results of the analysis mentioned above can be summarized in four hypothesis statements:

Hypothesis 1: The most dorsal segment of the PCL (as defined by Allison [42]) is vital for the joint's flexion stability. It helps the joint to extend back into the neutral position. In its absence, the joint might be locked in the flexion, or a snapping can be felt at a certain angle.

Hypothesis 2: ORL or a structure with the same function needs to exist for the coordinated motion of the IP joints. ORL also has a role of lowering the tendon force requirements to flex the PIP joint.

Hypothesis 3: A3 pulley redirects the tendon forces and enables the elevation of the palmar plate. This elevation depends on the position of the joint and the magnitude of the tendon forces. The ACL forces balance the tendons forces.

Hypothesis 4: ACL is a single continuous ligament originating from one side of the proximal phalanx, traveling under the palmar plate and attaching to the other side of the proximal phalanx.

Before concluding, it is required to mention the possible directions that future research can take. The first thing that comes to mind as a continuation of this study is to test the four hypotheses proposed above. Whether the results are positive or not, the capability of such a model is already demonstrate. Similar models can be utilized to analyze the controversial issues about the finger. A possible extension of this study could be the analysis of the extensor mechanism.

During the development process, the most challenging part was the lack of precise definitions of the ligamentous structures. More experimental studies are required to locate the origins and insertions of the ligaments more precisely.

Although it was not a concern in this study, obtaining and handling the 3D geometry of the bones is cumbersome. Currently, 3D geometries are obtained by scanning the bones using MRI, X-ray, etc. The resulting geometries are large and difficult to handle. The surfaces are approximated by triangular surfaces, introducing noise during contact modeling and increasing the simulation times. Instead of using a 3D mesh of the bone geometry, analytic surfaces can be used to model the bone surfaces. This would both decrease the file size and allow for a smoother simulation. The morphology of the phalanges is already well developed in the literature; there is an established name for every little tubercle and concavity found on the bone surfaces. Creating a parametric geometry of the phalangeal surfaces seems achievable. To the knowledge of the author, there is no such model in the literature. If this can be accomplished, one might obtain patient-specific geometry from a simple x-ray scan which would significantly speed up the modeling studies.

In conclusion, the model presented here is capable of explaining a wide range of phenomena, namely, the axis variation of the PIP joint, the excursion-flexion relation, the interphalangeal coordination, and the tendon force-angle relationship. The model was also used to develop four hypotheses about the controversial issues. Although these hypotheses are still subject to experimental validation, they demonstrate the capability of the overall model.

REFERENCES

[1] "Hand Series." https://radiopaedia.org/articles/hand-series (accessed Mar. 17, 2021).

[2] H. Drake, R. L., Vogl, W., Mitchell, A. W. M., & Gray, *Gray's anatomy for students*, 2nd ed. 2015.

[3] E. Q. Pang and J. Yao, "Anatomy and Biomechanics of the Finger Proximal Interphalangeal Joint," *Hand Clin.*, vol. 34, no. 2, pp. 121–126, 2018, doi: 10.1016/j.hcl.2017.12.002.

[4] B. Hirt, H. Seyhan, M. Wagner, and R. Zumhasch, *Hand and wrist anatomy and biomechanics: A comprehensive guide*. Stuttgart, Germany: Thieme Publishing Group, 2016.

[5] K. Kuczynski, "The proximal interphalangeal joint. Anatomy and causes of stiffness in the fingers.," *J. Bone Joint Surg. Br.*, vol. 50, no. 3, pp. 656–663, Aug. 1968, doi: 10.1302/0301-620x.50b3.656.

[6] S. W. Wolfe, W. C. Pederson, R. N. Hotchkiss, and S. H. Kozin, *Green's operative hand surgery: 2-Volume set*, 6th ed. New York, NY: Churchill Livingstone, 2010.

[7] J. M. F. LANDSMEER, "The Coordination of Finger-Joint Motions," *J. Bone Jt. Surg.*, vol. 45, no. 8, pp. 1654–1662, Dec. 1963, doi: 10.2106/00004623-196345080-00007.

[8] B. P. Kleinhenz and B. D. Adams, "Closed Sagittal Band Injury of the Metacarpophalangeal Joint," *J. Am. Acad. Orthop. Surg.*, vol. 23, no. 7, pp. 415–423, Jul. 2015, doi: 10.5435/JAAOS-D-13-00203.

[9] Y.-C. Fung, *Biomechanics*, 2nd ed. New York, NY: Springer New York, 1993.

[10] M. Benjamin and J. R. Ralphs, "Tendons and ligaments--an overview.," *Histol. Histopathol.*, vol. 12, no. 4, pp. 1135–1144, Oct. 1997.

[11] N. Özkaya, M. Nordin, D. Goldsheyder, and D. Leger, *Fundamentals of Biomechanics*, 3rd ed. New York, NY: Springer New York, 2012.

[12] B. C. Pridgen *et al.*, "Flexor Tendon Tissue Engineering: Acellularization of Human Flexor Tendons with Preservation of Biomechanical Properties and Biocompatibility," *Tissue Eng. Part C Methods*, vol. 17, no. 8, pp. 819–828, Aug. 2011, doi: 10.1089/ten.tec.2010.0457.

[13] F. Alshomer, C. Chaves, and D. M. Kalaskar, "Advances in Tendon and Ligament Tissue Engineering: Materials Perspective," *J. Mater.*, vol. 2018, pp. 1–17, Aug. 2018, doi: 10.1155/2018/9868151.

[14] M. J. Dolan and T. Drew, "UNIT 3-TENDONS & LIGAMENTS," 2005, [Online]. Available: http://www.orthonline.dundee.ac.uk/DLS/Orthopaedics Rehabilitation Technology/Module Group 2/Module 2 - Tissue Mechanics/Unit 3 - Tendon & Ligaments/files/assets/downloads/publication.pdf.

[15] B. H. Ng, S. M. Chou, B. H. Lim, and A. Chong, "Strain rate effect on the failure properties of tendons," *Proc. Inst. Mech. Eng. Part H J. Eng. Med.*, vol. 218, no. 3, pp. 203–206, 2004, doi: 10.1243/095441104323118923.

[16] K. Firoozbakhsh, I. S. Yi, M. S. Moneim, and Y. Umada, "A study of ulnar collateral ligament of the thumb metacarpophalangeal joint.," *Clin. Orthop. Relat. Res.*, no. 403, pp. 240–247, Oct. 2002, doi: 10.1097/00003086-200210000-00035.

[17] E. H. Harris, L. B. J. Walker, and B. R. Bass, "Stress-strain studies in cadaveric human tendon and an anomaly in the Young's modulus thereof.," *Med. Biol. Eng.*, vol. 4, no. 3, pp. 253–259, May 1966, doi: 10.1007/BF02474798.

[18] S. L. Woo, "Mechanical properties of tendons and ligaments. I. Quasi-static and nonlinear viscoelastic properties.," *Biorheology*, vol. 19, no. 3, pp. 385–396, 1982, doi: 10.3233/bir-1982-19301.

[19] J. J. Wu, “Quantitative Constitutive Behaviour and Viscoelastic Properties of Fresh Flexor Tendons,” *Int. J. Artif. Organs*, vol. 29, no. 9, pp. 852–857, 2006, doi: 10.1177/039139880602900906.

[20] F. R. Noyes and E. S. Grood, “The strength of the anterior cruciate ligament in humans and Rhesus monkeys.,” *J. Bone Joint Surg. Am.*, vol. 58, no. 8, pp. 1074–1082, Dec. 1976.

[21] N. Chandrashekar, H. Mansouri, J. Slauterbeck, and J. Hashemi, “Sex-based differences in the tensile properties of the human anterior cruciate ligament.,” *J. Biomech.*, vol. 39, no. 16, pp. 2943–2950, 2006, doi: 10.1016/j.jbiomech.2005.10.031.

[22] G. Criscenti *et al.*, “Material and structural tensile properties of the human medial patello-femoral ligament.,” *J. Mech. Behav. Biomed. Mater.*, vol. 54, pp. 141–148, Feb. 2016, doi: 10.1016/j.jmbbm.2015.09.030.

[23] G. A. Johnson, D. M. Tramaglini, R. E. Levine, K. Ohno, N. Y. Choi, and S. L. Woo, “Tensile and viscoelastic properties of human patellar tendon.,” *J. Orthop. Res. Off. Publ. Orthop. Res. Soc.*, vol. 12, no. 6, pp. 796–803, Nov. 1994, doi: 10.1002/jor.1100120607.

[24] K. M. Quapp and J. A. Weiss, “Material characterization of human medial collateral ligament.,” *J. Biomech. Eng.*, vol. 120, no. 6, pp. 757–763, Dec. 1998, doi: 10.1115/1.2834890.

[25] T. A. Wren, S. A. Yerby, G. S. Beaupré, and D. R. Carter, “Mechanical properties of the human achilles tendon.,” *Clin. Biomech. (Bristol, Avon)*, vol. 16, no. 3, pp. 245–251, Mar. 2001, doi: 10.1016/s0268-0033(00)00089-9.

[26] J. M. LANDSMEER, “Studies in the anatomy of articulation. I. The equilibrium of the ‘intercalated’ bone.,” *Acta Morphol. Neerl. Scand.*, vol. 3, pp. 287–303, 1961.

[27] K. N. An, E. Y. Chao, W. P. 3rd Cooney, and R. L. Linscheid, “Normative model of human hand for biomechanical analysis.,” *J. Biomech.*, vol. 12, no.

10, pp. 775–788, 1979, doi: 10.1016/0021-9290(79)90163-5.

[28] T. J. Armstrong and D. B. Chaffin, “An investigation of the relationship between displacements of the finger and wrist joints and the extrinsic finger flexor tendons.,” *J. Biomech.*, vol. 11, no. 3, pp. 119–128, 1978, doi: 10.1016/0021-9290(78)90004-0.

[29] A. M. Kociolek and P. J. Keir, “Modelling tendon excursions and moment arms of the finger flexors: anatomic fidelity versus function.,” *J. Biomech.*, vol. 44, no. 10, pp. 1967–1973, Jul. 2011, doi: 10.1016/j.jbiomech.2011.05.002.

[30] H. J. Buchner, M. J. Hines, and H. Hemami, “A dynamic model for finger interphalangeal coordination.,” *J. Biomech.*, vol. 21, no. 6, pp. 459–468, 1988, doi: 10.1016/0021-9290(88)90238-2.

[31] G. W. Fischer, “A treatise on the topographic anatomy of the long finger and a biomechanical investigation on its inter-joint movement,” University of Iowa, 1969.

[32] K. Hara, R. Yokogawa, and A. Yokogawa, “A graphical method for evaluating static characteristics of the human finger by force manipulability,” in *Proceedings. 1998 IEEE International Conference on Robotics and Automation (Cat. No.98CH36146)*, May 1998, vol. 2, pp. 1623–1628 vol.2, doi: 10.1109/ROBOT.1998.677383.

[33] N. Miyata, K. Yamaguchi, and Y. Maeda, “Measuring and modeling active maximum fingertip forces of a human index finger,” in *2007 IEEE/RSJ International Conference on Intelligent Robots and Systems*, Oct. 2007, pp. 2156–2161, doi: 10.1109/IROS.2007.4399243.

[34] J. Z. Wu, K.-N. An, R. G. Cutlip, K. Krajnak, D. Welcome, and R. G. Dong, “Analysis of musculoskeletal loading in an index finger during tapping.,” *J. Biomech.*, vol. 41, no. 3, pp. 668–676, 2008, doi: 10.1016/j.jbiomech.2007.09.025.

[35] D. L. Jindrich, A. D. Balakrishnan, and J. T. Dennerlein, “Finger joint impedance during tapping on a computer keyswitch.,” *J. Biomech.*, vol. 37, no. 10, pp. 1589–1596, Oct. 2004, doi: 10.1016/j.jbiomech.2004.01.001.

[36] N. Vignais and F. Marin, “Analysis of the musculoskeletal system of the hand and forearm during a cylinder grasping task,” *Int. J. Ind. Ergon.*, vol. 44, no. 4, pp. 535–543, 2014, doi: https://doi.org/10.1016/j.ergon.2014.03.006.

[37] J. L. Sancho-Bru, “A 3D Biomechanical Model of the Hand for Power Grip,” *J. Biomech. Eng.*, vol. 125, no. 1, p. 78, 2003, doi: 10.1115/1.1532791.

[38] F. Hess, P. Fürnstahl, L.-M. Gallo, and A. Schweizer, “3D analysis of the proximal interphalangeal joint kinematics during flexion.,” *Comput. Math. Methods Med.*, vol. 2013, p. 138063, 2013, doi: 10.1155/2013/138063.

[39] “Human Hand Bones,” 2018. http://www.thingiverse.com/thing:15342.

[40] H. E. Ash and A. Unsworth, “Design of a surface replacement prosthesis for the proximal interphalangeal joint,” *Proc. Inst. Mech. Eng. Part H J. Eng. Med.*, vol. 214, no. 2, pp. 151–163, 2000, doi: 10.1243/0954411001535327.

[41] W. H. Bowers, *The Interphalangeal Joints*. Churchill Livingstone, 1987.

[42] D. M. Allison, “Anatomy of the collateral ligaments of the proximal interphalangeal joint,” *J. Hand Surg. Am.*, vol. 30, no. 5, pp. 1026–1031, 2005, doi: 10.1016/j.jhsa.2005.05.015.

[43] P. Gad, “The anatomy of the volar part of the capsules of the finger joints.,” *J. Bone Joint Surg. Br.*, vol. 49, no. 2, pp. 362–7, May 1967, [Online]. Available: http://www.ncbi.nlm.nih.gov/pubmed/6026521.

[44] W. H. Bowers, J. W. Wolf, J. L. Nehil, and S. Bittinger, “The proximal interphalangeal joint volar plate. I. An anatomical and biomechanical study,” *J. Hand Surg. Am.*, vol. 5, no. 1, pp. 79–88, 1980, doi: 10.1016/S0363-5023(80)80049-9.

[45] E. H. Williams, E. McCarthy, and K. D. Bickel, “The histologic anatomy of the volar plate,” *J. Hand Surg. Am.*, vol. 23, no. 5, pp. 805–810, 1998, doi:

10.1016/S0363-5023(98)80154-8.

[46] S. W. J. Lee, Z. Y. Ng, and Q. A. Fogg, “Three-dimensional analysis of the palmar plate and collateral ligaments at the proximal interphalangeal joint,” *J. Hand Surg. Eur. Vol.*, vol. 39, no. 4, pp. 391–397, 2014, doi: 10.1177/1753193413492288.

[47] S. Saito and Y. Suzuki, “Biomechanics of the volar plate of the proximal interphalangeal joint: A dynamic ultrasonographic study,” *J. Hand Surg. Am.*, vol. 36, no. 2, pp. 265–271, 2011, doi: 10.1016/j.jhsa.2010.10.034.

[48] M. Kömürcü, Y. Kirici, C. E. M. Korkmaz, K. B. Alemdaroğlu, Y. Sanisoğlu, and M. B. Bozkurt, “Morphometric analysis of metacarpophalangeal and proximal interphalangeal palmar plates,” *Clin. Anat.*, vol. 21, no. 5, pp. 433–438, 2008, doi: 10.1002/ca.20631.

[49] T. Schreiber, P. Allenspach, B. Seifert, and A. Schweizer, “Connective tissue adaptations in the fingers of performance sport climbers,” *Eur. J. Sport Sci.*, vol. 15, no. 8, pp. 696–702, 2015, doi: 10.1080/17461391.2015.1048747.

[50] J. Chen, J. Tan, and A. X. Zhang, “In vivo length changes of the proximal interphalangeal joint proper and accessory collateral ligaments during flexion,” *J. Hand Surg. Am.*, vol. 40, no. 6, pp. 1130–1137, 2015, doi: 10.1016/j.jhsa.2014.11.032.

[51] J. M. F. Landsmeer, “The anatomy of the dorsal aponeurosis of the human finger and its functional significance,” *Anat. Rec.*, vol. 104, no. 1, pp. 31–44, May 1949, doi: 10.1002/ar.1091040105.

[52] R. W. HAINES, “The extensor apparatus of the finger.,” *J. Anat.*, vol. 85, no. 3, pp. 251–9, 1951, [Online]. Available: http://www.ncbi.nlm.nih.gov/pubmed/14850394%0Ahttp://www.pubmedcentral.nih.gov/articlerender.fcgi?artid=PMC1273517.

[53] H. G. Stack, “Muscle Function in the Fingers,” *J. Bone Joint Surg. Br.*, vol. 44-B, no. 4, pp. 899–909, 1962, doi: 10.1302/0301-620x.44b4.899.

[54] C. Harris and G. L. Rutledge, “The functional anatomy of the extensor mechanism of the finger.,” *J. Bone Joint Surg. Am.*, vol. 54, no. 4, pp. 713–26, Jun. 1972, [Online]. Available: http://www.ncbi.nlm.nih.gov/pubmed/5055166.

[55] M. M. Shrewsbury and R. K. Johnson, “A systematic study of the oblique retinacular ligament of the human finger: Its structure and function,” *J. Hand Surg. Am.*, vol. 2, no. 3, pp. 194–199, 1977, doi: 10.1016/S0363-5023(77)80069-5.

[56] T. A. El-Gammal, C. M. Steyers, W. F. Blair, and J. A. Maynard, “Anatomy of the oblique retinacular ligament of the index finger,” *J. Hand Surg. Am.*, vol. 18, no. 4, pp. 717–721, 1993, doi: 10.1016/0363-5023(93)90326-X.

[57] H. Ueba, N. Moradi, H. C. Erne, T. R. Gardner, and R. J. Strauch, “An anatomic and biomechanical study of the oblique retinacular ligament and its role in finger extension,” *J. Hand Surg. Am.*, vol. 36, no. 12, pp. 1959–1964, 2011, doi: 10.1016/j.jhsa.2011.09.033.

[58] W. F. Decraemer, M. A. Maes, and V. J. Vanhuyse, “An elastic stress-strain relation for soft biological tissues based on a structural model,” *J. Biomech.*, vol. 13, no. 6, pp. 463–468, 1980, doi: 10.1016/0021-9290(80)90338-3.

[59] A. SHIRAZI-ADL, A. M. AHMED, and S. C. SHRIVASTAVA, “Mechanical Response of a Lumbar Motion Segment in Axial Torque Alone and Combined with Compression,” *Spine (Phila. Pa. 1976).*, vol. 11, no. 9, pp. 914–927, Nov. 1986, doi: 10.1097/00007632-198611000-00012.

[60] F. R. Noyes, P. J. Torvik, W. B. Hyde, and J. L. DeLucas, “Biomechanics of ligament failure. II. An analysis of immobilization, exercise, and reconditioning effects in primates,” *J. Bone Jt. Surg. - Ser. A*, vol. 56, no. 7, pp. 1406–1418, 1974, doi: 10.2106/00004623-197456070-00009.

[61] S. L.-Y. Woo, M. A. Gomez, Y.-K. Woo, and W. H. Akeson, “Mechanical properties of tendons and ligaments,” *Biorheology*, vol. 19, no. 3, pp. 397–408, Jun. 1982, doi: 10.3233/BIR-1982-19302.

[62] F. L. Harwood and D. Amiel, “Differential metabolic responses of periarticular ligaments and tendon to joint immobilization,” *J. Appl. Physiol.*, vol. 72, no. 5, pp. 1687–1691, 1992, doi: 10.1152/jappl.1992.72.5.1687.

[63] R. D. Herbert and R. J. Balnave, “The effect of position of immobilisation on resting length, resting stiffness, and weight of the soleus muscle of the rabbit,” *J. Orthop. Res.*, vol. 11, no. 3, pp. 358–366, 1993, doi: 10.1002/jor.1100110307.

[64] R. D. Herbert and J. Crosbie, “Rest length and compliance of non-immobilised and immobilised rabbit soleus muscle and tendon,” *Eur. J. Appl. Physiol. Occup. Physiol.*, vol. 76, no. 5, pp. 472–479, 1997, doi: 10.1007/s004210050277.

[65] K. Yasuda and K. Hayashi, “Changes in biomechanical properties of tendons and ligaments from joint disuse,” *Osteoarthr. Cartil.*, vol. 7, no. 1, pp. 122–129, 1999, doi: 10.1053/joca.1998.0167.

[66] K. S. Lee and M. C. Jung, “Flexion and extension angles of resting fingers and wrist,” *Int. J. Occup. Saf. Ergon.*, vol. 20, no. 1, pp. 91–101, 2014, doi: 10.1080/10803548.2014.11077038.

[67] T. A. L. Wren, G. S. Beaupré, and D. R. Carter, “A model for loading-dependent growth, development, and adaptation of tendons and ligaments,” *J. Biomech.*, vol. 31, no. 2, pp. 107–114, 1997, doi: 10.1016/S0021-9290(97)00120-6.

[68] R. Endress *et al.*, “Tissue-engineered collateral ligament composite allografts for scapholunate ligament reconstruction: An experimental study,” *J. Hand Surg. Am.*, vol. 37, no. 8, pp. 1529–1537, 2012, doi: 10.1016/j.jhsa.2012.05.020.

[69] O. I. Franko, T. M. Winters, T. F. Tirrell, E. R. Hentzen, and R. L. Lieber, “Moment arms of the human digital flexors,” *J. Biomech.*, vol. 44, no. 10, pp. 1987–1990, 2011, doi: 10.1016/j.jbiomech.2011.04.025.

[70] K. N. An, Y. Ueba, E. Y. Chao, W. P. Cooney, and R. L. Linscheid, “Tendon excursion and moment arm of index finger muscles,” *J. Biomech.*, vol. 16, no. 6, pp. 419–425, 1983, doi: 10.1016/0021-9290(83)90074-X.

[71] S. Horibe, S. L. Woo, J. J. Spiegelman, J. P. Marcin, and R. H. Gelberman, “Excursion of the flexor digitorum profundus tendon: A kinematic study of the human and canine digits,” *J. Orthop. Res.*, vol. 8, no. 2, pp. 167–174, 1990, doi: 10.1002/jor.1100080203.

[72] W. G. Darling, K. J. Cole, and G. F. Miller, “Coordination of index finger movements,” *J. Biomech.*, vol. 27, no. 4, pp. 479–491, 1994, doi: 10.1016/0021-9290(94)90023-X.

[73] P. HAHN, H. KRIMMER, A. HRADETZKY, and U. LANZ, “Quantitative Analysis of the Linkage between the interphalangeal Joints of the Index Finger,” *J. Hand Surg. Am.*, vol. 20, no. 5, pp. 696–699, Oct. 1995, doi: 10.1016/S0266-7681(05)80139-1.

[74] K. J. Van Zwieten and G. J. Bex, “An analytical expression for the D . I . P .– P . I . P . flexion interdependence in human fingers,” no. May, 2015, doi: 10.5277/ABB-00078-2014-02.

[75] A. D. Nimbarte, R. Kaz, and Z. M. Li, “Finger joint motion generated by individual extrinsic muscles: A cadaveric study,” *J. Orthop. Surg. Res.*, vol. 3, no. 1, pp. 1–7, 2008, doi: 10.1186/1749-799X-3-27.

[76] H. Watanabe, H. Hashizume, H. Inoue, and T. Ogura, “Collagen framework of the volar plate of human proximal interphalangeal joint.,” *Acta Med. Okayama*, vol. 48, no. 2, pp. 101–108, Apr. 1994, doi: 10.18926/AMO/31103.

APPENDICES

A. Calculation of the Helical Axis Position Vector

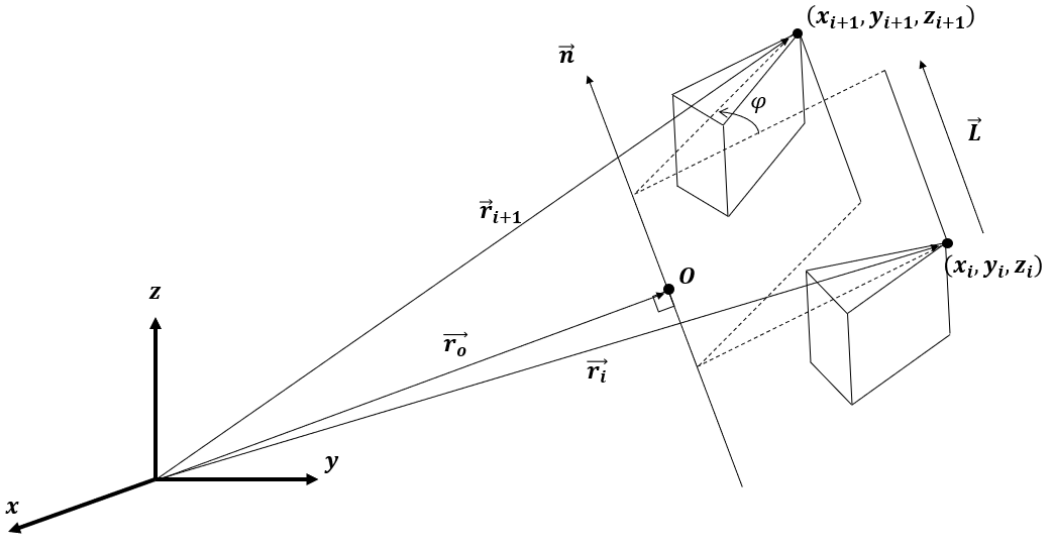

Figure A.1. Displacement of a point

The displacement of a point on a rigid body from frame i to $i+1$ is shown in Figure A1 as the combination of a rotation around the helical axis by an angle φ and a translation along it, $\vec{L}$. $\vec{n}$ is the unit vector in the direction of the helical axis. O is a point on the helical axis such that its position vector $\overrightarrow{r_o}$ is perpendicular to the helical axis. $\vec{r}_i$ and $\vec{r}_{i+1}$ are the position vectors of the point at frame i and $i+1$. Following equation can be written:

$$\{\vec{r}_{i+1} - \vec{r}_o\} = H\{\vec{r}_i - \vec{r}_o\} + \vec{L} \qquad \text{(Equation 30)}$$

H is the rotation matrix for rotating by an angle φ about an axis in the direction $\vec{n} = n_x\boldsymbol{i} + n_y\boldsymbol{j} + n_z\boldsymbol{k}$ passing through the origin.

$$H = [I - \cos(\varphi)]n \cdot n^t + \cos(\varphi)\, I + sin(\varphi)\tilde{n} \qquad \text{(Equation 31)}$$

In equation 31, $\tilde{n}$ is the cross-product matrix.

$\vec{L}$ is the component of the displacement along the helical axis and can be calculated as follows:

$$\vec{L} = L\vec{n} = \left(\vec{d} \cdot \vec{n}\right)\vec{n} \quad \text{(Equation 32)}$$

$$L = \left(\vec{d} \cdot \vec{n}\right) = (\vec{r}_{i+1} - \vec{r}_i) \cdot \vec{n} \quad \text{(Equation 33)}$$

To calculate the position of the helical axis, $\vec{r}_o$ Equation 30 is manipulated as follows:

$$H\{\vec{r}_o\} - \vec{r}_o = H\{\vec{r}_i\} + \vec{L} - \{\vec{r}_{i+1}\}$$

$$(I - H)\{\vec{r}_o\} = \{\vec{r}_{i+1}\} - H\{\vec{r}_i\} - \vec{L} \quad \text{(Equation 34)}$$

Expanding $(I - H)$ in Equation 34 using equation 31:

$$(I - H) = I - [I - \cos(\varphi)]n \cdot n^t - \cos(\varphi)\, I - sin(\varphi)\tilde{n}$$

$$= [I - \cos(\varphi)][I - n \cdot n^t] - sin(\varphi)\tilde{n} \quad \text{(Equation 35)}$$

Substituting Equation 35 to the left side of the equation 34:

$$(I - H)\{\vec{r}_o\} = \left[[I - \cos(\varphi)][I - nn^t] - sin(\varphi)\tilde{n}\right]\{\vec{r}_o\}$$

$$= [I - \cos(\varphi)]\{\vec{r}_o\} - [I - \cos(\varphi)]nn^t\{\vec{r}_o\} - sin(\varphi)\tilde{n}\{\vec{r}_o\} \quad \text{(Equation 36)}$$

In Equation 36 notice that $n^t\{\vec{r}_o\}$ in the second term is zero since $\vec{n}$ and $\vec{r}_o$ are perpendicular to each other:

$$(I - H)\{\vec{r}_o\} = [I - \cos(\varphi)]\{\vec{r}_o\} - sin(\varphi)\tilde{n}\{\vec{r}_o\} \quad \text{(Equation 37)}$$

Then from Equations 34 and 37, $\vec{r}_o$ is calculated as follows:

$$\{\vec{r}_o\} = \left[[I - \cos(\varphi)]\{\vec{r}_o\} - sin(\varphi)\tilde{n}\{\vec{r}_o\}\right]^{-1}\left[\{\vec{r}_{i+1}\} - H\{\vec{r}_i\} - \vec{L}\right] \quad \text{(Equation 38)}$$